UNIVERSITY OF CALIFORNIA, MERCED

Uncovering Unique Cellular and Molecular Drivers of Resistance to Post Traumatic Osteoarthritis

A dissertation submitted in partial satisfaction of the requirements for the degree Doctor of Philosophy

in

Quantitative and Systems Biology

by

Jillian L. McCool

Committee in charge:
Graduate Advisor: Dr. Gabriela G. Loots
Dr. Kara E. McCloskey, Chair
Dr. Katrina K. Hoyer
Dr. Patricia LiWang

2022

Signature Page

The Dissertation of Jillian L. McCool is approved, and it is acceptable in quality and form for publication on microfilm and electronically:

Gabriela G. Loots

Kara E. McCloskey

Katrina K. Hoyer

Patricia LiWang

Date

University of California, Merced

2022

Dedication

To my Mom and Dad. Thank you for forever pushing me to be the best I could be and always telling me the sky was the limit. Without your love and support, I wouldn't be where I am today.

Table of Contents

List of Abbreviations

ACL – Anterior Cruciate Ligament
AC – Articular Cartilage
B6 – C57Bl6/J
DAMP – Damage Associated Molecular Patterns
DMM – Destabilization of Medial Meniscus
ECM - Extracellular Matrix
ERK - Extracellular Signal-Regulated Kinase
Ex/Em – Excitation/Emission
FACS - Fluorescently Activate Cell sorting
FBS – Fetal Bovine Serum
FDR - False Discovery Rate
FGF – Fibroblast Growth Factor
GAG – Glycosaminoglycans
GO - Gene Ontology
HA - Hyaluronic Acid
IAF – Intraarticular Fracture
IFN – Interferon
MM- Medial Meniscus
MRL – MRL/MpJ
MSC – Mesenchymal stromal sell
NBF - Neutral Buffer Formalin
NK - Natural Killer T Cell
PBS – Phosphate Buffer Solution
PG - Proteoglycans
PAMP -Pathogen Associated Molecular Patterns
PRR – Pattern Recognition Receptor
RA – Rheumatoid Arthritis
scRNAseq - Single Cell RNA Sequencing
TCI – Tibial Compression Injury
TGF – Tumor Growth Factor
TNF – Tumor Necrosis Factor
VEGFa - Vascular Endothelial Growth Factor Alpha

List of Figures

Chapter 1

Chapter 2

Chapter 3

Chapter 4

List of Tables

Chapter 3

Chapter 4

Acknowledgements

First, I would like to acknowledge my thesis committee; Dr. Kara E. McCloskey, Dr. Patricia LiWang and Dr. Katrina K. Hoyer for their time, continued interest, and expertise. I would like to extend an additional thank you to Dr. Hoyer for her efforts to motivate and check in on me daily while at LLNL.

I would like to thank all the individuals at Lawrence Livermore National Lab who I have learned from throughout graduate school. Specifically, the members of Dr. Loots' Lab, who have mentored me, and who I have mentored. Each of them taught me invaluable lessons for life both in and out of the lab. I would like to acknowledge the funding that this research was supported by: LDRD 2020 20-LW-002, DOD PR192271 and PR180268. This work was performed under the auspices of the U.S. Department of Energy by Lawrence Livermore National Laboratory under Contract DE-AC52-07NA27344.

Dr. Kelly Martin, for her mentorship and friendship. I cannot thank you enough for dedicating late nights in lab, copious snacks, and well-deserved happy hours to sustain my sanity through graduate school. Also, Dr. Nicholas Hum for his constant technical and emotional support, as well as numerous coffee breaks and occasional procrastination when experimentation became overwhelmingly difficult. Last, Dr. Aimy Sebastian for providing continual mentorship during my graduate career. Her scientific and computational expertise has been a phenomenal addition to my training. These projects would not have progressed without your help.

I would like to extend the largest thank you to my advisor Dr. Gabriela Loots. Thank you for seeing a potential scientist in me years ago as an intern. I feel that I have grown so much in your lab. Not only technical skills, but I feel that I've learned more about myself as an individual by constantly being challenged by you and this project. I cannot wait to see what both of our new futures bring, and I wish you only the best moving forward in your career!

I would also like to thank each and every family member and friend who has watched me grow into the scientist I am today. Specifically, the unconditional love and daily support from my parents, Keith and Krishna, has been my guiding light while on this journey. Although it would take me paragraphs to express my gratitude, I cannot stress how much your support has meant to me. I hope that someday I will be as influential on someone as you have both been to me.

Although he will never read this, Pickles has been my motivation to stay healthy, active and mentally relaxed throughout this whirlwind of an adventure. Behind every scientist, is a great four-legged friend. When big experiments in lab turned into late nights coming home, having those shepherd ears poke through the windows and a "half tail" wagging to greet me, will always bring a smile to my face.

And last, but certainly not least, I would like to thank my partner in life, Dr. Kenny Swartz. Thank you for understanding every step of the way. For continuing to love and support me throughout all of my crazy. For pushing me to be a better human and a better scientist (and for occasionally helping me with Python). This last push of graduate school has been so much easier with you by my side to bring me snacks, coffees, and smiles from your obnoxious jokes. You're my favorite… to be picked on by.

Curriculum Vitae

Jillian L. McCool
Graduate Student Researcher
School of Natural Sciences
University of California Merced
530-521-9983
jillianmccool@gmail.com

Professional Preparation

California State University, Chico	Microbiology	BS, 2016
California State University, Chico	Science Education	BS, 2016
University of California, Merced	Quantitative & Systems Biology	PhD, 2022

Professional Experience

2017-Present Graduate Researcher; BBTD/PLS, LLNL, Livermore CA

Research Experience

University of California Merced, Quantitative & Systems Biology, Merced, CA
Doctoral Graduate Student, August 2017– Present

- Investigated cellular and molecular changes to knee joint populations in response to ACL injury.
    - Designed flow cytometry panels for cell population and FACS analysis from primary cells.
    - Developed primary murine chondrocyte isolation technique to perform single cell RNA sequencing
    - Identified injury induced changes to cartilage populations of interest based on gene expression
    - Performed immunohistochemical validation of changes to bone, cartilage, and immune populations
    - Characterized matrix protein changes between mouse strains ex vivo
- Collaborated with 10x Genomics for optimization of spatial transcriptomic analysis of bone and cartilage

Lawrence Livermore National Laboratory, BBTD/PLS, Livermore CA
Undergraduate Student Intern, Summer 2015, 2016, 2017

- Determined chemotherapeutic effects on mouse microbiome
- Optimized in vitro CRISPR/Cas9 system for cellular genetic editing
- Tracked prostate cancer extracellular vesicle in vitro via fluorescent microscopy

Teaching Experience

University of California Merced, School of Natural Sciences, Merced, CA

Teaching Assistant	**2017-2022**
Biology 002 Molecular Biology	2017

Biology 001 Cellular Biology 2018-2019
Biology 060 Nutrition 2019, 2021
Biology 151 Immunology 2022

Pleasant Valley High School, Chico Unified School District, Chico, CA
Substitute Teacher **2016-2017**
Physical & Life Sciences
Credential Candidate **2016-2017**
Biology & Anatomy

California State University, Chico, Chico CA **2012-2016**
Laboratory Assistant
Science Education Lab for K-12 students

Select Poster Presentations

1. **McCool, JL,** Sebastian, A, Hum, NR, Murugesh, DK, Wilson, SP, Amiri, B, Christiansen, BA, Loots, GG. Characterizing Immune Cell Infiltration in the Murine Joint Microenvironment after Traumatic Knee Injury. American Society for Bone and Mineral Research Annual Conference. September 8-12, 2022; Austin, TX. Poster 132.
2. **McCool, JL,** Sebastian, A, Hum, NR, Murugesh, DK, Christiansen, BA, Loots, GG. Identification of Chondrocyte Subpopulations Using Single-Cell RNA Sequencing to Determine Injury Induced Cellular and Molecular Changes of C57Bl6 and MRL/MpJ Arthritic Knee Joints. American Society for Bone and Mineral Research Annual Conference. October 1-4, 2021; San Diego, CA. Poster 079

Selected Publications

Full list of publications can be found at the following link:
https://www.ncbi.nlm.nih.gov/myncbi/jillian.mccool.2/bibliography/public/

1. **McCool, JL,** Sebastian, A, Hum, NR, Loots, GG. Isolation of Murine Articular Chondrocytes for Single Cell RNA or Bulk RNA Sequencing Analysis. Methods in Molecular Biology: Cartilage Tissue Engineering. Accepted for Publication Sept. 2022.
2. Sebastian, A, Hum, NR, **McCool, JL,** Wilson, SP, Rios-Arce, ND, Murugesh, DK, Christiansen, BA, Loots, GG. Single-Cell RNA-Seq Reveals Changes in Immune Landscape in Post-Traumatic Osteoarthritis. Front Immunol. 2022 July 29; 13:938075. doi: 10.3389/fimmu.2022.938075. PubMed PMID: 35967299. PubMed Central PMID: PMC9373730
3. Sebastian, A. **McCool, JL,** Hum, NR, Murugesh, DK, Wilson, SP, Christiansen, BA, Loots, GG. Single-Cell RNA Seq Reveals Transcriptomic Heterogeneity and Post-Traumatic Osteoarthritis-Associated Early Molecular Changes in Mouse Articular Chondrocytes. Cells. 2021 June 10;10[6]:1462. doi: 10.3390/cells10061462. PubMed PMID: 34200880. PubMed Central PMID: PMC8230441.
4. Sebastian, A, Murugesh, DK, Mendez, ME, Hum, NR, Rios-Arce, ND, **McCool, JL,** Christiansen, BA, Loots, GG. Global Gene Expression Analysis Identifies Age-Related Differences in Knee Joint Transcriptome During the Development of Post-Traumatic Osteoarthritis in Mice. Int J Mol Sci. 2020 Jan 6;21[1]:364. doi: 10.3390/ijms21010364. PMID: 31935848. PMCID: PMC6982134.
5. Mendez, ME, Sebastian, A, Murugesh, DK, Hum, NR, **McCool, JL**, Hsia, AW, Christiansen, BA and Loots, G.G. [2020], LPS -Induced Inflammation Prior to Injury Exacerbates the Development of Post-Traumatic Osteoarthritis in Mice. J Bone Miner Res. 2020 Nov;35[11]:2229-2241. doi: 10.1002/jbmr.4117. PMID: 32564401. PMCID: PMC7689775

Abstract

Uncovering Unique Cellular and Molecular Drivers of Resistance to Post Traumatic Osteoarthritis

By

Jillian L. McCool

Doctor of Philosophy

University of California Merced, 2022

Dr. Gabriela G. Loots
Dr. Kara E. McCloskey, Chair
Dr. Katrina K. Hoyer
Dr. Patricia LiWang

Post traumatic osteoarthritis or PTOA is characterized as a painful and debilitating joint disease. The physiological effects that occur during PTOA progression and chronic disease are severe joint pain, inhibition of movement, and extreme degradation of the cartilage and underlying bone. PTOA is rampant worldwide, affecting millions of individuals. In the United States alone, PTOA is the 5th leading cause of physical disability and carries the 8th highest financial burden on the healthcare system [1] . The articular knee joint is comprised of several tissues including cartilage on both the tibia and femur, as well as underlying trabecular bone known as the subchondral bone. Supporting the joint, is a soft membrane capsule known as the synovial lining which contains fluid essential in joint lubrication. The synovial fluid within the joint is crucial for maintaining joint movement and restraining the continual compressive stress induced by daily activities. For many individuals, these tissues will sustain their functionality into old age. Within the next two decades, health institutes like the Center for Disease Control [1] have projected a rise in osteoarthritis that correlates to the aging population in the United States. Additionally, nearly 12% of all cases of osteoarthritis [2] currently reported are induced by trauma. PTOA is rampant among all ages and has a similar pathogenesis as OA. Currently, there are no effective preventatives, extremely limited treatments, and poor biochemical prognosis for detecting OA, as well as progression to PTOA after trauma.

Nearly 50% of individuals who encounter a traumatic knee injury and do not proceed with reconstructive surgery are later diagnosed with PTOA. Interestingly, the remaining individuals spontaneously resolve this disease, continuing daily activities without pain, disability, and knee joint degradation. These individuals are thought to have a regenerative mechanism associated with their injury response. Due to the complex nature of attaining tissues from these individuals, researchers have begun using mouse strains with differing susceptibilities to PTOA to elucidate a potential regenerative mechanism associated with healing capabilities. This study identifies the MRL/MpJ mouse strain as a PTOA-resistant model in studying the onset of PTOA after tibial compression injury. By induction of an ACL rupture, we have identified several subpopulations of chondrocytes in addition to changes in joint supporting stromal cells, including endothelial cells, that aid in attenuating severe degradation of cartilage and bone through their interactions with the immune system. Additionally, a dynamic change in MRL/MpJ myeloid populations after injury indicates there is a shift in macrophage populations after injury that prompt the knee joint microenvironment towards an anti-inflammatory, wound healing phenotype. In short, this research identifies potential cellular and molecular targets for drug delivery and pharmacological intervention that may hinder the severe joint degradation seen in patients around the globe.

Chapter 1. Introduction

Osteoarthritis, also known as OA, is a degenerative joint disease that occurs in individuals of all ages. OA is characterized by severe degradation of cartilage and bone in articulated joints including hip, ankle, wrist, fingers, spine, and knee [3]. Currently, OA is the 5th leading cause if disability worldwide [1], affecting millions of individuals every year. In the United States, it is considered the leading mobility-related disability [4] Tissue degradation described in OA is usually caused by mechanical wear of the articular surface of the bone. OA can be divided into two classifications of disease: primary OA and secondary OA [1]. Primary OA is common among elderly individuals and its progression is primarily described as prolonged wear and tear of the joints causing deformation of the cartilage and bone over time [5]. Primary OA can be considered a chronic disease, with progression taking place on the scale of decades [5]. Additionally, primary OA can be caused by other factors such as obesity, diabetes, diet, gender, musculoskeletal disorders, and genetic predisposition [1]. On the other hand, secondary OA is caused by traumatic injury to the joint and is usually the result of an anterior cruciate ligament [6] tear, medial meniscus (MM) tear, or intra articular fracture (IAF) [7]. Secondary OA is known as Post Traumatic Osteoarthritis or PTOA. There is no defining age for PTOA, as it is an inducible disease that is prominent in many young, active individuals [8]. During the progression of PTOA, joint instability and inflammation begins immediately after trauma; intensifying degradation of the cartilage, bone, synovial tissue, meniscus, and remaining tendons and ligaments [9]. Currently, there are no cures or preventatives, as well as limited treatments available for this disease.

1.1 Osteoarthritis and Post Traumatic Osteoarthritis

1.1.1 Incidence and burden

Nearly 350 million people currently have arthritis [1] and in the United States (US), 1 in 4 adults have been diagnosed with arthritis [1]. In individuals with arthritis that are over 40, more than 22% have been diagnosed with knee joint OA [10]. Those individuals affected by OA suffer from a multitude of symptoms including severe joint pain, swelling, stiffness and potential loss of use due to the physiological changes that occur to articulated

joints. Osteoarthritis is a primary form of arthritis that is vastly studied due to its high incidence, lack of treatments and clinical burden. Over 32 million adults in the United States are currently affected by OA [4] and the Center for Disease Control [1] has estimated that by 2040, 78 million Americans that are 18 years of age or older will be diagnosed with OA. Musculoskeletal diseases cost for nearly $400 billion on average each year, accounts for nearly 49% of ambulatory care, 22% of Inpatient care, and 13% of prescribed pharmaceuticals [11]. Osteoarthritis care accounts for nearly $80 billion in medical spending costs, and accounts for nearly 27% of ambulatory care, 50% of Inpatient care, and 6% of prescribed pharmaceuticals [11]. Additionally, OA ranks 8th among health conditions for highest healthcare spending budget. Furthermore, PTOA management costs nearly $12 billion, with direct related costs reaching $3 billion. With the rise in age of the US population, OA is becoming a greater risk and burden on our healthcare systems.

1.2 Diagnosis and Treatment

1.2.1 Clinical Diagnostics

OA and PTOA are diagnosed very similarly due to their chronic onset. Usually, a consultation of an individual's medical history will be conducted to determine the current symptoms, if any, the patient is having. Additionally, questions on general health, family history, and habits will also be asked to determine risk and current disease state. In most cases, these diseases are then diagnosed through physical examination by a doctor. Following physical examination, patients are usually subjected to a radiograph, Magnetic Resonance Imaging (MRI) or Computed Tomography (CT); the most common method of the three being a radiograph [12]. While radiographs are not indicative of soft tissue damage, they are essential in identifying degradation of subchondral bone and thus severe OA or PTOA [13]. When used, traditional MRI and CT scans can diagnose changes to the cartilage matric and some damage to the surrounding joint tissues although early cases of OA and PTOA are commonly left undiagnosed using these methods.

MRI's use nonionizing radiation to temporarily align protons in the tissue of interest, and are dependent on magnetic field strength, pulse sequence, tissue thickness as

well as field of view [13]. Many new techniques for MRI imaging have arisen over the past decade, giving clinicians and researchers new methods for identifying cartilage damage early on in OA and PTOA progression. These include identification of and changes to certain ions or other molecules in the tissue i.e., Sodium, Glycosaminoglycans (GAGs) and Proteoglycans (PGs). Furthermore, CT scans identify tissue morphology by bending a beam of x-rays around the joint and detecting the reflection of the beam off the tissue. This information is then analyzed and converted into cross sections or three-dimensional models to identify severe changes to deeper tissues i.e., subchondral bone. To further analyze, anionic, iodine-based contrast agents can be used to label unhealthy cartilage [14]. When the cartilage is compromised, as it is in cases of OA and PTOA, there is uptake within the cartilage that can be detected using CT imaging [15]. GAGs repel these anionic agents, leaving the healthy cartilage free of signal, and regions of degradation or cartilage lesions concentrated with these anionic contrast agents.

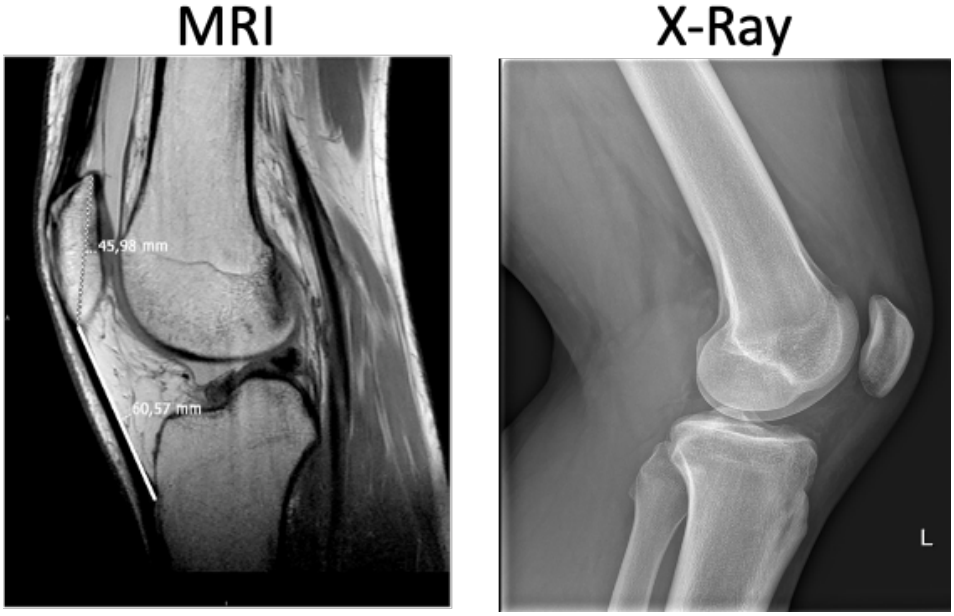

Figure **Error! No text of specified style in document.**.1**:** Examples of Current Diagnostics Available. MRI (left) and X-ray (right) are the main tools available for clinical diagnosis

of soft tissue and bone damage, respectfully. (Images adapted from Silvestri et al 2018 and Burgers et al 2016)

1.2.2 Current PTOA Treatments

While preventatives are extremely limited for chronic PTOA onset, treatment options are nearly as scarce. A majority of patients who suffer from chronic PTOA are limited to pain management strategies. Among these are pharmacological interventions, physical therapy and, in severe cases, replacement arthroplasty [16]. Individuals who suffer from chronic PTOA must live their lives managing pain pharmacologically. General pain relievers known as analgesics, are relatively common for mild to moderate pain management [17, 18]. In short, these over-the-counter drugs are readily available for individuals, although they have no effect on the joint itself. Nonsteroidal anti-inflammatory drugs (NSAIDs) are a more advanced pain reliever that acts as an anti-inflammatory by blocking cyclooxygenases (COX) [19] The COX enzyme is responsible for converting fatty acids in the body to smaller lipids known as prostaglandins. Prostaglandins are responsible for maintaining and mediating the bodies pro-inflammatory response [20]. Corticosteroids, also known as glucocorticoids, work in a similar manner to NSAIDs in that they reduce the inflammatory response by mimicking a natural hormone the body produces known as cortisol. Cortisol is responsible for managing the bodies stress response as well as regulating metabolism, inflammation, and the immune response [21].

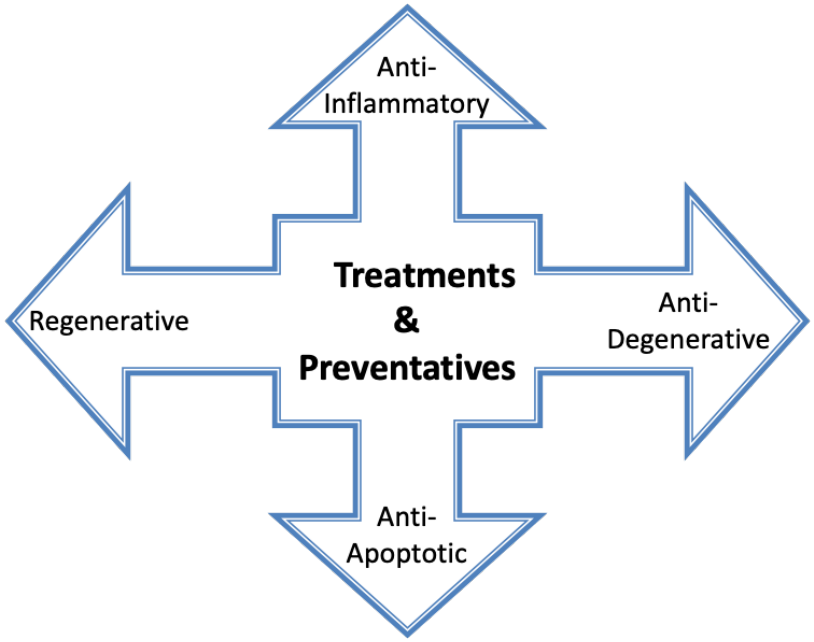

Figure **Error! No text of specified style in document.**.2 Research direction for PTOA Treatments and Preventatives. (Adapted from Khella et al 2022)

In addition to multiple available medicines for pain management, physical therapy (PT) has been essential in patient recovery. PT typically aims to improve the mobility of a patients affected joint to restore its use [22]. Additionally, it is responsible for increasing the strength of the joint and maintaining fitness; both necessary to continue performing daily tasks. Unfortunately, PT and pharmacologic intervention are simplified treatments that target managing the pain associated with joint trauma and do very little to actually heal the tissue. In many cases, patients must undergo a cartilage allograph or full knee replacement [23].

Overall, there is a severe lack of treatments available, and those currently in use are centered around symptom resolution rather than tissue healing. Due to the lack of growth in the articular cartilage, new treatments are needed to address the lack of lubrication, support and resistance that native cartilage supplies, by promoting regeneration of this tissue in the articular joint.

1.3 Synovial Knee Joint Composition

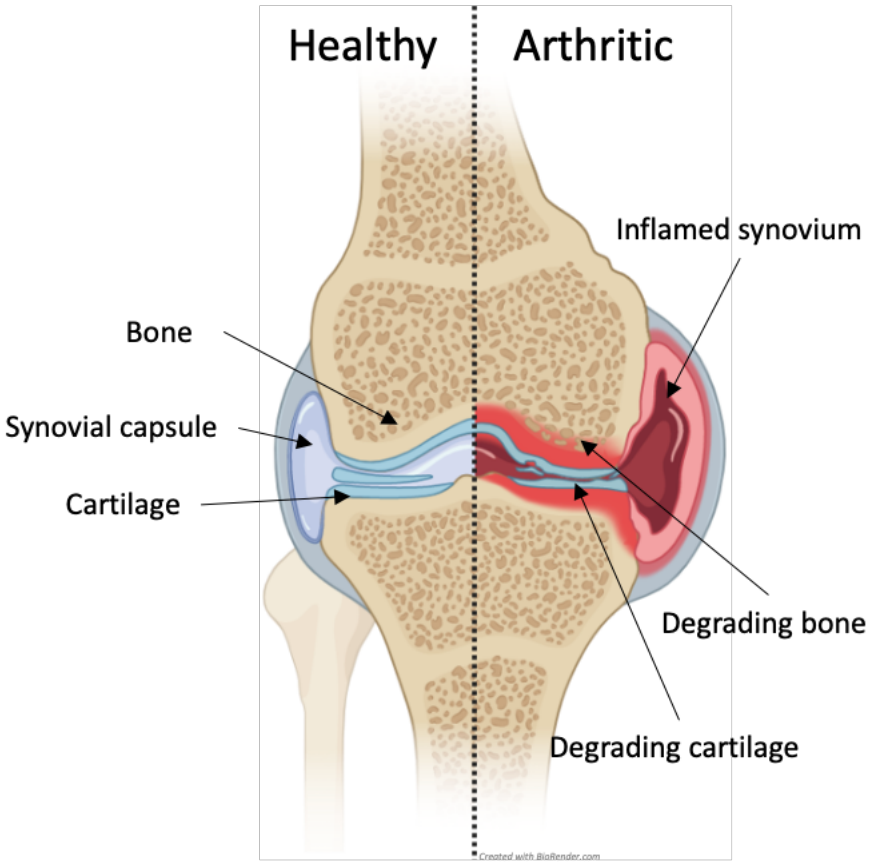

Figure **Error! No text of specified style in document.**.3 Schematic of healthy and degraded, arthritic knee joint

1.3.1 Cartilage

Synovial joints are comprised of several tissues including the articular cartilage [24]. The main function of cartilage is to protect, lubricate and cushion the boney areas that it covers [25]. Cartilage is comprised of mostly water, followed by several complex complex biomolecules, such as GAGs and PGs [26]. In addition, the extracellular matrix (ECM) of this tissue is high in collagen content as well as other sulfated proteoglycans i.e., aggrecan, chondroitin sulphate and hyaluronan [25].

Cartilage can be divided into three categories based on location and function. Fibrocartilage is highly resistant to tension and compression and is primarily found in the supporting ligaments surrounding joints. This cartilage is high in collagen 1 and is contains

lower amounts of proteoglycans than other cartilage types. [27]. Commonly found in the larynx and ear, elastic cartilage is an extremely flexible form of cartilage that is resistant to extreme pressure [28]. Last, hyaline cartilage is the most common cartilage in the body and is characterized by its blue-white color and glassy smooth appearance [29]. Additionally, hyaline cartilage is high in collagen 2 and proteoglycans. It is extremely resistant to compression and is commonly found on bone surfaces within joints [29]. Cartilage is a relatively avascular and aneural tissue [30]. Joint pain commonly associated with injury, like PTOA, is usually the result of inflammation and damage to the surrounding bone and synovium caused by immune infiltration [30]. Due to the avascular nature of the cartilage, chondrocytes rely on diffusion of nutrients through the ECM that is enhanced by regular compressive forces acting on the cartilage [31].

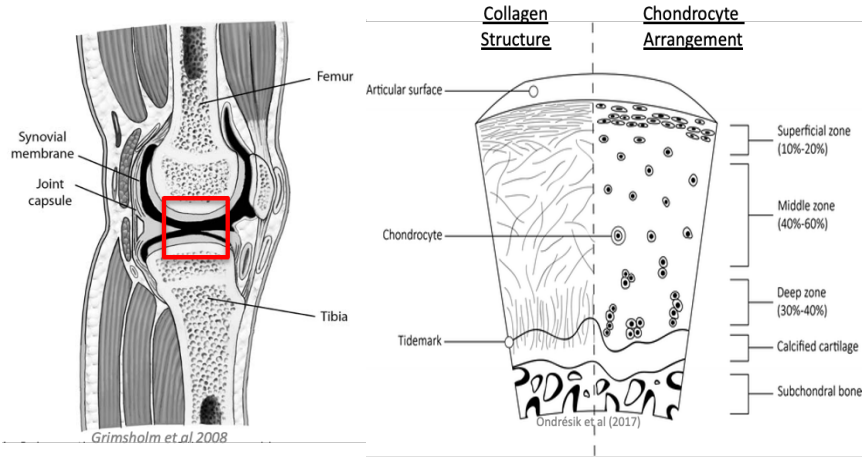

Figure **Error! No text of specified style in document.**.4 Schematic of articular cartilage composition at a cellular and protein level. (Adapted from Ondresik 2017 and Grimsholm 2008)

1.3.2 The Chondrocyte

Within the extracellular matrix are embedded the resident cells of the tissue known as chondrocytes. Chondrocytes reside in small cavities in the ECM known as lacunae and are responsible for secreting many of the proteins essential to maintaining the ECM [24]. Chondrocytes have adapted to survive in a nutrient poor, hypoxic environment, demonstrating the reasoning for their slow metabolic rates. While chondrocytes are normally in a resting steady state, they are still the main producers of ECM proteins [8]. Chondrocytes are not normally proliferative, but once trauma is induced, there is a spike

in their metabolic activity, and some undergo rampant proliferation, inducing a severe transformation to the composition and organization of the ECM [8]. Additionally, chondrocytes will respond to a change in their environment by producing oxygen free radicals and begin their terminal differentiation into hypertrophic chondrocytes [24]. Chondrocytes cause a positive feedback loop during tissue disturbance, by increasing the production of cartilage degrading enzymes such as aggrecanases, matrix metalloproteinases (MMPs), and other proteases responsible for degrading the ECM [8]. As these proteases are released, chondrocytes undergo apoptosis, resulting in cell death and continued loss of cartilage tissue eventually resulting in loss of subchondral bone [8].

1.3.3 Bone

Long bones are made up of two types of bone tissue: Cortical and Trabecular bone. Cortical bone primarily encompasses the long regions of each bone [32]. It is highly compact, tough, vascularized and provides a cavity for the bone marrow. Cortical bone is essential in supporting movement of the body and providing protection of internal organs. [32]. Cancellous bone, also known as trabecular or spongy bone, is a porous tissue found at the end of long bones under the cartilage region [33]. This bone can be thought of as an interconnected web of bone rods and plates essential in providing strength to the bone [34]. Additionally, it aids in dispersing load away from the joint cavity and towards the cortical bone [33]. Under the cartilage is a region of trabecular bone known as the subchondral bone. This bone region is essential in supporting the cartilage and in severe cases of OA is prone to damage and severe degradation caused by mechanical stress [35]. Additionally, this bone region encompasses a network of vessels and nerves that provide mechanical and nutritional support to the cartilage [35].

1.3.4 Synovium and Infrapatellar Fat Pad

The soft supporting region known as the synovium is a capsule like tissue that surrounds the bone and cartilage of synovial joints [36]. The synovium is necessary to provide additional nutrients to the cartilage as well as regulate the lubrication and movement of the joint without damage [37]. Within the joint capsule is the synovial fluid,

which is comprised of several proteins and enzymes essential in maintenance of the joint tissue. These include collagenases, proteinases, lubricin, hyaluronan, and prostaglandins. In addition to these molecules, the synovial tissue and synovial fluid are home to many resident immune cells [38]. Additionally, when the joint is challenged, mechanically or through infection, there is in influx of immune cells into the synovium and synovial fluid that are essential in tissue recovery and healing [38]. In a healthy joint, the synovial lining is comprised of several layers known as the intima and subintima. Over the subintima is a later of highly vascularized connective tissue that is home to synoviocytes and fibroblast [39]. Synoviocytes are metabolically active cells, while fibroblasts are critical for collagen production and secretion [39, 40].

Beneath the synovial lining, in the anterior region of the knee, is the infrapatellar fat pad (IPFP) [41] [42]. This adipose tissue is responsible for reduction of impact and protection from mechanical damage [41] [42]. In addition to resident adipocytes, the IPFP is home to many immune cells including leukocytes, macrophages, and other phagocytotic cells essential in joint maintenance and trauma response [41]. During trauma, there is an influx of immune cells into the IPFP, leading to joint swelling and local necrosis that structurally alters the joints physiology [41]. Additionally, the IPFP and resident immune cells are producers of several adipokines, and cytokines produced after trauma to signal an inflammatory response essential in maintaining joint integrity [43] and remodeling [44].

1.3.5 Immune Cells

The immune system is a robust array of organs, specialized cells, humoral factors, and cytokines, all with multiple functions in the body [45]. This system is essential in maintaining healthy tissue by fighting disease, removing dead tissue, signaling to local cells, and promoting tissue regeneration [45, 46]. The immune system is split into two highly interactive sub-systems known as the adaptive and innate immune systems [45].

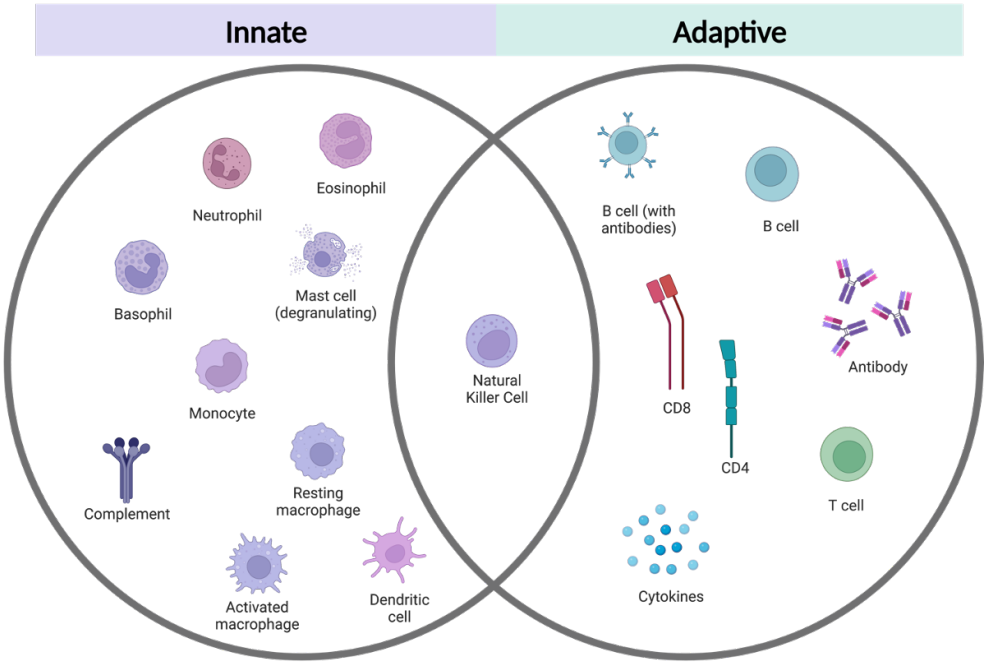

Figure **Error! No text of specified style in document.**.5 Components of the innate and adaptive immune system (Created with Biorender)

The innate immune response is an inherent, non-specific, immediate response and acts as the first line of defense in recognizing foreign antigens in the body [47]. The innate immune system protects the body through physical (i.e., skin, mucus membranes, hair, cilia) and chemical (i.e., lysosomes, saliva, pH) barriers [48]. The innate immune response is comprised of myeloid derived cells that are either phagocytotic or granulocytic in nature. These cells include macrophages, monocytes, mast cells, dendritic cells, as well as neutrophils, basophils and eosinophils and complement proteins [48]. Additionally, some natural killer T cells are also lymphocytic cells that do not have antigen specificity and thus are considered to be part of both innate and adaptive immunity [49]. On the other hand, the adaptive immune response is primarily comprised if lymphoid cells essential in specificity, immunological memory, and self-antigen recognition. Cells of the adaptive immune system include B lymphocytes and T lymphocytes. Within these two cell populations are several subcategories of functionally unique cells including plasma cells, memory B cells, T helper cells, and cytotoxic T cells [49]. These cells are highly specific in their responses to foreign invaders and act as the second line of defense against specific pathogens or damage that occurs to the body [50].

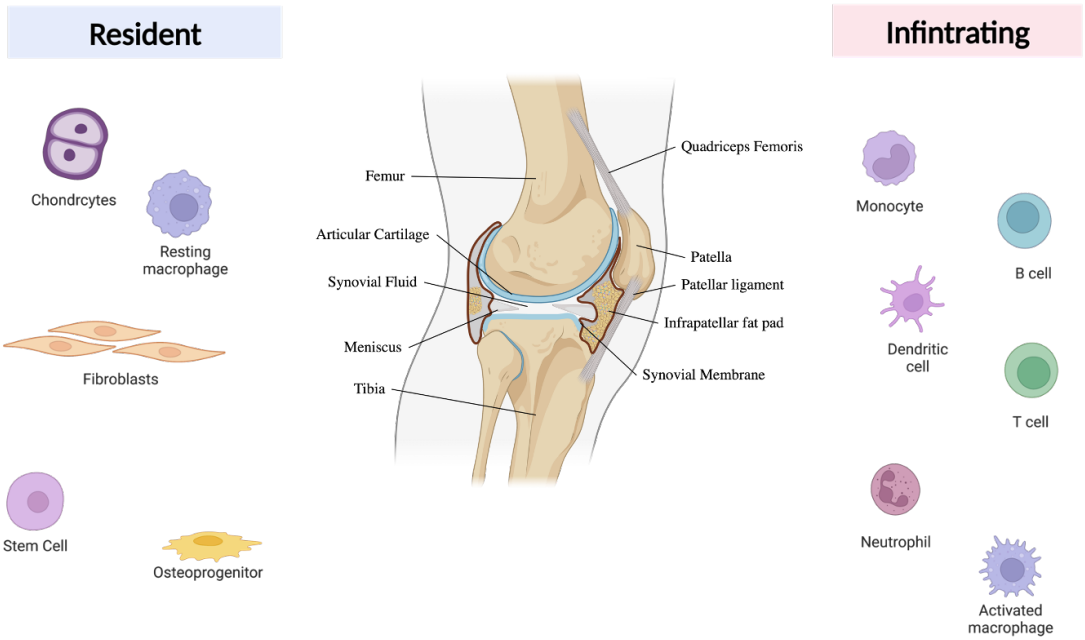

Figure **Error! No text of specified style in document.**.6 Resident and infiltrating immune components in the synovial knee joint (Created with BioRender)

Within the synovial joint, there are resident immune cells native to local tissues that aid in regulating the mechanical stress and signaling between cells. In the context of joint diseases, like OA or PTOA, these resident immune cells mainly include macrophages [51]. During injury, additional macrophages as well as monocytes, neutrophils, mast cells, T and B cells are recruited into the synovial joint [52]. Initially, the joint enters a pro-inflammatory state by recognizing molecules known as damage-associated molecular patterns (DAMPS) via pattern recognition receptors (PRRS) on the surface of resident cells [53, 54]. Secondly, inflammatory signaling pathways are activated by cellular cytokine or chemokine production, (i.e., interleukins (IL), colony stimulating factors (CSF), interferons (IFN), tumor necrosis factors (TNF), tumor growth factors (TGF)). Finally, specialized immune cells called lymphocytes are recruited to the site of trauma [55]. From this state, the damaged tissue is mediated by additional cell signaling molecule to extend the proinflammatory state or begin tissue remodeling. In arthritic synovial joints, neutrophils have been shown mediate the inflammatory response by recruitment of NK cells [51, 56] . Additionally, neutrophils have also been shown to assist in the migration of monocytes and dendritic cells into the tissue through cytokine signaling [57].

Additionally, monocytes and steady state macrophages have a similar function to neutrophils in initiating inflammation but are also vital in resolving it via anti-inflammatory signaling. When prompted infiltrating monocytes can differentiate into macrophages which are functionally distinct from tissue resident macrophages in the synovium [58]. These monocyte-derived macrophages are activated by the inflammatory environment and depending on the array of cytokines being produced, will transform into either a classically activated, proinflammatory, M1 macrophage or an alternatively activated, anti-inflammatory, M2 macrophage [59]. While these stages are traditionally thought of as two distinct populations, current research has shown that this polarization is represented by more of a spectrum of activation states [60]. Current research shows that alternatively activated M2 macrophages may be essential in joint maintenance after trauma [60, 61].

1.4 Disease Pathogenesis

1.4.1 Phases of PTOA

The progression of PTOA can be split into several phases of physiologic changes that occur to the tissue [62]. **Figure 1. 1** showcases the onset of PTOA after traumatic injury. Initially, the joint responds in injury by entering the immediate phase [63]. In this phase, cellular necrosis begins in multiple cell types as a response to injury. Additionally, the ECM of the articular cartilage begins to lose its integrity through collagen rupture, cartilage swelling, and loss of proteoglycans [63]. Last, hemarthrosis, or “joint bleeding” begins to occur when vessels rupture in the joint space, mixing with debris from damage tissue and cells, which leads to swelling of the joint [64].

The second phase of PTOA is known as the acute phase. This phase is characterized by the infiltration of immune cells into the joint space, severe ECM degradation, decreases in joint lubrication including the synovial fluid, and an increases in chondrocyte apoptosis [64]. After the initial immune response has subsided, the knee joint enters into an asymptomatic phase in which tissue damage can progress without surgical intervention [64]. It is at this stage that most individuals will opt into reconstructive surgery and begin surgical recovery. For those individuals that do not elect

surgery, joints will either progress to painful, chronic PTOA or spontaneously resolve the disease, leaving individuals to live a healthy pain free life [65]. The mechanism of this dichotomy is still unknown, leaving patients who suffer from knee trauma and progress to chronic PTOA without treatments or preventatives.

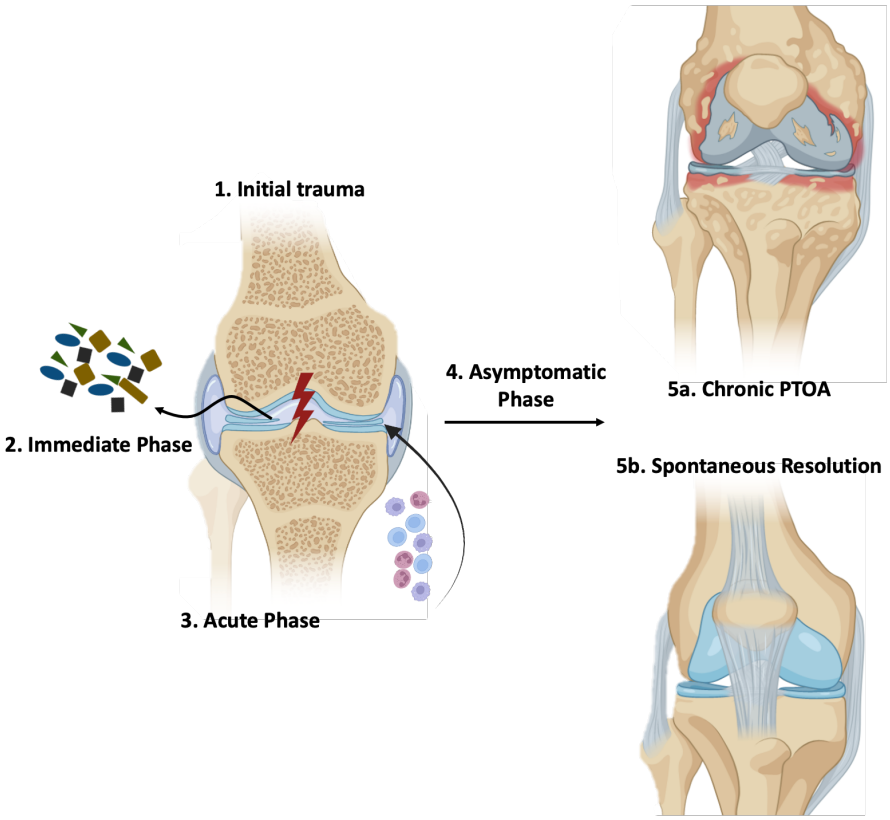

Figure 1. 1 Phases of Post Traumatic Osteoarthritic Progression. Disease progression includes the four phases followed by chronic PTOA onset or spontaneous resolution of the disease. (Created with Biorender)

1.5 Methods of studying PTOA

1.5.1 *In vitro* vs. *in vivo* research

For the past few decades, PTOA research has focused on understanding PTOA progression in later stages when it can be physically diagnosed, and damage has already occurred. While understanding chronic PTOA is essential in determining which tissues and cells are affected by this disease, novel research of early mechanisms directly after injury

is essential in prevention of chronic PTOA. Researchers have since turned to identifying immediate cellular response to trauma.

In the past, *in vitro* cell culture methodologies using fibroblast cell lines differentiated into "chondrocyte-like" cells have been used to determine the direct affects that cytokines, proteases, growth factors and other signaling molecules have directly on chondrocytes. While these studies have laid a foundation for understanding chondrocyte response, current research has shown that chondrocytes are highly reliant on their microenvironment within the joint and without it are prone to de-differentiation into fibroblasts. Thus, crosstalk between cell types is essential in maintaining a healthy joint, and includes not only chondrocytes, but resident cells in the bone, synovium, fat, and immune system.

To combat the lack of support provided by monolayer culture, new *in vitro* culturing techniques have arisen that include pellet culture [66], 3-dimensional spheroid culture [67], co-culture [68] and supplemented media [69]. Additionally, more studies have moved to *in vivo* models to fully recapitulate healthy and diseased joint environments. Multiple techniques have been used to mimic common injuries in humans that consistently lead to chronic PTOA, the most common being damage to the ACL and MM [70]. By employing surgical methods, researchers have been able to study the environment and cellular responses of a destabilized joint and track the progression of PTOA until chronic onset has occurred [71]. While mouse models of PTOA may not completely recapitulate human disease, it allows researchers to identify early changes to the joint that occurs after trauma; a feat otherwise impossible when analyzing arthritic cartilage from joints replacement surgeries [72] .

1.6 MRL/MpJ "Super-healer" Mice

To better identify the cellular mechanisms associated with the onset of PTOA, researchers have used mouse models to replicate injury and disease progression. One such, is the MRL/MpJ (MRL) mouse strain. This strain was initially selected for its larger than average size [73]. In the past few decades, the MRL mouse has been shown to have

regenerative capabilities in several tissues including cornea, skin, nervous system, muscle, and of interest, reparation of ear punch wounds and full thickness cartilage lesions [74-77] [78]. The healing capabilities of these mice has given them the colloquial name of "super-healers." As previously shown, MRL have an exquisite capability to regenerate tissue as opposed to healing through the production of disorganized collagen that forms scar tissue [79]. This regeneration is defined as the ability to form a blastema, breakdown the basement membrane and reestablish tissue with normal architecture and function [79].

Regeneration is common in tissues like the liver [80] and skeletal muscle [81] but is extremely rare in avascular tissues such as the cartilage. In addition, MRL possess the capability to pass this trait on to their offspring [79]. Previous evaluation of MRL ear cartilage demonstrates that these animals have normal chondrogenesis and angiogenesis after injury, indicating that this regenerated cartilage is functionally the same as uninjured tissue [82]. In addition, the articular cartilage of these mice also possesses the capability to regenerate after full thickness lesions are induced [74]. Fitzgerald et al evaluated proteoglycan, collagen 2, and collagen 6 levels in uninjured and regenerated cartilage, showing that MRL possess the capability to not only deposit cartilage with normal ECM and proteoglycan levels but also retain collagen concentrations [74]. While their mechanism of regeneration is still poorly understood, new research suggests that MRL mice may have enhanced healing capabilities in the cartilage [62, 73], in addition to a complex immune system that may aid in their regenerative mechanisms [83]. By using the MRL strain to study disease prevention, researcher will be able to identify cellular and molecular targets for potential preventative measures and pharmacological interventions to combat the progression of PTOA in humans.

1.7 Significance & statement of work

The global burden, prevalence, and financial liability associated with PTOA emphasizes the need to understand disease progression at a cellular level. Mechanistically, PTOA is poorly understood, and thus the development of new treatments is lacking. By increasing our knowledge of not only the normal function of cells in a healthy joint but also those early on in PTOA progression, researchers can further elucidate the mechanism

of tissue degradation and immune response in hopes of developing future treatments. Additionally, identification of potential cartilage regenerative mechanisms is essential in the prevention of cartilage deterioration in both OA and PTOA. Current research in PTOA has been limited to mouse models and validations *in vitro* which limit the environmental impact of the joints as a tissue. With the advent of next generation sequencing technologies, non-invasive PTOA induction models and advancement of computational tools, the molecular mechanisms associated with PTOA will no longer perplex researchers and clinicians. The shift in identifying the joint as a whole tissue as opposed to individual pieces has moved the fields progress in finding clinical treatments and preventatives forward exponentially.

Despite this progress, there are still technical challenges that limit using these new technological capabilities. This research identifies a technical gap in the field and employs new sequencing technologies to further elucidate the cellular composition of murine articular cartilage. Chapter 2 describes a novel method for genetically targeting chondrocytes using a modified reporter protein for isolation of primary cells. By using a transgenic mouse line that fluorescently tags collagen 2 expressing cells, this study was able to enrich for primary chondrocytes from the articular cartilage of the knee joint using Fluorescently Activated Cell Sorting (FACS). Chapter 3 expands on the changes to articular chondrocytes that are induced by trauma by analyzing an assortment of joint cells. This study used the novel method established in Chapter 2 to isolate murine articular chondrocytes from different strains of mice with varying susceptibilities to PTOA as well as joint supporting stromal populations. These cells were then analyzed using single cell RNA sequencing and transcriptionally unique subpopulations of chondrocytes were identified in healthy joints as well as over the course of PTOA progression.

Osteoimmunology is a vast field that primarily focuses on the bone marrow microenvironment and establishment of the bone's relationship with the immune system. While studies have identified that there is a large flux of immune cells into the synovial joint, it has only been in the last decade that researchers have begun to reveal the function of the immune system during PTOA progression. Chapter 4 utilizes single cell RNA

sequencing paired with an optimized synovial joint digest from murine knee joints to identify the foundational populations of immune cells within the joint. In addition, this study identifies trends in multiple immune populations as they respond to injury in the same mouse strains used in Chapter 3. The knowledge gained in these studies has changed the foundation of what is currently known about the cellular composition of the synovial joint. Not only have new subpopulations been identified in both immune and chondrocyte populations, but their direct response to injury gives future research a foundation for new pharmacological developments and potential early biomarkers of PTOA onset.

Chapter 2. Isolation of Murine Articular Chondrocytes for Single-Cell RNA or Bulk RNA Sequencing Analysis

Abstract

The interactions of cells within the joint microenvironment are relatively unknown in [84] studying joint diseases such as PTOA. To date, cartilage and bone have been extremely difficult to study at the cellular level due to their densely packed matrices and sparce cellular nature; requiring most transcriptomic research to date being conducted using RNA from whole bone tissues or through *in vitro* studies. With the increased interest in studying the cellular components of tissues like bone and cartilage, there has been a push to improve next generation sequencing technologies from generic bulk RNA sequencing to help identify specific transcriptional changes to individual cells within the tissue. Single-cell RNA Sequencing (scRNAseq) is a novel technology that is highly sensitive to transcriptional changes within cell populations of a tissue and has allowed the field to gain information on cellular interactions and subpopulations in numerous tissues, including articulated joints. Because scRNAseq can elucidate the cellular composition of a tissue of interest, it increases opportunities for bone and cartilage researchers to understand which cells are embedded in these tissues and how those cells interact and respond to trauma or other stimuli. Currently, protocols for isolating viable, intact cells from soft tissues are well established, while bone and cartilage have been limited to *in vitro* studies or embryonic chondrocytes. Due to the dense, fibrous extracellular matrix, obtaining a single cell suspension of adult murine chondrocytes for scRNAseq is extremely difficult. This chapter highlights a successful protocol using a collagen specific transgenic reporter mouse to successfully isolate articular chondrocytes from murine knee joints. The subsequent chapters demonstrate that chondrocytes and other joint interacting cells can be enriched through flow cytometry and analyzed via single-cell RNA sequencing using this optimized enzymatic cartilage digest from murine long bones.

Introduction

Osteoarthritis [2] is degenerative joint disease characterized by degradation of bone, cartilage, and connective tissue within an articulated joint [1]. OA and other inflammatory diseases related to orthopedic trauma and joint degeneration are the leading causes of disability worldwide [1]. This painful disease is highly studied at late disease stages, although the cellular response to disease early in progression is poorly understood due to the complexity of joint tissues such as cartilage and bone.

Individuals diagnosed with OA must rely on pain management strategies to combat symptoms of this disease caused by the mechanical degradation of the articulated joint. This is usually caused by significant physical and molecular changes that occur to the articular cartilage, synovial capsule, tendons, ligaments, skeletal muscles and bone [85, 86]. Over the past 30 years, scientists have emphasized the need for better "omics" technologies for analyzing biological systems at the cellular and molecular level. By better understanding the genomic, transcriptomic, proteomic, and metabolomic data essential in studying health and disease, researchers and clinicians can develop better targets for treating pain, decreasing tissue damage, and preventing disease onset. New sequencing technologies are important in understanding the protein interactions, gene expressions, and epigenetics of cells in response to stressors on the body. Additionally new sequencing tools have become crucial in finding causal relationships between cellular identity, function and phenotype of disease progression previously not discovered [87].

The need for new "omic" technologies began in large part with the start of the Human Genome Project in the late 1980s supported by the National Institute of Health where scientists aimed to create a complete map of the human genome. In determining the exact sequence using early genomic tools, the Human Genome Project laid the foundation for many technologies we use today, including advanced sequencing techniques. More recently, the Human Cell Atlas project was established in 2016 to help transform our current understanding of the human body in health and disease. This project has helped increase progress of new "omics" technologies with its goal of understanding cellular sub-types, locations, states, development, and processes. By combining clinical, translational,

and computational data, the Human Cell Atlas has created a catalog of the nearly 40 trillion cells in the human body. This “cellular reference map” permits researchers and clinicians to analyze molecular mechanisms and cellular interactions and to study the biological changes that are associated with different diseases [88, 89]. This project provides a vast collection of information essential for identifying markers of cellular resistance, tissue degradation, and disease prevention. [88, 89].

Musculoskeletal diseases benefit greatly from these advances in “omics” technologies due to their high burden and lack of treatments. Single-cell RNA sequencing (scRNAseq) is a relatively new transcriptomic analysis tool that has changed the perception of studying soft tissue diseases, e.g. ailments of the lung, liver or brain, as well as many types of cancer [88, 90, 91]. Soft tissues require a much simpler approach to perform single-cell sequencing, with cell dissociation from bulk tissue being much more straightforward than highly fibrous or calcified tissues such as bone and cartilage. Although human tissue research using scRNAseq has been extremely valuable for identifying cellular changes in diseased tissues *ex vivo* [92], obtaining viable tissues from individuals to define a healthy baseline is extremely difficult. Alternatively, researchers have used animal models to study disease progression that may mimic human pathology. Although animal models may not replicate the exact disease state and cellular response of humans, they help scientists create a database of cellular networks and disease responses to identify targets of drug development and prevention.

Musculoskeletal diseases such as OA and Post-Traumatic OA are extremely difficult to study in humans due to the lack of healthy bone and cartilage samples available. In addition, there is an increased need to optimize these sequencing technologies for dense and fibrous tissues with low cellularity. This chapter provides a novel technique for isolating viable chondrocytes from murine articulated joints and long bones. This research is essential for enriching primary cells from cartilage to perform an in-depth analysis using scRNAseq through a series of enzymatic digestions, flow cytometric analysis, and Florescence Activated Cell Sorting (FACS).

Materials and Methods

Murine Animal Models

Transgenic Ai9;Col2a1-CreER^{T2} (Ai9Col2) were generated in house as previously described [93, 94]. In short, homozygous Ai9 reporter mice (Jackson Laboratory, Bar Harbor, ME, USA; Stock No: 007905) were purchased from Jackson Laboratory and bred with Col2a1-CreER^{T2} to generate offspring with specific expression of the Ai9 reporter in collagen 2 expressing cells. Pups were injected with tamoxifen for five days at 2-weeks of age, as previously described [95], to induce robust cre expression in the articular cartilage and growth plate of the hindimbs. MRL (MRL/MpJ, Stock # 000486), and B6 (C57Bl6/J, Stock # 000664) animals were purchased from Jackson Laboratory and bred in house using standard procedures. Mice were allowed free range of the cage while on 12h light/dark prior to euthanasia. All experiments were conducted using male animals and all experimental procedures were completed in accordance with the Institutional Animal Care and Use Committee (IACUC) guidance at Lawrence Livermore National Laboratory in AAALAC-accredited facilities.

Murine hindlimb dissection and joint cleanup

Male Ai9Col2 mice were euthanized humanely under CO2 at 1.72 L/min followed by cardiac puncture to collect serum for potential future analysis. Skin was removed manually by snipping the ventral side of the animal and pulled to expose the hindlimbs. The hindlimbs were cleared of excess muscle by cutting the Achilles tendon for removal of gastrocnemius and trimming the medial hamstring muscle until the hip joint was reached. The quadriceps femoris muscle was removed by creating a single incision above the patella and peeling the muscle back towards the hip joint. Dislocation of the hip joint was accomplished by applying an upward force to the hip to completely remove the femur from the ischium. The entire hindlimb was removed after cutting away the remaining muscles. Excess muscle and fat were removed from the femur and tibia by trimming with scissors.

Articular Cartilage Isoaltion from Murine Long Bones

Murine knee joints were separated at the joint cavity by carefully sawing through the patellar tendon, ACL, and fibular collateral ligament to separate the femur and tibia. Epiphyses were cleaned of remaining muscle using a Kimwipe. Ligaments and tendons were trimmed using scissors to expose the articular cartilage of the knee joint. Cleaned long bones were micro-dissected using a scalpel in which ~1mm of tissue was removed from the articular surface, freeing the articular cartilage from the subchondral bone.

Chondrocyte Dissociation from Articular Cartilage Tissue

The articular cartilage was minced using dissecting scissors and placed into 15mL conical tube for enzymatic digestion using 5ml of enzymatic cocktail comprised of 2% Collagenase 2 (17101015, GIBCO, Thermo Fisher, Waltham, MA) in FBS free Dulbecco's Minimal Essential Media. Cartilage tissue was digested at 37^{o}C for four, 30-minute intervals while shaking. After each interval, digestion media was filtered through a 70um cell strainer into a 50mL conical tube, topped with 5mL DMEM+10% FBS and kept on ice for the remainder of the digestions. Fresh digestion media was added to the 15mL conical tube containing the partially digested tissue for another round of digestion.

Digested Sample Cleanup

Following four rounds of digestion, the digested cell solution was centrifuged at 4oC for 10 minutes at 800 g to pellet cells and any remaining debris. Supernatant was removed and contaminating red blood cells were lysed using Ammonium-Chloride-Potassium (ACK) Red Blood Cell Lysis Buffer (A1049201, Thermo Fisher, Waltham, MA) for 10 minutes on ice. 1x PBS was added to each sample to bring the total volume to ~1.5 ml, then filtered through a 70um cell strained, and transferred to a 2mL Eppendorf tube. Filtered cells were pelleted by centrifuging at 600 g for 6 minutes at room temperature and supernatant was removed via pipette.

Antibody staining of primary chondrocytes for scRNAseq prep

Digested cells were blocked using BD Fc Block (Cat. No. 553142, BD Bioscienced, San Jose, CA) for 15 minutes on ice and then stained using 100ul of an antibody cocktail

diluted in 1X PBS + 10% FBS specific for contaminating immune and erythroid cells including: CD45 APC-Cy7 (1:100, 103116, BioLegend, San Diego, CA, USA), Ter119 APC (1:10, 130-102-290, Miltenyi Biotec, Bergisch Gladbach, Germany), and DAPI (Thermo Fisher Scientific, Waltham, MA, USA). Cells were incubated for 15 minutes on ice in the dark. Following incubation, cells were diluted with 1ml PBS, centrifuged to pellet at 600g for 6 mintues, resuspended in 250ul of 1x PBS + 1% FBS, and transferred to flow cytometry tubes for analysis and sorting. Prior to FACS, the total viable cells count was completed using trypan blue dead cell stain and the Thermofisher Countess™ II (Thermo Fisher, Waltham, MA). Samples were loaded into a BD FACSMelody Instrument for analysis and sorting of the Ai9-positive population and CD45/Ter119 double negative cells.

Collagen 2 staining for flow cytomatric anlaysis of primary chondrocytes

After sorting, Ai9+ chondrocytes were split based on condition (fixed or unfixed). The "fixed" condition cells were incubated with BD Cytofix/Cytoperm Fixation/Permeabilization Solution Kit (Cat. No. 554714, BD Biosciences, San Jose CA) according to manufacturer's instructions. Briefly, cells were blocked using BD Fc Block (Cat. No. 553142, BD Biosciences, San Jose, CA) for 15 minutes on ice followed by a fixation/permeibilization step for 20 minutes at 4^{o}C in BD Fixation/Permeabilization solution. Cells were then washed with BD Perm/Wash Buffer and stained with 100ul of a 1:100 solution of mouse anti-Collagen 2 antibody (MA5-12789, Thermo Fisher, Waltham, MA) for 1hr at RT. Cells were centrifuged, washed, then stained in the dark for 30 min at room temperature with 100 ul of secondary antibody solution using a 1:1000 dilution of Goat anti-Mouse IgG2a Cross-Adsorbed Secondary Antibody, Alexa Fluor 488 (A21131, Thermo Fisher, Waltham, MA). Following incubation, cells were washed and resuspended in 1x PBS + 1% FBS, then transferred to flow cytometry tubes for analysis using the BD FACSMelody Flow Cytometer for analysis of collagen 2 positive staining.

Cell Culture and Imaging

Sorted CD45 negative, Ter119 negative cells were plated in a 6-well tissue culture plate containing in DMEM + 10% FBS and supplemented with 1 x penicillin/streptomycin.

Cells were culture for 5 days and allowed to adhere to the plate before imaging on a Leica inverted microscope controlled using Metamorph imaging software (Molecular Devices, Sunnyvale, CA) using a Texas Red filter (ex/em = 586/603 nm). Images were pseudo colored and merged using ImageJ V1.53 Software [96].

Joint Processing for Cryosectioning

Hindlimbs were collected from 10-week-old Ai9Col2 male mice and cleaned of extraneous muscle while keeping the joint cavity intact. Joints were fixed in 10mL of 10% Neutral Buffer Formalin (NBF) for 24 hours at room temperature while shaking. Joints were washed three times for >1hr each with 1x PBS, cryoprotected by incubating with 30% Sucrose overnight at 4ºC, placed in a cryomold, then coated in TissueTEK Optimal Cutting Temperature (OCT) Compound. Coated samples were snap frozen in liquid nitrogen and stored in an airtight container at -80ºC until sectioned. Selected samples were sectioned at 10um using the Leica CM1860 Cryostat (Leica Biosystems,Wetzlar, Germany), placed on charged slides and mounted with Prolong Gold + DAPI (P36935, Thermo Fisher, Waltham, MA). Samples were imaged using a Leica DM5000 microscope, ImagePro Plus V7.0 Software, and QIClick CCD camera (QImaging, Surrey, BC, Canada). ImageJ V1.53 Software was used for imaging and photo editing [96].

Results

Reporter expression is restricted to articular cartilage of murine hindlimbs

Ai9Col2 mice were subjected to histological assessment through an optimized cryosectioning protocol of knee joints. A nuclear counterstain was applied to sections to identify the individual nuclei of cells in addition to the cellular expression of Collagen 2 (

Figure 2. 1). Expression of the tdtomato reporter protein in Ai9Col2 murine hindlimbs was present exclusively in the articular cartilage (

Figure 2. 1a,b) and growth plate (

Figure 2. 1d, e) as previously described by Nagao et al [97].

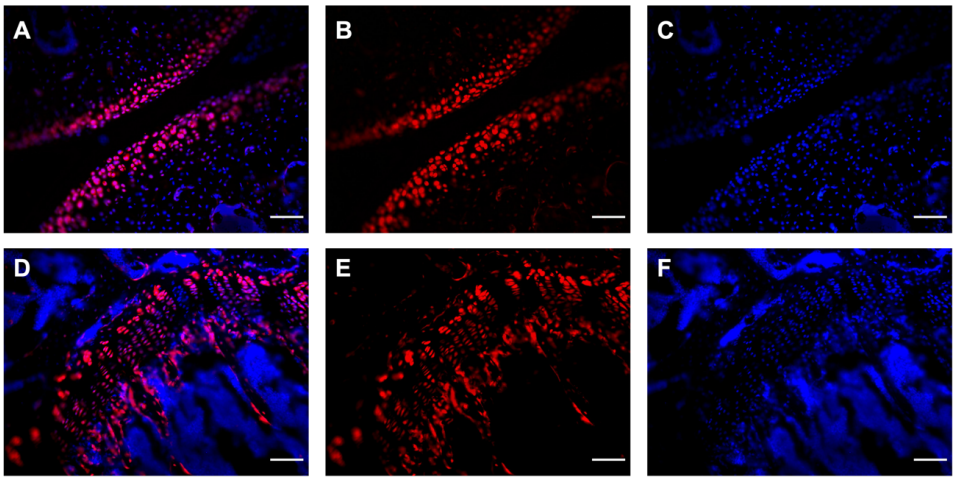

Figure 2. 1 tdTomato expression in transgenic reporter Ai9Col2a1-CreERT2 mouse hindlimbs Fluorescent imaging of murine hindlimb joints identifying tdTomoto expression in articular (top) and growth plate (bottom) chondrocytes. Merged (A,D) tdTomato/594nm only (B,E) and DAPI stained (C,F). Scale bars: 100um.

Fluorescence of the tdtomato reporter in Ai9Col2 corresponded to protein expression of Collagen 2, a well-known transcriptional marker of chondrocytes, by use of immunohistochemistry (IHC). Collagen 2 is also a highly important component of the extracellular matrix excreted by chondrocytes that makes up the articular cartilage. Analysis of joints by IHC showed Collagen 2 expression in the articular cartilage of hindlimb knee joints (

Figure 2. 1a-c, Figure 2. 2), and growth plate chondrocytes (

Figure 2. 1d-f).

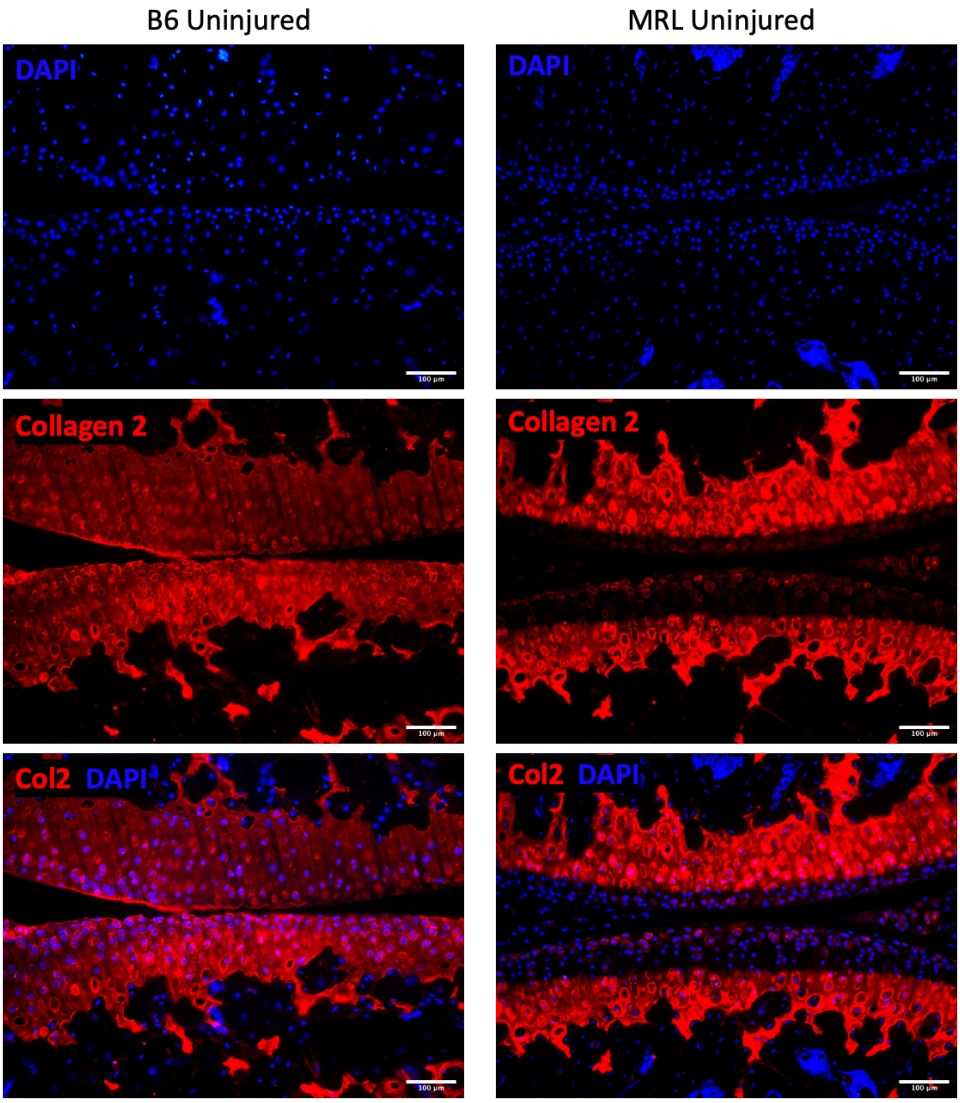

Figure 2. 2: Collagen expression in murine synovial joint. Immunohistochemical analysis of Collagen 2 expression in the articular cartialge of knee joints from MRL/MpJ and C57Bl6J mice. Scalebar 100um. Magnification 20x. Collagen 2 expression in red (594nm) and nuclei are stained using DAPI (405nm).

Collagen 2 can be targeted for enrichment of murine chondrocytes ex vivo

Preparation and enzymatic digestion of micro-dissected articular cartilage from Ai9Col2 mice was essential in dissociating chondrocytes from the extracellular matrix of the tissue and processing for flow cytometry. This optimized protocol, produced fluorescently labeled, viable chondrocytes for further analysis (Figure 2. 3).

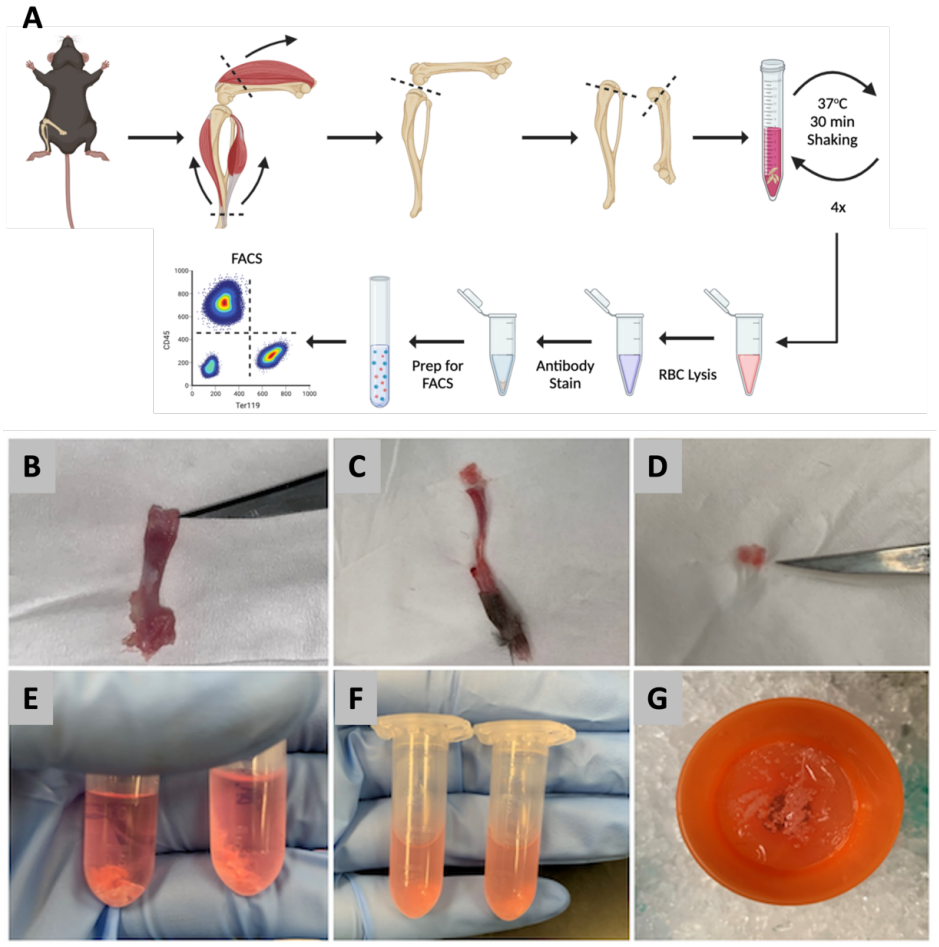

Figure 2. 3 Optimized microdissection and isolation of articular chondrocytes. Schematic for cartilage microdissection technique and digestion steps to attain single cell suspension (A) Region of microdissection shown on femurs (B) Articular cartilage dissection from tip of femur and cartilage (C, D) Minced cartilage prior to enzymatic digest (E). Cartilage after one round of digestion (F) Remaining tissue after final enzymatic digest (G).

Microdissection of both tibia and femur removed the soft cartilage capsule at the end of each long bone, resulting in little residual bone and marrow contamination being detected (Figure 2. 3B-D). When tissues were subjected to enzymatic digest, digestion media was left cloudy indicating cellular dissociation from the cartilage tissue (Figure 2. 3E,F). Final visual inspection of the digested tissue resulted in small, hard fragments of tissue remaining indicating some subchondral bone was removed during microdissection, and contamination by osteoblasts, osteoclasts, and fibroblasts was possible.

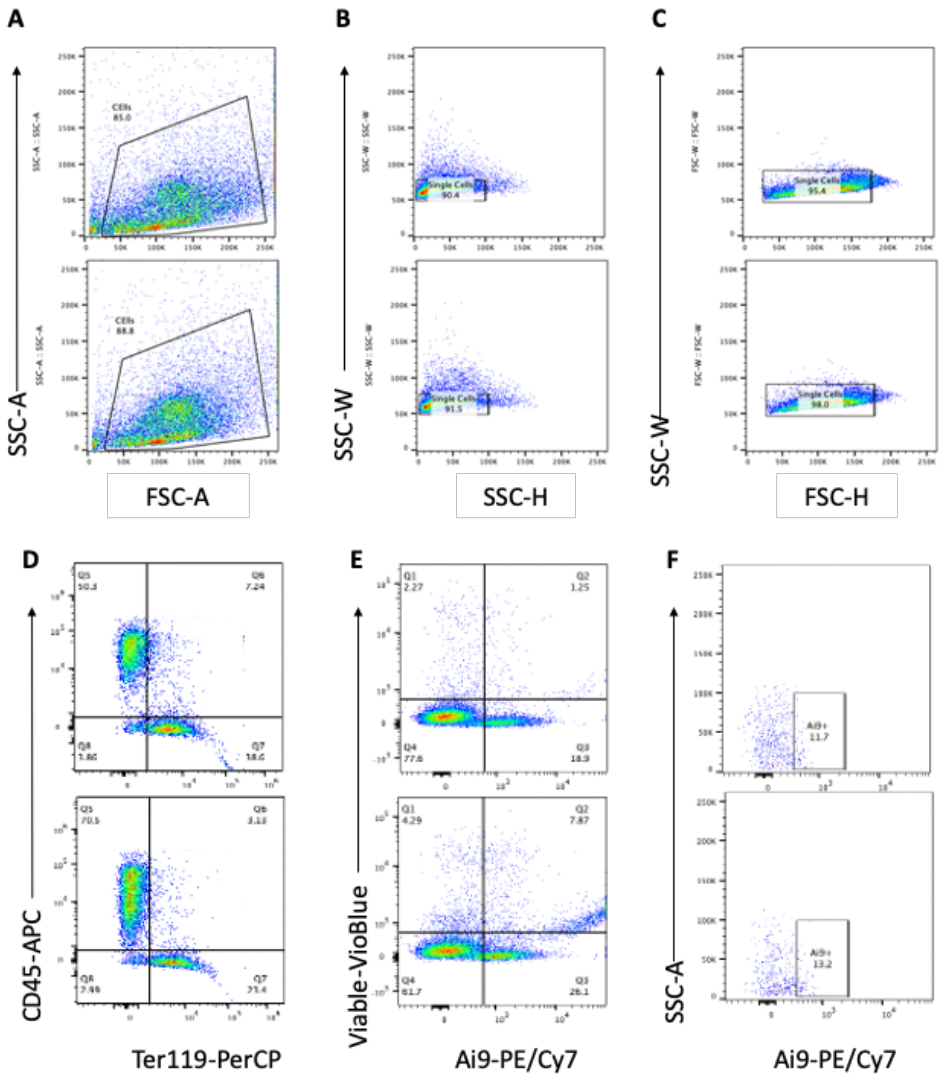

Figure 2. 4. Flow cytometric analysis of Ai9;Col2CreERT2 digested cells. Gating Strategy for all cells (A), and doublets using side scatter (SSC) (B) and forward scatter (FSC) (C) Cells stained with CD45-APC and Ter119-PerCP for identification of immune and erythroid cells, respectively (D) Identification of Ai9+ cells and Ai9- cells in total digested sample gated off FSC (E) Double negative (CD45-Ter119-) cells from Panel D reanalyzed as proportion of CD45-Ter119-Ai9+ cells (indicating chondrocytes) and CD45-Ter119-Ai9- (indicating non-chondrogenic cells) (F).

Ai9 reporter aids in enrichment of chondrocytes via flow cytometry

After dissociation to a single cell suspension, cells were stained for immune and erythroid cell markers to identify contaminating bone marrow and blood cells in samples. Analyzed samples had roughly 50-70% of digested cells that were CD45+ immune cells, while between 25-35% of digested cells were Ter119+ erythroid cells. On average, about 5% of cells were double positive for CD45 and Ter119 (Figure 2. 4A). Roughly 20% of all

cells analyzed were Ai9+, regardless of their expression of CD45 or Ter119 (Figure 2. 4B). Cells from the double negative population (CD45-Ter119-) of Figure 2. 4A were analyzed for positive Ai9 expression. Just over 10% of CD45-Ter119- cells were Ai9+, while most cells were CD45-Ter119-Ai9- (Figure 2. 4C). CD45-Ter119-Ai9+ cells were sorted and plated for imaging after 5 days without differentiation media. Fluorescent imaging using a Texas red filter showed a large proportion of Ai9+ cells in culture that had adhered to the plate indicating a chondrocyte like cellular phenotype (Figure 2. 5). These cells had a round to oblong morphology, characteristic of cultured murine chondrocytes [98]. In addition, not all adherent cells expressed Ai9, as shown in the brightfield image (Figure 2. 5, left).

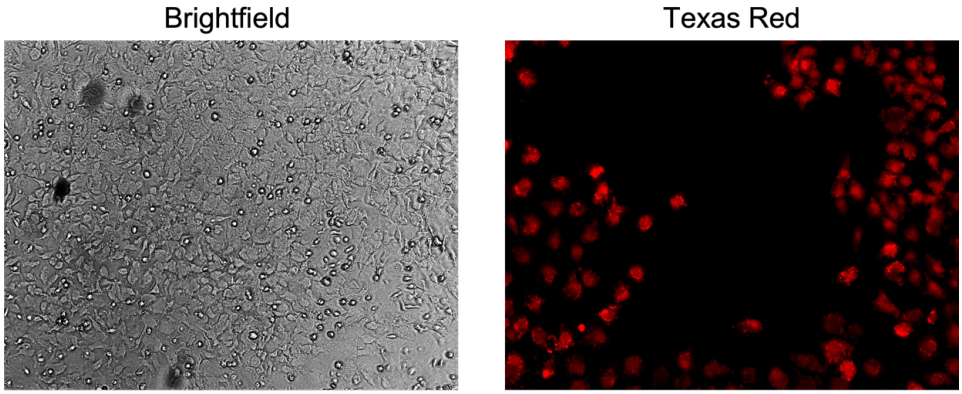

Figure 2. 5. Fluorescent imaging of sorted CD45-Ter119-Ai9+ cells. Ai9+ cells from digested cartilage of Ai9;Col2a1-CreER^{T2} mice were plated in DMEM/F12 + 10% FBS. Cells were grown for 5 days at 37ºC + 5% CO2. Brightfield image of plated cells showing confluent population (Left). Florescent imaging showing RFP expression of the tdtomato reporter in collagen 2 expressing cells (right).

Discussion

Previous bone and cartilage research has been dependent on the isolation of RNA from whole bone or joint samples for bulk RNA sequencing [99]. With the advent of new sequencing platforms in the last decade, like scRNAseq, optimized tissue preparation techniques must be established to further study cellular heterogeneity in healthy and diseased tissues using these new tools. The generation of new protocols for bone and cartilage research will aid in furth[84]er exploration of OA, RA, and other bone diseases by using single-cell RNA sequencing to study adult murine long bones and synovial joints.

Resident cells of the cartilage, known as chondrocytes, secrete many molecules responsible for lubrication and impact management of the joint, such as proteoglycans (PGs), glycosaminoglycans (GAGs) and collagens [100]. The most relevant and well-studied of these molecules is Collagen 2 [101-103]. ECM proteins, specifically collagens, are essential in maximizing tensile strength and managing compressive forces [102]. Immunohistochemical analysis of murine cartilage in B6 and MRL strains showed that this protein is expressed mainly in the matrix surrounding chondrocytes (Figure 2. 2, red stain). Additionally, Collagen 2 expression is restricted to the cartilage tissue and growth plate regions of the tibia and femur as expected [104]. An in-depth analysis (Figure 2. 2) shows that mice strains differ in their robust expression of Collagen 2 in the articular cartilage and express alternative matrix associated molecules, like Aggrecan. The response to injury and role of matrix composition of MRL and B6 are phenomena discussed later in Chapter 3.

Identification and isolation of chondrocytes from normal murine cartilage tissue is extremely difficult due to the fibrous complexity of the tissue, but also the lack of cell surface markers on individual chondrocytes. Chondrocytes are transcriptionally classified based on their expression of excreted collagens, PGs, GAGs and nuclear proteins (e.g. Sox9), [105, 106] unlike cells with abundant membrane protein targets on their surface, e.g., immune cells. The lack of surface antigens makes targeting viable cells for isolation from bulk joint tissue difficult using common techniques, such as magnetic separations or FACS. Instead chondrocytes require membrane permeabilization for intracellular antigens and current diagnostic tools are incapable of targeting secreted protein products. Consequently, this study focused on the development of a new isolation for murine articular chondrocytes from hindlimb knee joints using a transgenic reporter animal to combat the need for membrane permeability and targetable cell surface antigens.

To further identify targets for flow cytometry and FACS, primary chondrocytes were treated with a fixative and stained for intracellular and extracellular markers [107]. Due to the lack of targetable antigens, collagen 2 was the primary target tested (Figure 2. 6). Upon flow cytometric analysis of Ai9+ chondrocytes, it was clear that untreated samples lacked a collagen 2 population. Indeed, validating that chondrocytes required

fixation and permeabilization of their membranes to better identify and isolate these cells from a heterogenous population using FACS. Sequencing of fixed RNA is a relatively new technology that has only started being used within the last few years. Due to the novelty of fixed RNA sequencing, previous studies describing chondrocytes transcriptomics have been limited to traditional bulk sequencing of all joint cells in the tissue or those from *in vitro* stem cell differentiation [108]. While bulk-seq has allowed researchers to identify large transcriptional changes that occur in heterogeneous tissues, it restricts identification of cellular identities, interactions, and functions within the joint. Additionally, studies of joint cell responses early in OA progression cannot be done using cartilage tissue isolated from late-stage OA knee replacements.

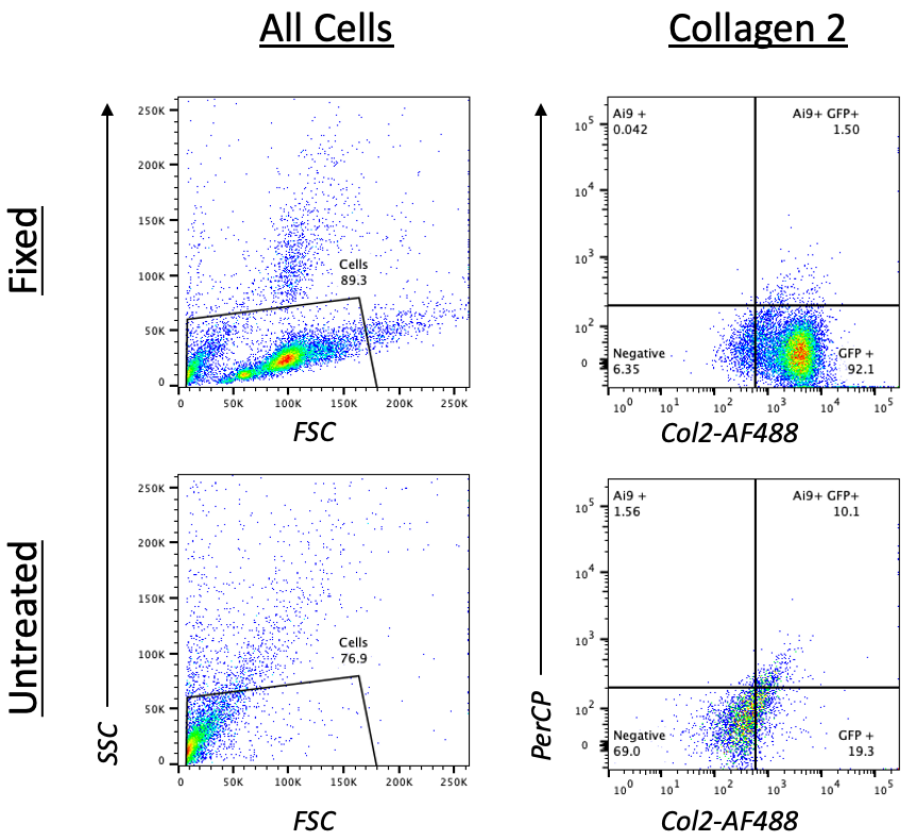

Figure 2. 6 Immunocytochemistry of primary chondrocytes read on flow cytometry. Primary cells isolated from murine cartilage were either untreated (Bottom Row) or subjected to fixation using CytoFix solution (Top Row). Cells were stained with a mouse anti-collagen 2 primary and anti-mouse 488nm secondary for flow cytometric analysis

(Right Column). Fixed samples show a GFP+ population while unfixed samples have very limited signal.

In practice, many researchers use primary stem cells isolated from bone marrow or differentiate fibroblast cells lines into chondrocytes using a combination of growth factors (Transforming Growth Factor-β3/TGF-β3) and metabolites like sodium pyruvate, ascorbic acid, proline, and Insulin-Transferrin-Selenium (ITS). When grown in culture, these stem cells and fibroblast lines can take up to three weeks to fully differentiate into chondrocytes [109]. In addition, these *in vitro* studies lack the mechanical stimuli and joint microenvironment to successfully recapitulate an *in vivo* disease phenotype [69]. Although many culturing techniques have attempted to replicate the joint microenvironment through pellet and gel culture, *in vitro* studies cannot fully replicate joint trauma and disease. The inability to grow chondrocytes in their native environment, further exacerbates the need for primary cell isolations from early post-injury to perform homogeneous chondrocyte studies [6]. This chapter outlines a new method for enrichment of viable articular chondrocytes, enabling single-cell RNA sequencing in animal models to better understand all stages of PTOA progression.

Chapter 3. Single-Cell RNA Sequencing Reveals Transcriptomic Heterogeneity in Articular Chondrocytes of PTOA-Susceptible and PTOA-Resistant Mouse Strains

Abstract

Post Traumatic Osteoarthritis (PTOA) is a painful joint disease characterized by degradation of bone, cartilage and connective tissue that is initiated by a traumatic injury such as an anterior cruciate ligament or medial meniscus tear. In humans, about 50% of joint injuries progress to PTOA, while the remainder spontaneously resolve without progressive degeneration. This study utilizes a PTOA-susceptible mouse strain, C57Bl6/J (B6) and PTOA-resistant "Super-healer" MRL/MpJ (MRL) to explore the cellular composition of both strains prior to and in response to injury. Previous research has shown that MRL mice show a sustained resistant phenotype, with little cartilage degradation for up to 12 weeks after Anterior Cruciate. Ligament rupture using a tibial compression induced (TCI) injury [99]. Meanwhile B6 mice exhibit significant joint degradation as early as 2 weeks post injury, and progress to severe PTOA by 4 weeks after injury. This method recapitulates human ACL tears in a non-invasive manner, also inhibiting an additional immune response caused by common surgical induction like DMM or ACL translocation. Currently, there is a limited understanding of the regenerative potential and cellular heterogeneity within the joint of these PTOA resistant MRL mice. In addition, there is limited research detailing the transcriptomic response of chondrocytes to injury *in vivo.* This study uses single cell RNA sequencing (scRNA-seq) to characterize not only the differences between B6 and MRL knee joints, but also identifies changes in stromal populations as well as subpopulations of chondrocytes previously unknown. Additionally, the abundance, heterogeneity and expression of chondrocyte and stromal populations in MRL joints a may reveal new targets within the injured joint that can be used to protected individuals from PTOA.

Introduction

A subset of Osteoarthritis [2], known as Post Traumatic Osteoarthritis (PTOA), is caused by mechanical injury to the joint. Knee joint specific PTOA is rampant worldwide and accounts for nearly 12.5% of PTOA cases in the United States [1]. Knee joint PTOA is usually caused by a tear to the anterior cruciate ligament [6] or meniscus, or sometimes intra-articular fracture, that leads to destabilization of the joint. This instability leads to disruption of the normal joint physiology, i.e. cartilage degradation and subchondral bone loss, in nearly 50% of individuals who do not have reconstructive surgery. Mysteriously, other individuals spontaneously resolve without damage or pain [2]. The risk factors that determine PTOA likelihood are not understood well and therefore much is left to study in the field of PTOA resistance. To further exacerbate this disease, there are no cures or preventatives. Additionally, limited treatments are available, and little is understood about the molecular pathogenesis of PTOA. Thus, patients are limited to primitive treatments such as pain management or physical therapy. Patients and practitioners alike are eager for new research to fill these gaps in knowledge.

The articular knee joint is comprised of several tissues including bone, hyaline cartilage, synovium, tendons, and ligaments for stabilization. Each component of the joint microenvironment is essential for normal joint function, and damage to any of them can alter the functionality of the knee joint at a cellular and molecular level. The articular cartilage (AC) of the knee is a thin layer of tissue located at the ends of each of the long bones that is essential for joint support and mechanical load. This tissue is comprised mostly of water and is supplemented by extracellular matrix (ECM) proteins and resident chondrocytes. These ECM proteins are essential in bearing weight during activity and lubrication of the joint, and their highly organized structure has an extremely protein rich composition. These proteins are essential for the elastic structure of the AC and include different sized proteoglycans (PG), multiple collagen types, and glycosaminoglycans [110] such as hyaluronic acid, chondroitin sulphate; all responsible and crucial for the AC to function properly. Proteoglycans and glycosaminoglycans are the main protein components that make up the articular cartilage. GAGs can be broken down into three

classifications: keratin sulphate, chondroitin sulfate, and hyaluronic acid (HA). A combination of these GAGs creates macromolecules known as PGs which are critical for the elasticity of the cartilage and extremely important in the flow of fluid and nutrients throughout the tissue [3]. Aggrecan, the main large aggregating molecule, is highly prevalent in the articular cartilage and forms an entwined network of fibrils with native collagen molecules and other small leucine rich proteoglycans such as biglycan, lubricin, decorin, and fibromodulin. In addition to PGs and GAGs, the cartilage is rich in collagen fibrils and relies on the arrangement of them for its mechanical properties. Collagen II accounts for nearly 90% of the collagen content in the AC, followed by collagen XI and collagen IX. Collagen XI forms covalent bonds with collagen II and acts as an internal regulator of fibril formation in the AC. In addition to collagen IX, collagen VI is localized to the pericellular regions of the cartilage and forms complexes with collagen II/XI complexes. It is highly important in facilitating the connection of the chondrocyte with the matrix itself through the pericellular matrix of the cell [4]. Finally, collagen X is essential in mineralization and is a molecular indicator of calcification, chondrocyte hypertrophy, and OA onset. This microstructure is essential for maintaining the integrity of the cartilage, controlling microfluidics within the tissue, and aiding in mechanical load distribution [5]. These matrix proteins form a complex environment that degrades and changes composition when disturbed by trauma [6], [7].

The AC has been divided into four zones [8] based on matrix composition and is specific to collagen fibril arrangement and chondrocyte morphology. Chondrocytes make up less than 5% of the entire cartilage tissue, yet play a major role in secretion of the ECM [111]. They are embedded in the ECM in small cavities known as lacunae and separated from each other cytoplasmically. Chondrocytes are surrounded by a thin pericellular matrix, which protects the cell and aids in regulating its metabolism by detecting changes to its microenvironment through mechanical and biochemical stimuli. These cells are specifically restricted to each of the cartilaginous zones and vary in size, shape, and concentration depending on their depth in the AC zones [111].

Healthy cartilage can be divided into four zones: superficial, intermediate, deep, and calcified. The superficial zone of the AC is the outmost layer, consisting of morphologically flat, horizontally aligned chondrocytes and collagen fibrils, which accounts for about 15% of the AC. The superficial zone is primarily responsible for lubrication of the joint, i.e. providing a surface for surrounding tissue to glide along the cartilage without damage[112, 113]. The ECM in this zone is comprised of high amounts of Lubricin (a glycoprotein responsible for this slick structure), fibronectin, and water. The intermediate zone, which accounts for about half of the AC, is less dense in terms of chondrocyte number than the superficial layer and morphologically more spherical. The ECM of the intermediate zone is comprised of a random alignment of thicker collagen fibrils and a high concentration of the GAG rich protein aggrecan [114]. Beneath the intermediate zone is the third zone of the AC known as the deep zone. This region accounts for nearly 30% of the tissue, is extremely rich in collagen fibrils and proteoglycans, and has the least number of chondrocytes. The cells in this region are spherical in shape and stacked into columns perpendicular to the surface of the AC [115]. Connecting the intermediate and deep zone of the articular cartilage is a small layer of cartilage known as the "tidemark" [116]. This region is dense with compacted collagen fibrils thought to act as an anchor for the more malleable upper layers of cartilage to the calcified region of cartilage above the subchondral bone. Below the tidemarks is the basal layer of cartilage known as the deep zone or calcified cartilage. This region has an extremely sparse population of chondrocytes. The chondrocytes that do exist here are much smaller, have a hypertrophic appearance, and are usually surrounded by ECM, giving them the appearance of having a matrix "shell." These cells have an extremely low metabolism based on their low levels of endoplasmic reticulum and golgi [117]. The ECM in this region primarily consists of calcified matrix and is high in Collagen X, which is essential for bearing load and transferring mechanical force to the subchondral bone below. These chondrocyte layers have been characterized using generic histologic techniques [118], but the cellular function of each layer has yet to be elucidated in response to knee joint injury.

In addition to its complex protein structure, the cartilage is extremely avascular, lacks innervation, and has no lymphatic drainage, leaving mature chondrocytes to rely heavily on the surrounding synovial tissue for nutrients [105]. Articular chondrocytes lack the capacity to proliferate under normal conditions and have evolved to survive in this hypoxic environment [119]. The synovial capsule is comprised of a membrane and hyaluronic acid rich fluid. The synovium is essential in supplying chondrocytes with nutrients, aids in the transportation of waste material away from the cells, and provides additional lubrication to the joint. In addition, the synovium is also home to several subsets of immune and stem cells including neutrophils, synoviocytes, lymphocytes, and monocytes [120-123]. In general, cartilage tissue normally lacks regenerative capabilities after damage has occurred, [124], although recent studies of these joint supporting cells allude to a healing mechanism attributed to the interaction of cells in the cartilage and synovium.

While generic histological profiling can differentiate the morphological changes that occur to the cartilage as a whole tissue, transcriptomic profiling of these joint resident cells has still not been fully evaluated, especially after joint damage has already occurred. Several models of tissue injury and mouse strain have been studied using bulk RNA sequencing [99, 125-127]. Although traditional bulk RNA sequencing has allowed for new insights to the transcriptomic changes occurring to tissues under different conditions, [99, 128] it still lacks the capacity to determine cell specific changes and reveal heterogeneity in tissues of interest. Over the past decade, single-cell RNA sequencing has overcome the challenges faced by bulk RNA sequencing; it has been essential both for identifying cell specific transcriptomic changes under differing disease conditions and revealing the tissue complexity that is otherwise missed using bulk RNA-sequencing. This study uses a previously established tibial compression injury (TCI) model that recapitulates clinical knee injury parameters of an ACL tear [129]. Bulk sequencing paired with scRNA sequencing provides an in-depth analysis of injury induced transcriptomic changes that occur to articular chondrocytes.

This chapter compares a mouse strain that is moderately susceptible to PTOA to a strain that has previously been identified as PTOA resistant. The MRL/MpJ strain is known for its regenerative wound healing capabilities in several tissues [73, 74] as well as its resistance to severe joint degradation after ACL injury for up to 12 weeks after injury [99]. By utilizing scRNA sequencing technology, we were able to identify baseline and injury-responsive populations in the cartilage of the knee joint that were previously unknown in murine models and may play a role in the resistance to cartilage deterioration. This study provides insight to potential healing mechanisms responsible for this resistant phenotype by profiling ECM components and comparing joint populations to those found in osteoarthritic cartilage from humans undergoing a full knee replacement.

In addition, the recent development of an articular cartilage digest for enzymatic isolation of articular chondrocytes in Chapter 2 paired with flow cytometric analysis has aided the field by providing a reproducible method to selectively isolate primary chondrocytes from knee tissues while simultaneously limiting contaminates, e.g. immune and stromal cells. In this chapter, several previously published chondrocytes sub-populations [118, 130] are identified and changes to these populations after injury in the PTOA-Susceptible C57Bl/6J mouse strain are revealed. Notably, both transcriptional and spatial changes that occur to cells and the tissue across injury conditions were identified at the population level through scRNAseq using immunohistochemical validation. These technologies have aided the understanding of basic PTOA progression and response to injury using animal models representative of human disease.

Materials and Methods

Animal Care and Tibial Compression Joint Injury

All animal experimental procedures were completed in accordance with the Institutional Animal Care and Use Committee (IACUC) guidance at Lawrence Livermore National Laboratory and the University of California, Davis in AAALAC-accredited facilities. C57Bl6/J (B6; Stock No: 000664) and MRL/MpJ (MRL; Stock No: 000486)

animals were purchased from Jackson Laboratory (Bar Harbor, ME, USA) and housed until 10 weeks of age while allowed to roam free in normal caging. At 10-weeks of age, mice were placed under anesthesia using isoflurane inhalation and placed in a horizontal position to prepare for a non-surgical knee joint injury [129]. The right tibia was placed between two plates and subjected to single tibial compression overload of 12-18N force at 1 mm/s displacement rate until anterior cruciate ligament rupture was complete using an electromagnetic material testing system (ElectroForce 3200, TA Instruments, New Castle, DE, USA). Mice were given a single 50uL dose of 0.9% sterile saline (Becton, Dickinson and Company, Franklin Lakes, NJ, USA), and a single dose of Buprenorphine (0.01 mg/kg) administered immediately post-injury for pain relief. Following injury, mice were allowed free range of the cage while on 12h light/dark cycles prior to euthanasia for 3-day, 7-day and 4 weeks post injury.

Histological Assessment of PTOA Progression

Right hindlimbs were collected from uninjured (D0), 3-days post injury (3DPI), 7-day post injury (7DPI), 4-weeks post injury (4WPI) and 6-weeks post injury (6WPI) from both C57Bl6/J and MRL/MpJ animals. Joints were processed for histological evaluation by fixation in 10% neutral buffered formalin (NBF), decalcification using a weight loss-weight gain method in 0.5 M ethylenediamine tetra-acetic acid (EDTA), and processing for paraffin embedding. Joints were then sectioned into 6μm slices in the sagittal plane. Serial medial sections were prepared for histological assessment of joint tissue integrity by staining 0.1% Safranin-O (0.1%, Sigma, St. Louis, MO, USA; S8884) and 0.05% Fast Green (0.05%, Sigma, St. Louis, MO, USA; F7252) using standard procedures (IHC World, Woodstock, MD, USA) to identify the structure of bone, cartilage, and bone marrow. Slides were imaged using a Leica DM5000 microscope (Leica Microsystems, Wetzlar, Germany). ImagePro Plus V7.0 Software, a QIClick CCD camera (QImaging, Surrey, BC, Canada), and ImageJ V1.53 Software was used for imaging and photo editing.

Immunohistochemistry (IHC)

Sagittal sections from uninjured D7PI and 4WPI hindlimbs of MRL and B6 mice were used for IHC ($n \geq 3$/group). Slides were dewaxed and dehydrated using standard

protocols (IHC World, Woodstock, MD, USA). Primary antibodies were incubated overnight at 4 °C in a dark, humid chamber following antigen retrieval (Table 3. 1: Antibody vendor, dilution, and retrieval methods). Secondary antibodies were incubated for 2 h at room temperature in a dark, humid chamber at 1:500. Negative control slides were incubated with secondary antibody only. Stained slides were mounted with Prolong Gold with DAPI (Molecular Probes, Eugene, OR, USA). Slides were imaged using a Leica DM5000 microscope (Leica Microsystems, Wetzlar, Germany). ImagePro Plus V7.0 Software, a QIClick CCD camera (QImaging, Surrey, BC, Canada), and ImageJ V1.53 Software were used for imaging and photo editing. Secondary antibodies included: Chicken anti-rabbit 488 (Thermofisher, Waltham, MA, USA; A21441), Chicken anti-rabbit 594 (Thermofisher, Waltham, MA, USA; 21442), and Donkey anti-goat 594 (Thermofisher, Waltham, MA, USA; A11058).

Table 3. 1: Antibody vendor, dilution, and retrieval methods

Primary Antibody	**Stock#**	**Dilution**	**Antigen Retrieval**
Collagen 2	Thermo: MA512789	1:100	30m Pepsin A @ RT
Aggrecan	Abcam: AB3778	1:200	30m Pepsin A @ RT
Matrilin 3	R&D: AF3357	1:200	30m Unitrieve + 30m Hyaluronidase @ 65ºC
Cytl1	Thermo: 158561AP	1:75	1hr Tris-EDTA @ 65ºC
Chi3l1	Thermo: MA536122	1:100	30m Unitrieve @ 65ºC
Cilp2	Thermo: 118131AP	1:200	30m Hyaluronidase @ 65ºC

Cartilage Histomorphometry

Measurements of thickness and cell number in the articular cartilage of both MRL and B6 were manually assessed using standardized methods [131]. Briefly, slides from uninjured and 4WPI knee joints were stained with Safranin-O and Fast Green, as previously. The articular cartilage of five biological replicates (n=5) were measured using the ‘Measure’ command in ImageJ V1.53 Software at 5 regions of the tibia’s articular cartilage for all samples. Statistics were performed in GraphPad Prism by using an ordinary one-way ANOVA and post-hoc Turkey’s correction. All results were considered statistically significant for $p< 0.05$.

Single-Cell RNA Sequencing (scRNAseq)

Uninjured, 3DPI, and 7DPI, and 4WPI hindlimbs (n = 5/group) were used for scRNAseq analysis. Mice were euthanized humanely under CO2 and entire hindlimbs were removed after cutting away remaining skin and muscles. Excess muscle and fat were removed from the bones of the femur and tibia by trimming with scissors and using a Kimwipe. Murine knee joints were separated at the joint cavity and cleaned long bones were micro-dissected using a scalpel to remove ~1mm of tissue from the articular surface, freeing the articular cartilage from the subchondral bone as described in Chapter 1. For each experimental group, cartilage tissue from 5 mice was pooled and digested to a homogenous single-cell suspension. The articular cartilage was minced using dissecting scissors and placed into 15mL conical tube with 5ml of an enzymatic cocktail comprised of 0.2% Collagenase 2 (2 mg/mL Thermo Fisher Scientific, Waltham, MA, USA)) in FBS free Dulbecco's Modified Eagle Medium Nutrient Mixture F-12 (DMEM/F-12) (Thermo Fisher Scientific, Waltham, MA, USA). Cartilage tissue was digested at 37ºC for four 30-minute intervals while shaking. After each interval, digestion media was filtered through a 70μm cell strainer into a 50mL conical tube kept on ice for the remainder of the digestions. Fresh digestion media was added to the 15mL conical tube containing the partially digested tissue for another round of digestion. After the final digestion interval, cells were pelleted via 4 °C centrifugation for 10 min at 500g and subjected to a red blood cells lysis for 10 minutes on ice using Ammonium-Chloride-Potassium (ACK) Red Blood Cell Lysis Buffer (Thermo Fisher Scientific, Waltham, MA, USA)). Digested cells were stained for fluorescently activated cell sorting (FACS) analysis using 100μl of an antibody cocktail containing: CD45 APC-Cy7 (BioLegend, San Diego, CA, USA, 103116 (1:100)), Ter119 APC (Miltenyi Biotec, Bergisch Gladbach, Germany, 130-102-290, (1:10)), and DAPI (Thermo Fisher Scientific, Waltham, MA, USA). Contaminating immune and erythroid cells were depleted through double-negative selection (CD45-Ter119-) using a BD FACSMelody (San Jose, CA, USA). Final cell counts of enriched chondrocytes (CD45-Ter119-) were performed manually using a hemocytometer. Cells were resuspended in 1xPBS + 0.04% non-acetylated BSA for preparation of scRNAseq using a Chromium Controller (10× Genomics, Pleasanton, CA, USA). Library preparation was performed

using Chromium Single Cell 3′ GEM, Library & Gel Bead Kit v3 (10× Genomics, Pleasanton, CA, USA; Catalog no. 1000075) following the manufacturer's protocol and sequenced using Illumina NextSeq 500 targeting approximately 50,000 reads per cells.

scRNA-seq Data Analysis of Chondrocytes from Uninjured Joints

Alignment of scRNA-seq data to the mouse genome (mm10) and gene counting was completed utilizing the 10× Genomics Cell Ranger pipeline (10× Genomics, Pleasanton, CA, USA). Subsequently, output files from the Cell Ranger 'count' were read into Seurat v3 [20] for further analysis. Cells with fewer than 500 detected genes or genes that were expressed by fewer than 5 cells were excluded from the analysis. Dead cells and doublets were also removed during flow cytometry. After removing all the unwanted cells from the dataset, the data was normalized by employing a global-scaling normalization method 'LogNormalize'. Subsequently, the 2000 most variable genes were identified, the data were scaled, and the dimensionality of the data was reduced by principal component analysis (PCA). Subsequently, we constructed a K-nearest-neighbor (KNN) graph based on the Euclidean distance in PCA space using the 'FindNeighbors' function and applied Louvain algorithm to iteratively group cells together by the 'FindClusters' function. A non-linear dimensional reduction was then performed via uniform manifold approximation and projection (UMAP) and various cell clusters were identified. Then, clusters expressing immune and blood cell markers were removed and the remaining data were normalized, scaled, and, after variable feature identification, the data were re-clustered to identify clusters of non-immune cells in the joint. To identify chondrocyte subtypes, clusters expressing chondrocyte markers Acan, Sox9, and Col2a were extracted and further analyzed as described above. Marker genes per cluster were calculated using Seurat's 'FindAllMarkers' function and the 'wilcox' test option. All scRNA-seq data was deposited in the Gene Expression Omnibus [132] database.

Analysis of Human Chondrocyte scRNA-seq Data

Previously published human chondrocyte scRNA-seq data was downloaded from Gene Expression Omnibus [132] database (GSE104782) and a text file was obtained with raw expression values. The data were analyzed using Seurat, as described above to identify

various cell types. Subclusters were annotated based on the markers provided by Ji et al [130]

Comparison of Chondrocytes from Uninjured and Injured Joints

scRNA-seq data from uninjured, 3DPI, and 7DPI joints were analyzed using Seurat v3 [6]. After data pre-processing, variable features were selected based on a variance stabilizing transformation ('vst'). Then, we identified anchors for data integration using the 'FindIntegrationAnchors' function. Next, these anchors were passed to the 'IntegrateData' function and a new integrated matrix with all 3 datasets were generated. Subsequent dimensionality reduction, clustering, and visualization were performed in Seurat as described above. Clusters of cells expressing the chondrocyte markers Sox9, Acan, and Col2a1 were extracted and further analyzed to identify various chondrocyte subpopulations. Genes differentially expressed between chondrocyte subtypes at various timepoints were identified using 'FindMarkers' function implemented in Seurat.

Pseudotime Trajectory Finding

Pseudotime trajectory of chondrocytes was constructed with Monocle [133-135]. Expression data, phenotype data, and feature data were extracted from the Seurat object and a Monocle 'CellDataSet' object was constructed. Highly variable genes from Seurat object were used as ordering genes in Monocle. Dimensionality reduction was performed using the DDRTree algorithm implemented Monocle via the 'reduceDimension' function. Cells were ordered along the trajectory using the 'orderCells' method with default parameters.

Ontology Enrichment Analysis

Genes enriched in each chondrocyte subtype were identified using 'FindAllMarkers' function from Seurat [84]. Genes with >1.25-fold enrichment in each cluster with an adjusted p-value < 0.1 were used for ontology enrichment analysis using ToppGene Suite [136-138] and Metascape [139] Dot plots of enriched ontology terms were generated in R using the ggplot2 package.

Population Specific Gene Enrichment Analysis

Single cell gene expression from chondrocyte, osteoblast, synovial fibroblast, and fibroblast clusters were evaluated for population specific expression using Venny 2.1. Genes from each cluster were filtered based on an adjusted $p< 0.05$ and fold enrichment >1.5. Filtered gene lists were entered into Venny 2.1 to identify potential cell type specific markers. Genes specific to each population were then input into PANTHER 17.0 for ontology enrichment analysis and overrepresentation testing. Ontologies are expressed as $-\log_{10}$(FoldChange).

Results

MRL joints show resistance to cartilage degradation after TCI injury

Histological evaluation of MRL and B6 articular knee joints was completed by staining with safranin-o and fast green. Tissue staining indicated that by 4-weeks after injury, proteoglycan loss was restricted to the deep layers of the cartilage in MRL without severe tissue loss. Meanwhile, B6 showed severe loss of joint tissue including subchondral (Figure 3. 1a). OARSI scoring suggested that there was no significant difference between uninjured B6 and MRL, as indicated by low OARSI scores of 0.71 and 0.83 on average, respectively (Figure 3. 1b). This signified that no OA phenotype was present in either joint. At 4WPI, B6 had severe loss of proteoglycan staining in both tibia and femur, as well as stark tissue loss of cartilage and bone. OARSI scoring validated that B6 joints had a severe OA phenotype, as noted by an average score of 4.5. OARSI scores of MRL were on average much lower than B6 with an average value of 2.5. at 4WPI, there was a significant OA phenotype in both MRL and B6 when compared to uninjured counterparts, although MRL had significantly lower OARSI scores after injury than B6.

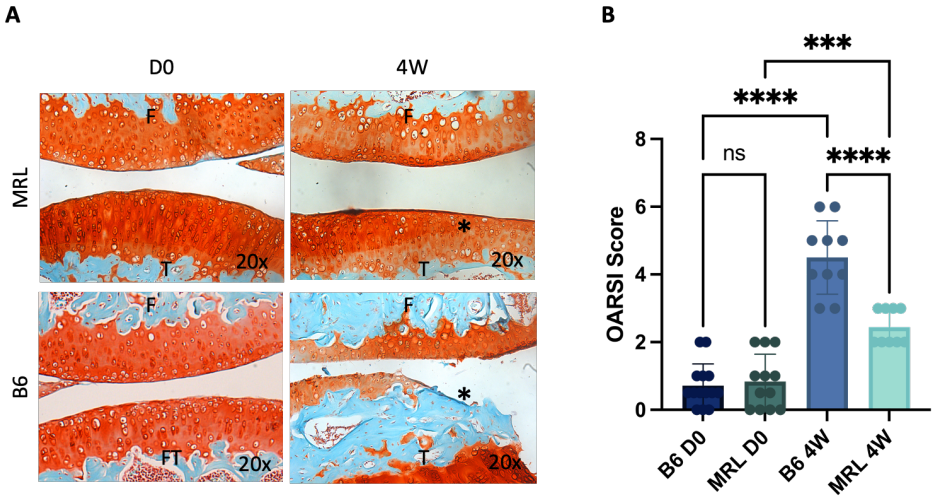

Figure 3. 1 Histological Assessment of PTOA onset in MRL and B6. Formalin-fixed, paraffin embedded knee joints were stained using safranin-o and fast green. PTOA resistant MRL (top row) had little loss of staining after injury in the articular cartilage (red) of the femur and tibia (top right, * asterisk). PTOA susceptible B6 (bottom row) had severe degradation of bone (blue,) and cartilage (red) in the tibia, and loss of some cartilage in the femur after injury (bottom right, * asterisk). Scale bar = 100um. Magnification 20X. F-Femur, T-Tibia. (A) OARSI scoring indicative of PTOA severity and joint tissue loss before (D0) and after (4W) injury in MRL and B6. ns=not significant. ***p<0.001, ****p<0.0001 (B)

Single-cell RNA identification of stromal populations in murine synovial joints

Analysis of murine hindlimb joints used an optimized digest protocol to isolate CD45-Ter119- stromal cells for scRNAseq (Figure 3. 2a). Cells were collected from uninjured (D0) and injured joints at D1, D3, D7, 2W, and 4W post injury of both B6 and MRL. Further analysis of B6 and MRL at D0 and 4W identified 11 populations of cells including: endothelial, fibroblasts, osteoblasts, chondrocytes, synovial fibroblasts, pericytes, skeletal muscle, peripheral nervous system cells, and lymphatic cells (Figure 3. 2b). Stromal populations were classified using widely accepted gene markers (Figure 3. 3, Figure 3. 4a) and highest expression of significant genes (Figure 3. 3). Cluster 0 and cluster 7 had robust expression of *Pecam, Fit1, CD36* and *Cdh5* (Figure 3. 4a) indicating transcriptionally that these cells were endothelial cells. Cluster 1 highly expressed fibroblast genes *Pdgfra, Dcn, Has1, Col1a1/2,* and *Myoc.* Cluster 2 had high expression of *Postn, Col1a1/2, Mmp13, and Bglap, which are* genes robustly expressed in osteoblast populations. Additionally, a small population of contaminating immune cells was also present with high expression of *Ptprc*, which is the gene for CD45, a known immune cell marker (34039664).

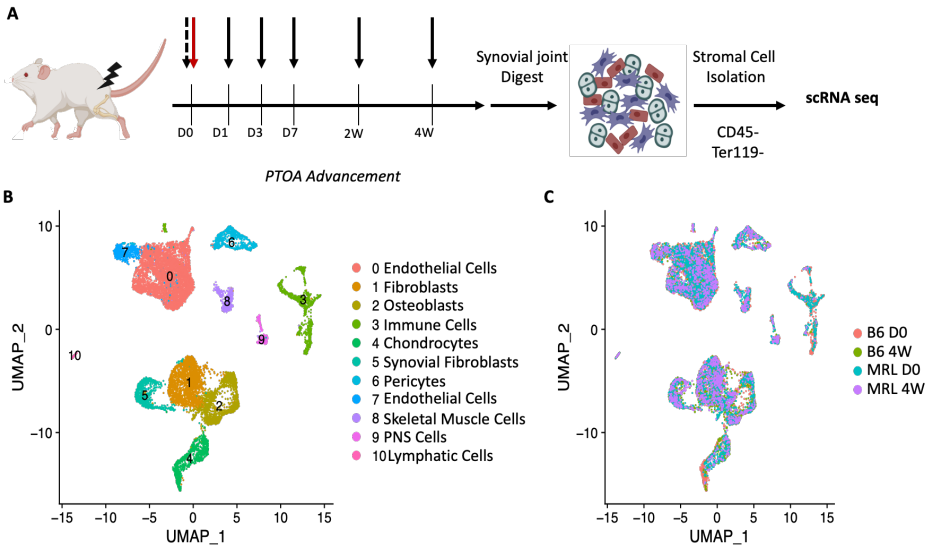

Figure 3. 2: Single-cell RNA sequencing of uninjured B6 articular joints. Schematic of knee joint digest specific for isolation of all stromal cell populations within the joint. Uninjured (D0, Black dotted arrow) joints and injured (injury, red arrow) joints at D1, D3, D7, 2W and 4W (black solid arrow) were processed for scRNASeq (A). Merged UMAP of all populations identified from stromal cells sequenced (B). Merged UMAP representative of all CD45-Ter119- cells in knee joints of all conditions (C).

Cluster 4 was classified as chondrocytes based on strong expression of *Col2a1*, *Acan*, *Col9a3* and *Col11a2*. Cluster 5 had extensive expression of *Prg4*, previously shown to be a marker of synovial fibroblast populations [140]. Pericytes are classically defined by their expression of *a-SMA*, *Rgs5*, and *Myd11* [141], genes all highly expressed in cluster 6. Cluster 8 robustly expressed *Myod1*, a gene known as a myogenic regulatory factor [142]. Cluster 9 expressed *MBP* and *MPZ*, genes important in regulating myelin sheaths [143] in peripheral nerve cells. Last, cluster 10 expressed *Lyve1* and *Prox1*, both highly expressed in lymphatic cells [144].

Interestingly, nearly all clusters were represented in all conditions (B6 D0, B6 4W, MRL D0, MRL 4W) (Figure 3. 2c, Figure 3. 4b).

Table 3. 2 describes each population's percent of total cells sequenced for all timepoints. Of note, B6 suffered from a nearly 23% loss of endothelial cells after injury, while MRL had only a 5% loss in endothelial cells. Additionally, B6 gained nearly 11% more fibroblasts after injury whereas MRL only gained about 6% after injury. B6 had a large increase in osteoblasts of 12% from baseline levels, compared to MRL populations

which lost ~1% of osteoblasts. Another large population increase occurred in synovial fibroblasts, where the B6 population rose nearly 9% after injury while MRLs only had a 3% increase after injury. Additionally, a large portion of the chondrocyte population was present only in B6 joints Figure 3. 2c, Figure 3. 4b). Both injured and uninjured B6 had roughly 10% of cells clustered as chondrocytes, while MRL had nearly half in both injured (3.5%) and injured (4.9%) conditions (

Table 3. 2). Skeletal muscle cells, PNS cells and lymphatic cells were relatively consistent across strains and injury timepoints and showed negligible changes to their population in response to injury (Figure 3. 4b).

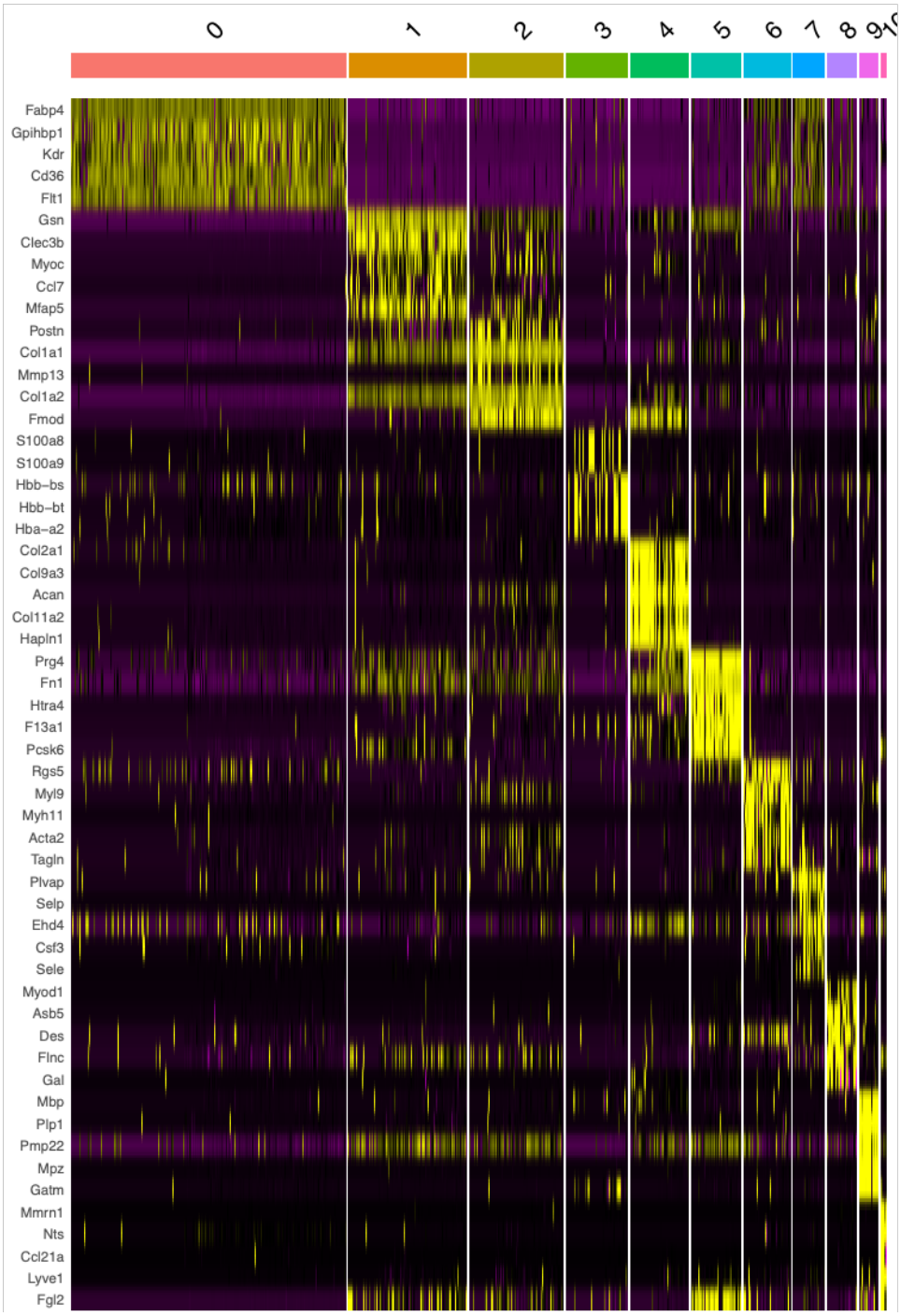

Figure 3. 3: Heatmap of all stromal cell gene expression. Heatmap of top expressed genes per cell population in stromal single-cell data set. Upregulated genes expressed in yellow while downregulated genes expressed in purple.

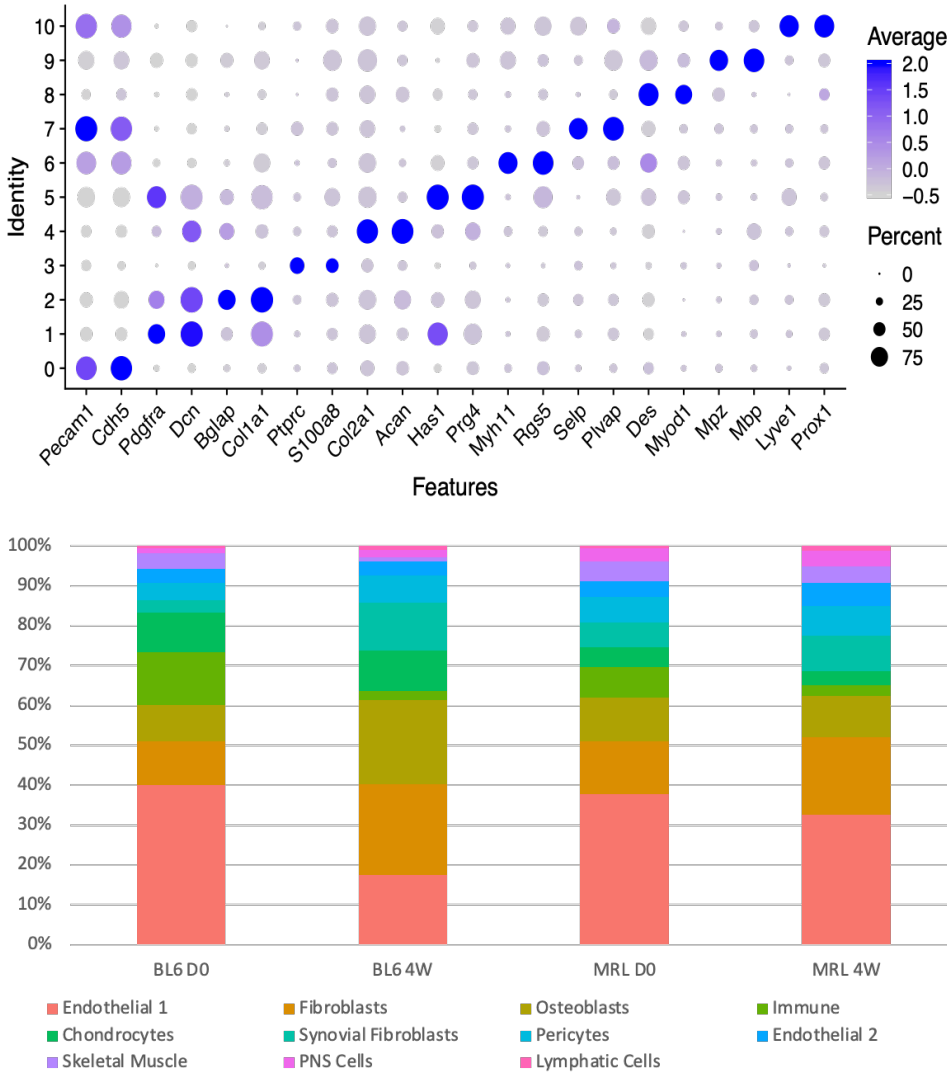

Figure 3. 4: Stromal population gene expression and population ratios. Dot plot of representative markers used in identifying each stromal population from scRNAseq. Average expression of genes is expressed by color of dot and percent of each cluster expressing gene is represented by size of dot (A) Graphical representation of the percent of total cells in each identified population in B6 and MRL uninjured joints and 4-weeks after injury (B)

Table 3. 2: Percent of stromal (CD45-) cells per cluster out of total sequenced cells

Cluster	0	1	2	3	4	5	6	7	8	9	10
Cell Type	Endothelial 1	Fibroblasts	Osteoblasts	Immune	Chondrocytes	Synovial Fibroblasts	Pericytes	Endothelial 2	Skeletal Muscle	PNS Cells	Lymphatic Cells
BL6 D0	*40.1*	*11.0*	*9.1*	*13.2*	*10.0*	*3.1*	*4.2*	*3.6*	*3.9*	*1.2*	*0.6*
BL6 4W	*17.6*	*22.6*	*21.2*	*2.2*	*10.2*	*11.8*	*7.0*	*3.4*	*1.0*	*1.9*	*1.0*
MRL D0	*37.8*	*13.2*	*11.0*	*7.6*	*4.9*	*6.2*	*6.6*	*3.9*	*4.8*	*3.3*	*0.6*
MRL 4W	*32.6*	*19.6*	*10.3*	*2.5*	*3.5*	*8.9*	*7.4*	*5.9*	*4.2*	*3.8*	*1.3*

MRL chondrocyte numbers are consistently lower than B6 in scRNAseq data

Examination of chondrocytes in the stromal scRNAseq dataset revealed that the B6 populations of chondrocytes prior to injury had a Col2a1+Acan+ subpopulation (cluster 0) of cells that does not appear in the other conditions sequenced (Figure 3. 5). While these conditions were all treated the same for cellular isolations, injured B6, uninjured MRL, and injured MRL were lacking this population (Figure 3. 5b). Immunohistochemistry was employed to further explore this phenomenon and evaluate where these cells resided spatially in the knee joint as well as if their presence was truly missing within the articular cartilage.

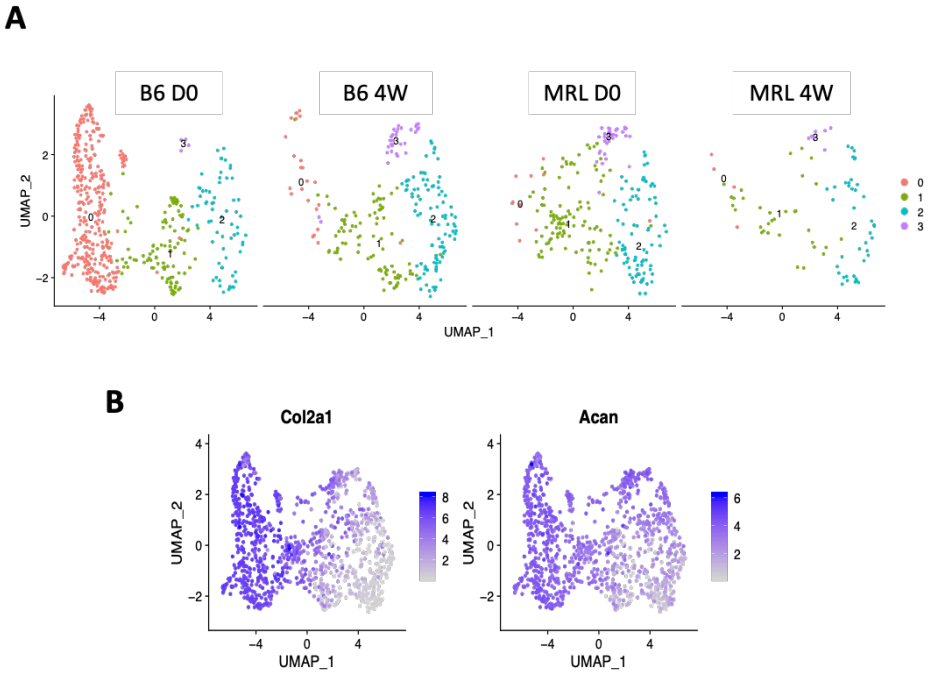

Figure 3. 5: Chondrocyte expression from stromal parent identifies sub-populations. Re-clustering of the chondrocyte subpopulation in scRNAseq data gives rise to four transcriptionally distinct chondrocyte sub-populations. Cluster plots identify different sub-populations of chondrocytes based on gene expression (A) Feature plots identify populations specific markers including collagen 2, aggrecan, and other restricted genes (B).

Immunohistochemical analysis of MRL and B6 cartilage (Figure 3. 6) identified populations of collagen 2 expressing cells and aggrecan expressing cells that formed individual layers in the articular cartilage of the knee. These populations were present in tibias of both strains prior to and at 4 weeks post injury. In uninjured knee joints, MRL had

a significantly thicker layer of aggrecan positive chondrocytes than B6, that resided primarily in the superficial and intermediate layers of the tissue. Additionally, MRL seemed to have a smaller population of collagen 2 positive cells that were restricted to the deep and calcified layer of the cartilage. However, B6 had an expansion of collagen 2 expression; cells in the calcified, deep, and some intermediate layer expressed high amounts of collagen 2. Additionally, B6 had a very thin layer of aggrecan that included some superficial chondrocytes but mostly cells residing in the intermediate layer.

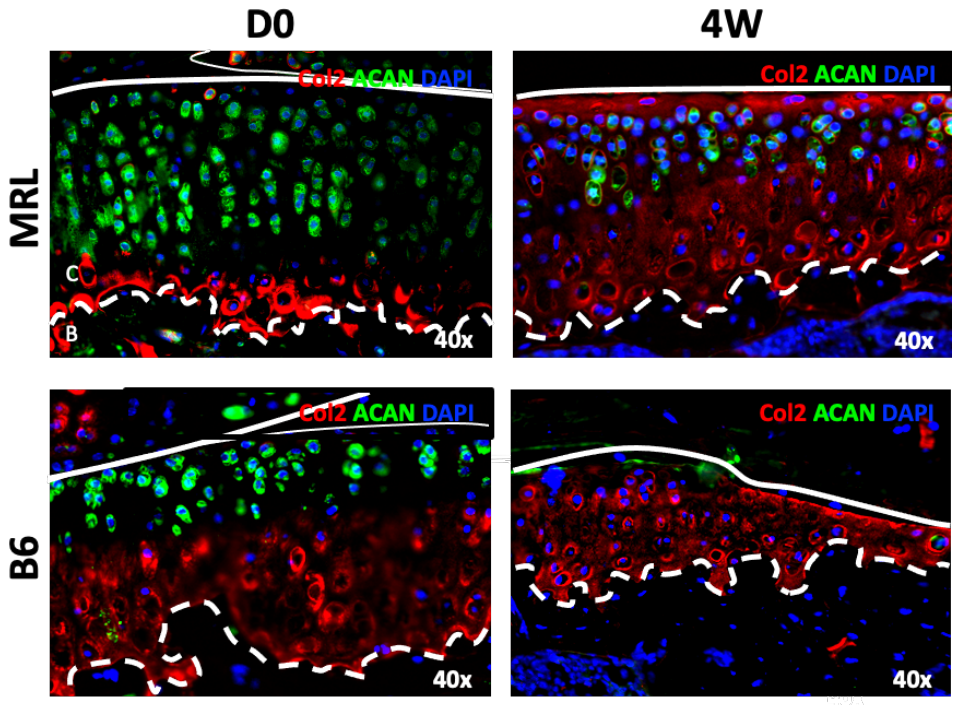

Figure 3. 6: Immunohistochemical validation of ECM protein expression in MRL and B6. Visualization of the protein expression of collagen 2 and aggrecan in the articular cartilage through immunohistochemistry prior to and after injury. Collagen 2, red. Aggrecan, green. Nuclei, DAPI. All images at 40x magnification. Solid line: outline of cartilage or meniscus tissues. Dotted line: interface of cartilage and subchondral bone.

By 4 weeks after injury, there was a severe loss of nearly all aggrecan signal in B6 tibias. In addition, there was also a significant region of cartilage in which collagen 2 signal was lost. MRL, on the other hand, had an expansion in expression of collagen 2 into the entire upper regions of the cartilage tissue, while retaining some aggrecan expression in the intermediate layer of the tissue. This also corresponded to the appearance of collagen 2 expressing superficial chondrocytes that were not present prior to injury (Figure 3. *6*).

Chondrocyte populations from both strains have distinct gene profiles and predicted functions

Gene expression of each cluster identified distinct transcriptomic profiles of each single cell RNA sequencing subpopulation of chondrocytes. Four clusters were identified (Figure 3. 7a), each having distinct up and down regulated gene expression. Cluster 0 was high in collagen 9 (*Col9a1/2/3*) and collagen 11 (*Col11a2*), as well as other known matrix proteins like matrilin 3 (*Matn3*), melanoma inhibitory activity (*Mia),* chondromodulin (*Cnmd*), and inorganic pyrophosphatase 1 (*Ppa1*) (Figure 3. 7).

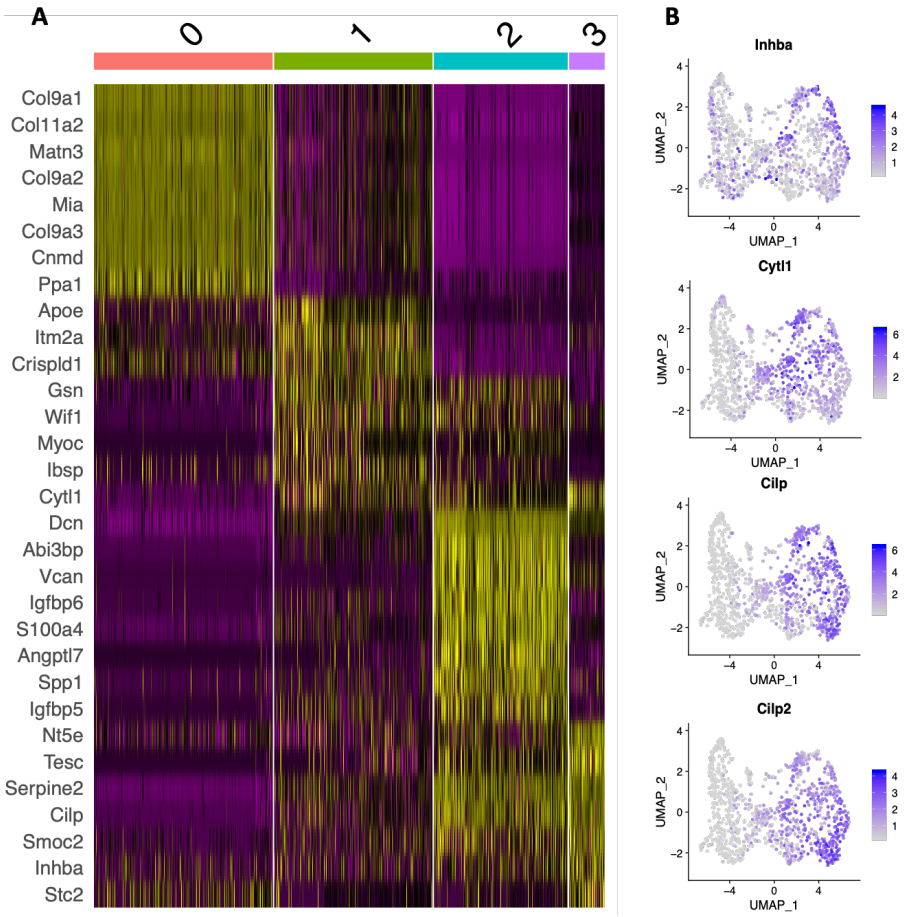

Figure 3. 7: Top genes restricted to each chondrocyte sub-cluster: Highly expressed genes in each subpopulation of chondrocytes determined by re-clustering. Upregulated genes expressed in yellow while downregulated genes expressed in purple (A). Feature plots describing gene expression of previously published markers present in the articular cartilage of murine knee joints (B)

This population has a gene expression profile unlike the other three. Additionally, Enricher analysis grouped genes into ontologies related to ECM structure reorganization

and collagen fibril organization. Pathway analysis revealed they were high in NCAM interactions, syndecan pathways and collagen/ECM synthesis (Figure 3. 8). Cluster 1 was high in genes associated with Rho protein signaling, cell projection organization and neuron development (Figure 8) including *Apoe, Itm2a, Gsn, Wif1, Myoc, Ibsp,* and *Cytl1 (*Figure 3. 7*)*. These genes were also associated with pathways of bone mineralization regulation, caspase-mediated protein cleavage, osteoblast signaling, and lipid transport (Figure 3. 8). Cluster 2 genes grouped into ontologies and pathways related to sulphated proteoglycan/glycosaminoglycan synthesis and organization (

). These genes included ECM proteins, like Decorin (*Dcn*), as well as *Vcan, Igfbp5/6, Spp1, Abi3bp,* and *Angptl7 (*Figure 3. 7). Cluster 2 and cluster 3 also expressed similar genes, although *Nt5e, Tesc, Serpine2, Cilp, Smoc2, Inhba,* and *Stc2* were restricted

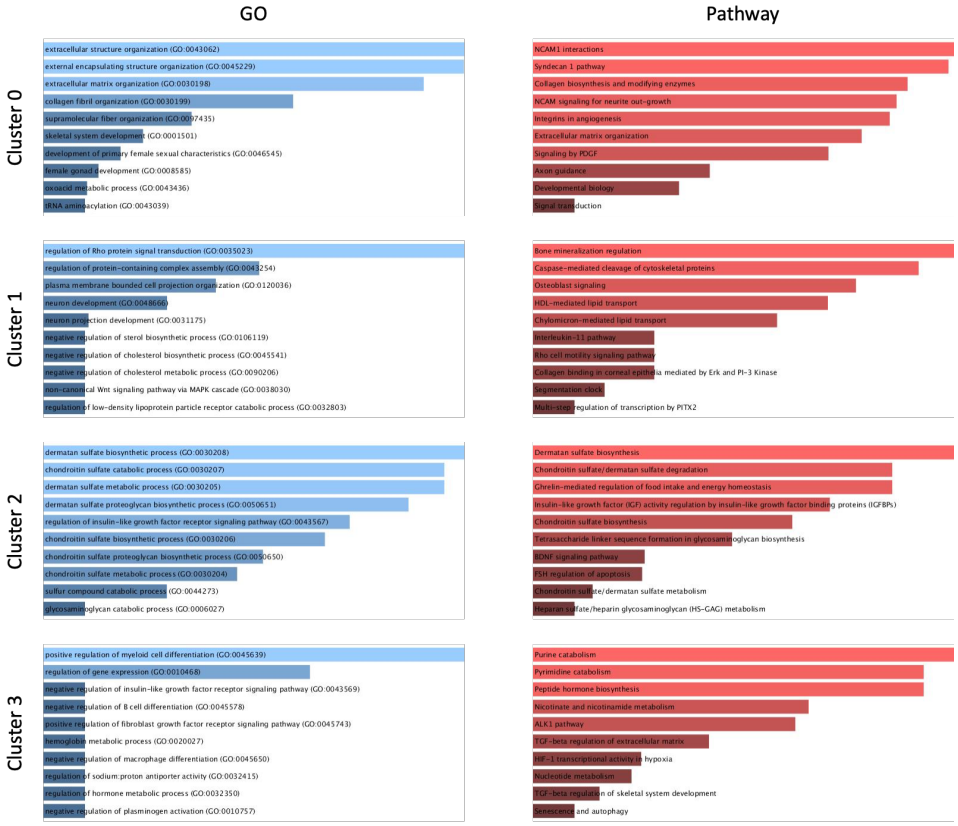

Figure 3. 8: Gene ontology and Pathway analysis via Enrichr. Chondrocyte subpopulations from stromal scRNAseq was analyzed for Gene Ontology (Left, Blue) and Pathways

(Right, Red) associated with each subpopulation. Analysis showed distinct potential functions of each chondrocyte cluster based on top genes restricted to individual clusters.

to cluster 3 (Figure 3. 7). In addition, ontologies associated with cluster 3 were relatively limited, showing high association with regulating myeloid cell differentiation and cellular metabolism regulation (Figure 3. 8).

Chondrocyte specific gene markers exhibit variable expression after injury

Furthermore, all clusters all had strong expression of Collagen 2, Aggrecan and *Sox9*; these genes are known as robust chondrocyte markers [145] (Figure 3. 9). Additionally, feature plot expression of Clusters 1, 2 and 3 showed *Cytl1* expression at various levels in all clusters (Figure 3. 7), while violin plots identified that the expression was relatively low in all clusters except in uninjured B6 (Figure 3. 9). Similarly, *Cilp* expression was limited to Clusters 2 and 3 in the feature plots (Figure 3. 7) while expression was variable in both strains at all timepoints. B6 had a small population of cells that highly expressed *Cilp* that decreased after injury. MRL on the other hand, had a relatively stable population of these cells regardless of injury status (Figure 3. 9). While there was some expression of Inhibin-$\beta\alpha$ (*Inhba*) in Clusters 0, 1 and 2, the highest expression was in Cluster 4 (Figure 3. 7b, Figure 3. 8). *Inhba* levels were extremely low in both uninjured and injured B6 joints, while there seemed to be an increase in expression as well as an expansion of these cells after injury in MRL (Figure 3. 9).

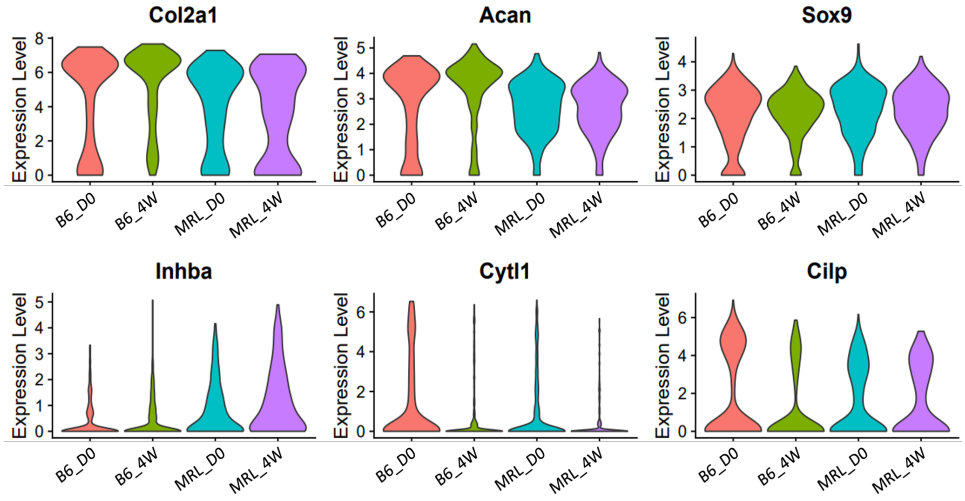

Figure 3. 9 Specific chondrocyte marker expression in populations from scRNAseq stromal cells. Violin plots representing common chondrocyte genes present in uninjured and

injured B6 and MRL from stromal scRNAseq. Height is equivalent to gene expression and width is cell number with a specific gene expression value. Colors are representative of Sample Conditions: B6 uninjured (D0), B6 injured (4W), MRL uninjured (D0), MRL injured (4W)

Additional examination of stromal cells identified 133 genes specific to the chondrocyte population that were not present in osteoblasts, fibroblasts, and synovial fibroblasts (**Figure 3. *10***a). These genes were enriched for ontology terms that included: bone morphogenesis, collagen fibril organization, cartilage development, cell aggregation and chondrocyte differentiation (**Figure 3. *10***b). Furthermore, osteoblasts had 81 population specific genes while fibroblasts and synovial fibroblasts had 54 and 52, respectively.

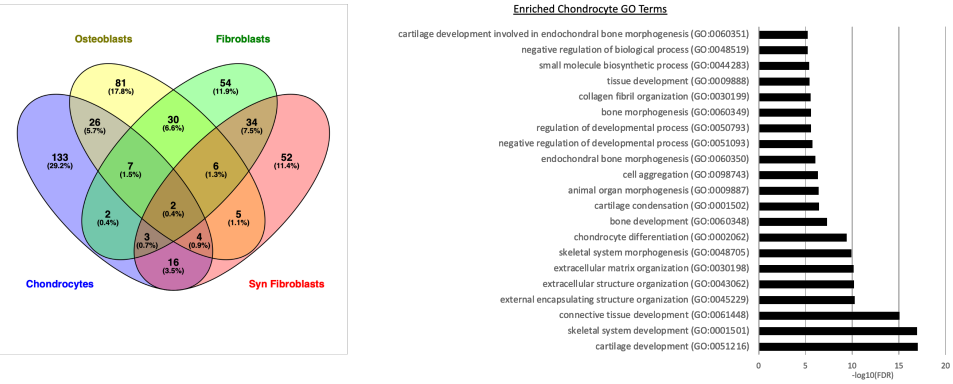

Figure 3. 10: Gene expression specific to function of chondrocytes. Venn diagram representing top significant genes in Osteoblasts, Fibroblasts, Synovial Fibroblasts and Chondrocytes from stromal scRNAseq (A) Gene ontology identifying potential function of genes restricted to chondrocytes (B)

Cartilage specific digest identifies stromal and bone cell populations in B6 joints

A modification of dissection and digestion, in addition to another single cell RNA sequencing analysis identified 10 transcriptionally unique populations of cells in the knee joints of B6 mice (Figure 3. **11**a, b). Five of these populations robustly expressed Aggrecan (*Acan)(*Figure 3. **11** *b)*, and were labeled as Chondrocytes (clusters 0, 1, 3, and 4), and Proliferating Chondrocytes (cluster 7) (Figure 3. **11***c)*. In addition to these cells, there were also large populations of Mesenchymal Stromal cells, Fibroblasts, Osteoblasts, Endothelial Cells, Pericytes, and Synovial Intimal Fibroblasts.

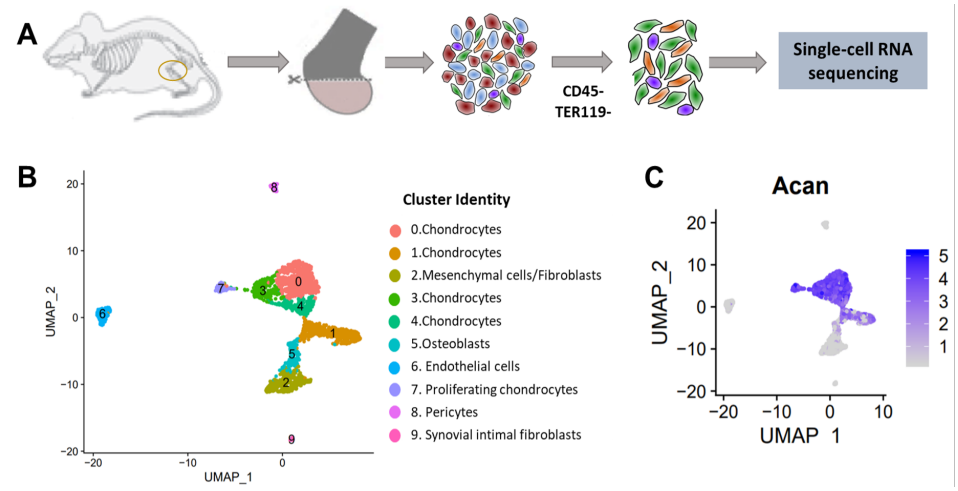

Figure 3. 11:Single-cell analysis of 10-week-old BL6 mouse knee joints. A) Graphical representation of the experimental workflow. Cartilage from mouse knee joints were dissected, dissociated into single cells, and subjected to immune and blood cell depletion. Viable cells from the remaining fraction were subjected to single cell sequencing. B) Cell clusters from scRNA-seq analysis visualized by Uniform Manifold Approximation and Projection (UMAP). Colors indicate clusters of various cell types. C) Feature plot showing the expression of chondrocyte marker Acan.

Each population had a distinct gene profile represented by known markers of these populations (Figure 3. 12a). The chondrocyte populations also had high expression of multiple collagens (*Col2, 9, 11, 27*) as well as other known secreted ECM proteins such as matrilin-3 (*Matn3*), chondroadherin (*Chad*), upper zone of growth plate and cartilage matrix associated protein (*Ucma*), and chondrocyte intermediate layer proteins (*Cilp1/2*). Chondrocyte populations (clusters 0, 1, 3, 4, and 7) also expressed distinct markers like *Wwp2, Sdc4,* and *Scrg1(*Figure 3. 12*a)*, while only Cluster 1 chondrocytes had robust expression of *Tnfrs11b, Wif1, Cilp1/2, Cytl1, Ibsp*, and *Clu* Figure 3. 12*b,c)* Cluster 1 appeared to be transcriptionally unique compared to other chondrocyte populations. Furthermore, Clusters 0, 3, 4, and 7 all shared robust expression of *Col9a1, Hapln1, Matn3* and *Cnmd*.

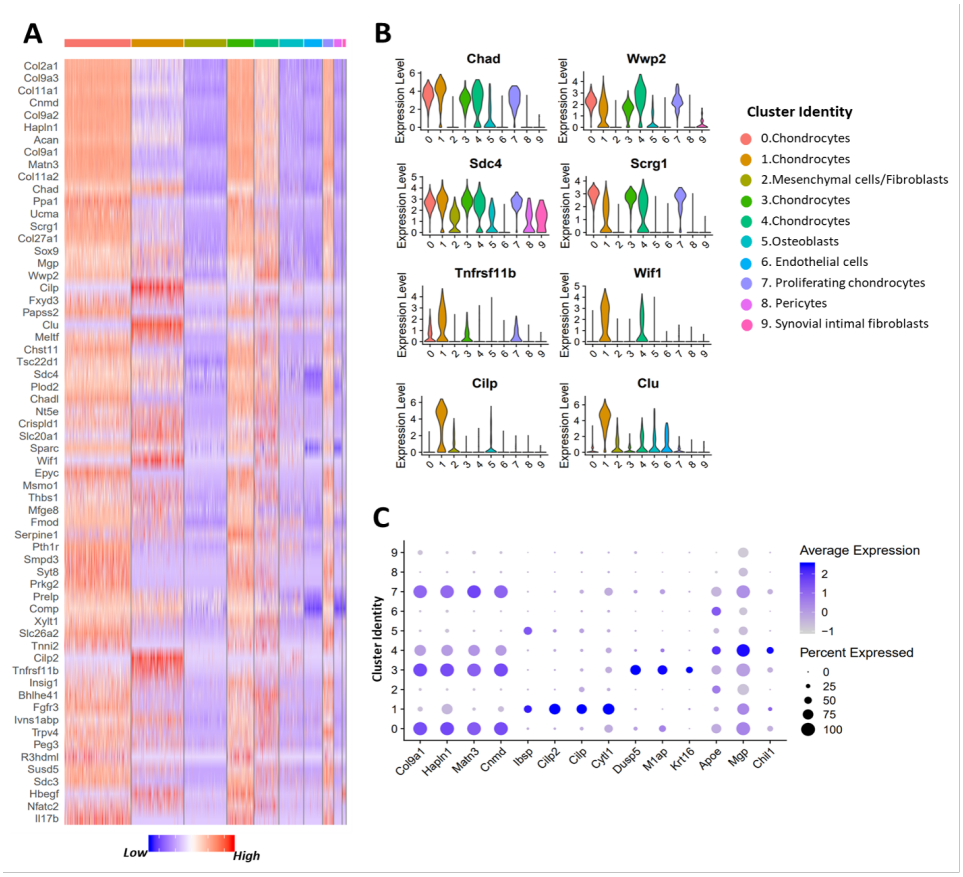

Figure 3. 12:. Identification of OA targets enriched in chondrocytes. A) Heatmap showing potential OA targets enriched in chondrocyte clusters compared to other connective-tissue forming cell types in the joint. B) Violin plot showing the expression of selected OA targets. C) Dot plot showing the expression of selected markers of various chondrocyte clusters. Dot size represents the fraction of cells expressing a specific marker in a particular cluster and intensity of color indicates the average expression level in that cluster.

B6 Chondrocytes are transcriptionally unique and may represent different stages of differentiation

Supplementary analysis identified 9 subpopulations of chondrocytes all expressing Sox9, Col2a1, Acan, and Chad (Figure 3. *13*a) while also having different transcriptomic profiles (Figure 3. *13*b, Figure 3. *14*). Cluster 2 cells were named the Mef2c^{high} population due to their robust expression of Mef2c, as well as Ihh, Alpl, and Pth1r. Cluster 3 robustly expressed Keratin-16 (Krt16), Srnx, and

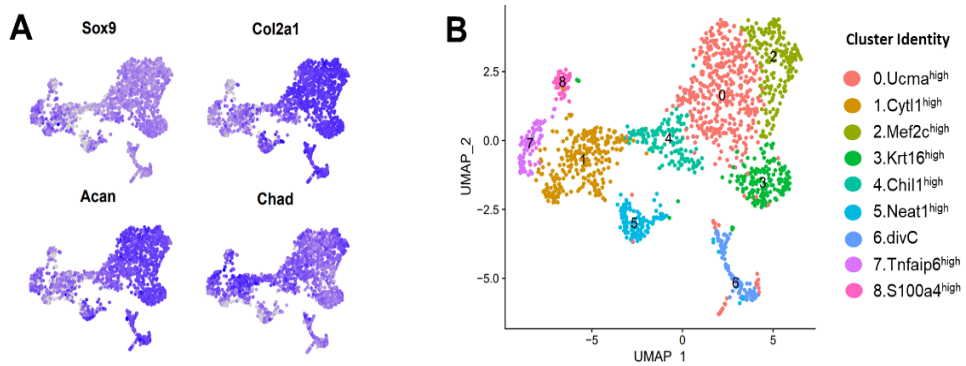

Figure 3. 13: Characterization of chondrocyte subtypes. A) Feature plots showing the expression of key chondrocyte markers. Purple: high expression, grey: low expression. B) UMAP plots of chondrocyte subpopulations in B6 joints.

M1ap and was named the Krt16high subpopulation. Cluster 4 had strict expression of Chil1 and high expression of Efemp1, and Spon. Thus, this cluster was named Chil1high subpopulation. Clusters 6, 7, and 8, had robust expression of Top2a, Tnfia6, and S100a4, respectively, and were labeled as Dividing Chondrocytes (divC), Tnfaip6high, and s100a4high subpopulations (Figure 3. 14c, d). While nearly all cluster (except for 1, 5 and 8) had strong expression in many cells in that cluster, Cluster 0 had broad expression of Ucma, Matn3, and Scrg1, and was named the Umcahigh subpopulation (Figure 3. 14c, d). While all clusters expressed Neat1, Cluster 5 had the highest expression and was named the Neat1high subpopulation.

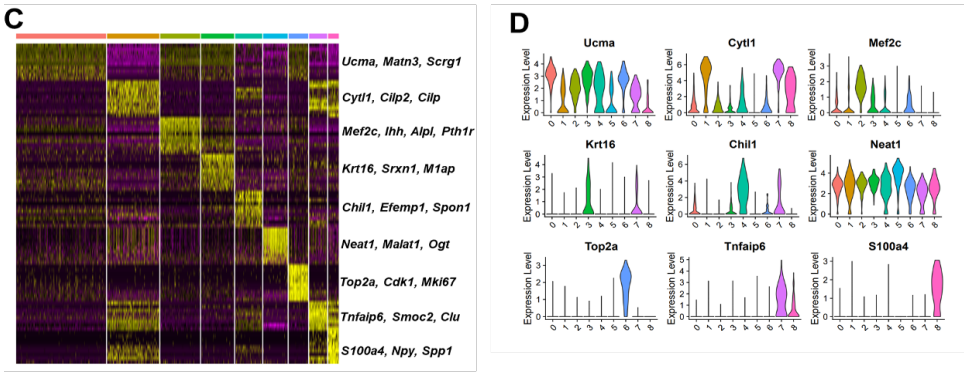

Figure 3. 14:Characterization of chondrocyte subtypes C) Heatmap showing the scaled expression of top genes expressed in each cluster. D) Violin plot showing the expression of selected markers of various chondrocyte subtypes.

In addition to their robust gene expression profiles, each subpopulation also had a distant potential differentiation state when analyzed by pseudo-time trajectory analysis using Monocle (Figure 3. 15e, f). When analyzed together, chondrocyte populations formed three branches that met in the center. *Top2a* expressing cells appeared at the end of

one branch while *Krt16* and *Mef2c* expressing cells appeared at the end of a second branch. These two subpopulations of chondrocytes met in the middle where a large proportion of the Ucma^{high} cells resided. The third branch showed that *Chil1*^{high} cells clustered near the *Ucma*^{high} subpopulation, and were followed by the *Cytl1*, *Tnfaip6* and *S100a4* subpopulations towards the end of the branch.

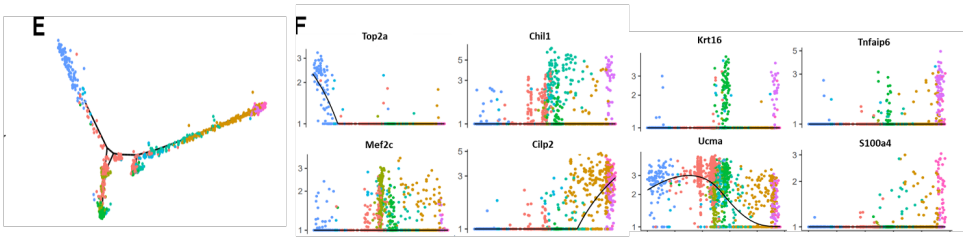

Figure 3. 15:. Characterization of chondrocyte subtypes E) Monocle pseudospace trajectory colored based on chondrocyte clusters in Figure 3. *13*b). F) Expression of chondrocyte markers on a pseudotime scale.

Four cluster specific markers were chosen from the scRNAseq data that were all restricted to certain subpopulations of chondrocytes (Figure 3. 16c) for spatial validation. Matrilin-3 (*Matn3*) was used to mark *Umca*^{high}, *Mef2c* ^{high}, *Krt16* ^{high}, and *Chil1* ^{high} subpopulations. *Cytl1* was used to mark the *Cytl1* ^{high}, *Tnfaip6* ^{high}, and *s100a4* ^{high} subpopulations. *Chil1* was restricted to the *Chil1* ^{high} population, and *Spp1* was used to further identify the *Tnfaip6* ^{high}, and *s100a4* ^{high} subpopulations (Figure 3. 16c). Immunohistochemistry was conducted to further identify the location of chondrocyte subpopulations within the cartilage tissue (Figure 3. 16d-f). Thorough analysis of B6 articular cartilage showed *Matn3* expression was present in both superficial and deep, calcified chondrocytes (Figure 3. 16d, red), while Cytl1 (Figure 3. 16d, green) and Cilp1 (Figure 3. 16e, red) had robust expression throughout the intermediate layer of chondrocytes. In addition, the deep, calcified layer of chondrocytes and calcified meniscus were also labeled using *Spp1* (Figure 3. 16f).

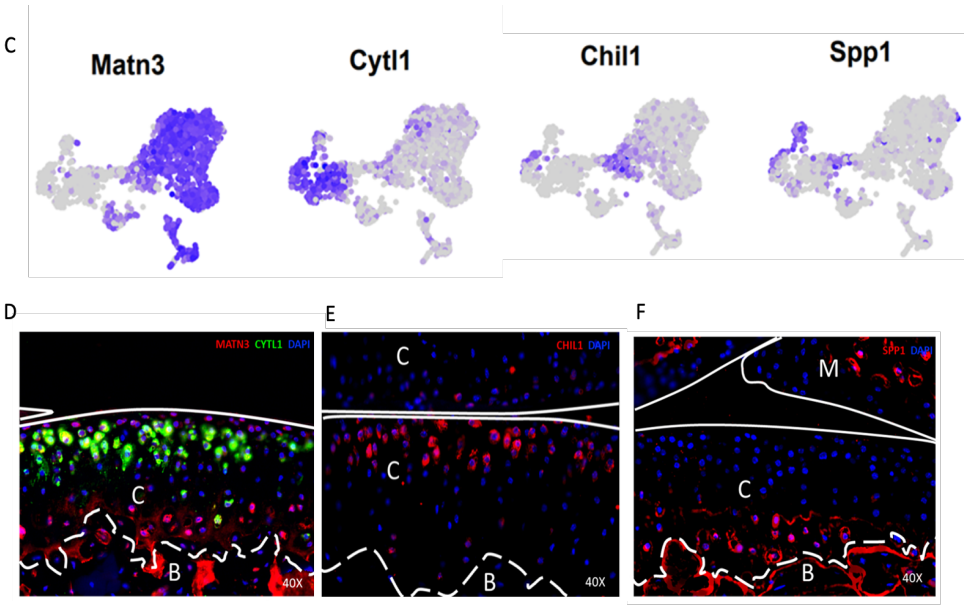

Figure 3. 16:Spatial characterization of chondrocyte subtypes. C)Feature plots showing the expression of Matn3, Cytl1, Spp1 and Chil1. D) Protein-level expression of Matn3 (red) and Cytl1 (green). E) Protein-level expression of Chil1 (red). F) Protein-level expression of Spp1 (red). DAPI marking the nucleus is in blue. C: Cartilage; B: Bone; M: Meniscus.

B6 subpopulations are recapitulated in scRNAseq of arthritic cartilage from human knee joints

Previous research [130] of human arthritic chondrocytes identified multiple populations of chondrocytes present. Samples from 10 patients undergoing a full knee arthroplasty identified 7 subpopulations that were defined as phenotypes within the OA knee which included: proliferative chondrocytes (ProC), pre-hypertrophic chondrocytes (PreHTC), hypertrophic chondrocytes (HTC), Regulatory Chondrocytes (RegC), Homeostatic Chondrocytes (HomC), Fibrocartilage (FC) and Effector Chondrocytes (EC). Single-cell sequencing data from this study was reanalyzed and seven clusters were identified that were also present in chondrocyte data from B6 joints (Figure 3. 17a). Of the seven previously identified human populations, Homeostatic, Hypertrophic and Fibrocartilage populations were identified in the new analysis. Additionally, human cartilage also had populations present in the B6 data including: *Cytl1* ^{high}, *Tnfaip6* ^{high} *Krt16* ^{high}, and *Chil1* ^{high}. Each cluster was high in *Acan* and had a unique transcriptomic profile that was restricted to each computationally identified cluster (Figure 3. 17b). Nearly all clusters had some expression of *Cytl1,* while HTC and FC populations were extremely high in *Col10a1* (Figure 3. 17c). Additionally, the FC population and Tnfaip6^{high} population

were high in genes indicative of fibrotic cells, fibroblasts and osteoblasts including *Col1a1, Thy1, Pdgfra, Mmp13, Alpl, Mef2c Pth1r Tnfaip6, Abi3bp, Prg4* and *s100a4* (Figure 3. 17d). Furthermore, homeostatic chondrocytes had high expression of transcription factors *Jun*, *Fos*, and *Fosb,* which were also present in mouse chondrocyte scRNASeq data (Figure 3. 17d, e).

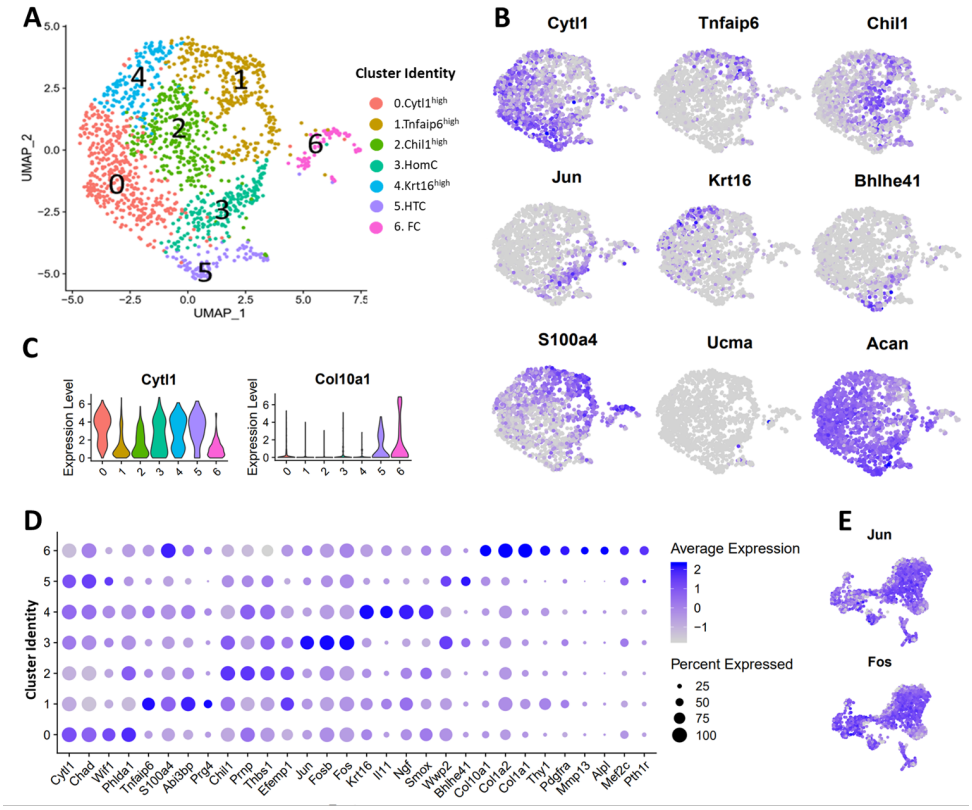

Figure 3. 17:Comparison of human and mouse articular chondrocytes. A) UMAP plots of various chondrocyte subtypes in human osteoarthritic knee joints. Colors indicate clusters of various cell types with distinct gene expression profiles. B) Feature plots showing the expression of key chondrocyte markers in human chondrocytes. Blue: high expression, grey: low expression. C) Violin plot showing the expression of Cytl1 and Col10a1 in human chondrocyte subtypes. D) Dot plot showing the expression of selected markers of various clusters. Dot size represents the fraction of cells expressing a specific marker in a particular cluster and intensity of color indicates the average expression level in that cluster. E) Feature plots showing the expression Jun and Fos in mouse chondrocytes

Strain specific differences occur at later timepoints after injury in knee joints populations

Single-cell RNA sequencing was employed to further elucidate the differences in murine cartilage between MRL and B6. There were 13 populations identified, including fibroblasts, osteoblasts, chondrocytes, endothelial, immune, erythroid,

mesenchymal stromal cells, and proliferating cells (Figure 3. *18*a). All stromal populations were distinctive in their gene expression profiles and robustly expressed known markers of cartilage, bone, and other joints supporting tissues (Figure 3. *18*b). Of interest, there were three populations of chondrocytes present in the data represented by clusters 1, 2 and 9, that were all high in expression of Acan. The proliferating population (cluster 9) also had expression of Mki67, a known gene of proliferating cells [146] (Figure 3. *18*b). Additionally, a small population of Osteoblasts (cluster 6) was high in Bglap or osteocalcin. Synovial fibroblasts (cluster 7) and fibroblast (cluster 0) populations were distinguished by their expression in Pdgfra, but synovial fibroblasts were also high in expression of Prg4.

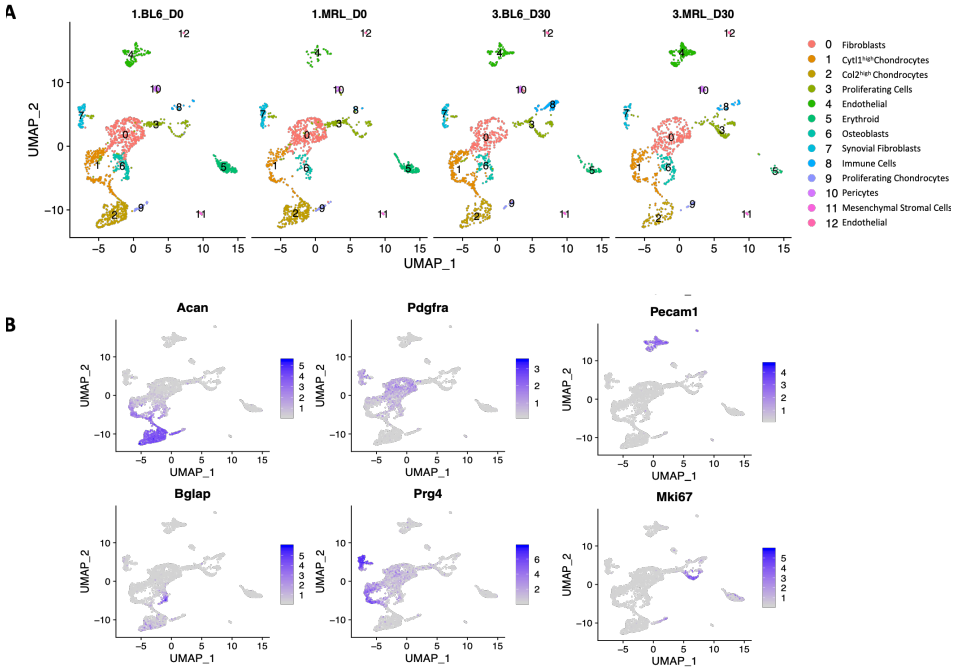

Figure 3. 18: Stromal Cell populations of B6 and MRL knee joints. UMAP of all cells sequenced identifying stromal and chondrocyte populations in uninjured (D0) and 4-weeks post injury (4W) knee joints of MRL and B6 animals (A) Feature plots describing key markers of stromal, bone and chondrocyte population. Purple color is representative of expression value (B)

Analysis of each population at all timepoints showed that MRL have significantly more fibroblasts at both timepoints than B6, as well as more proliferating cells (**Figure 3. *19***). MRL also have a lower number of Cytl1^{high} expressing chondrocytes compared to B6, although this population expanded after injury. In addition, MRL had a severe drop in

Col2^{high} cells after injury but show an extremely large expansion of endothelial cells compared to B6 as well as compared to their uninjured counterparts.

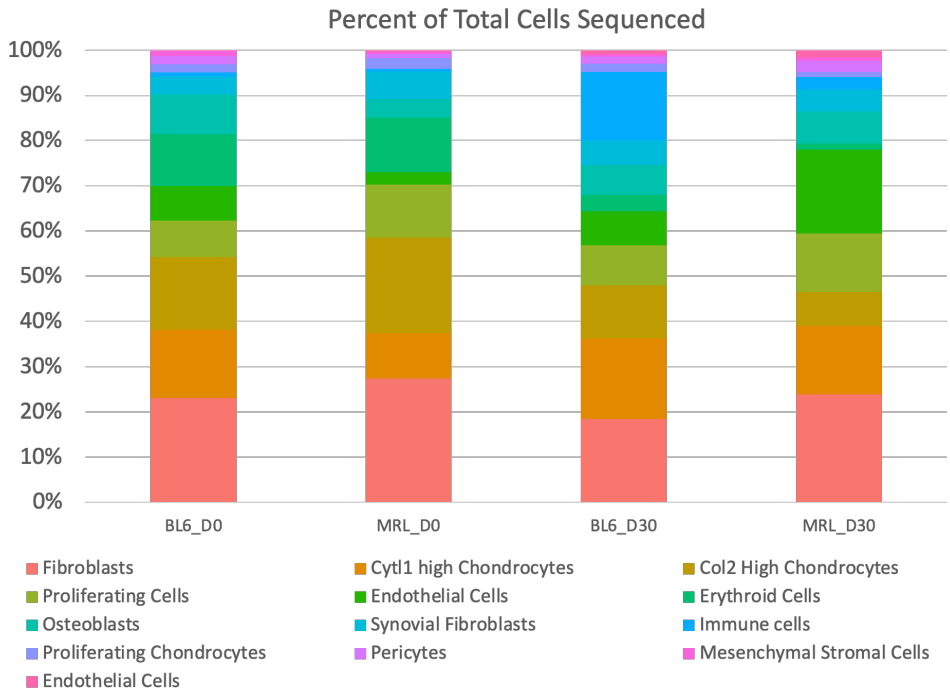

Figure 3. 19: Representation of each population as percent of total cells sequenced. Histogram representing all cell populations identified in single cell sequencing. Injured (4W) and uninjured (D0) of B6 and MRL are present as separate columns. Populations colors are based on cluster identified in *Figure 3.18*

Supplemental analysis of bone and cartilage populations identified additional changes to these cells occurring after injury and between strains (**Figure 3. *19***, **Figure 3. *20***). MRL still had an increased fibroblast population characterized by expression of *Pdgfra (***Figure 3. *21***). In addition, both B6 and MRL had an expansion of Cytl1^{high} chondrocytes, while MRL actually had less Col2^{high} chondrocytes. Prior to injury, MRL had significantly less osteoblasts, but had a stark increase after injury. MRL had significantly more proliferating chondrocytes than B6 prior to injury, which severely decreased after injury. In addition, B6 had a much higher number of mesenchymal-like cells that express multiple fibroblast markers prior to injury than MRL. This population decreased in both strains after injury and was named mesenchymal progenitors (**Figure 3. *20***, **Figure 3. *21***).

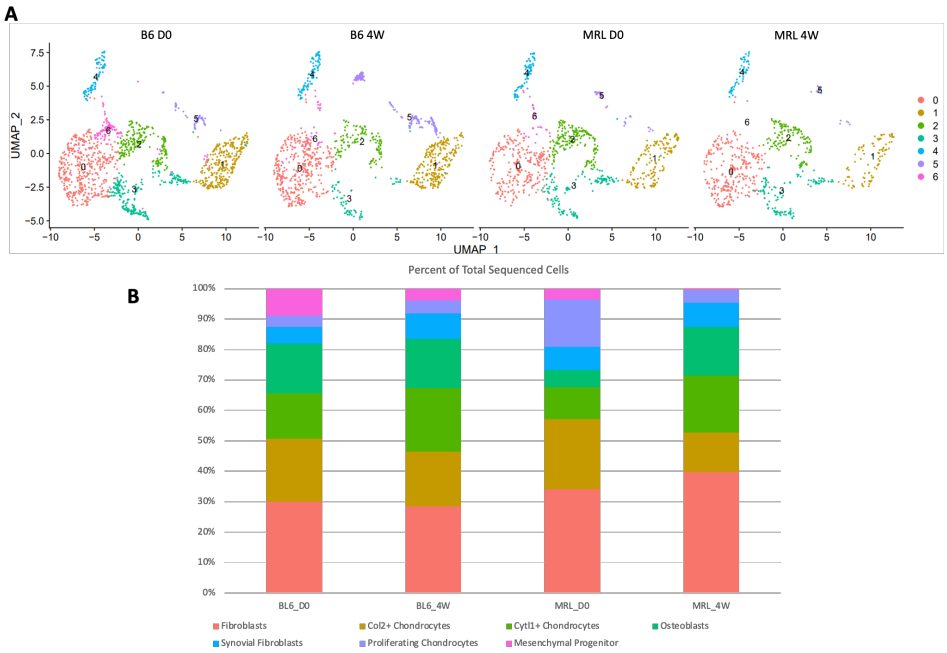

Figure 3. 20: Joint cells present omitting immune and erythroid contamination. Subpopulations of bone, cartilage and other joints supporting cells reclustered and split by timepoint (A). Histogram representation of MRL and B6 uninjured (D0) and 4-week post injury (4W) joints as a percent of total bone, cartilage, and joint supporting cells (B).

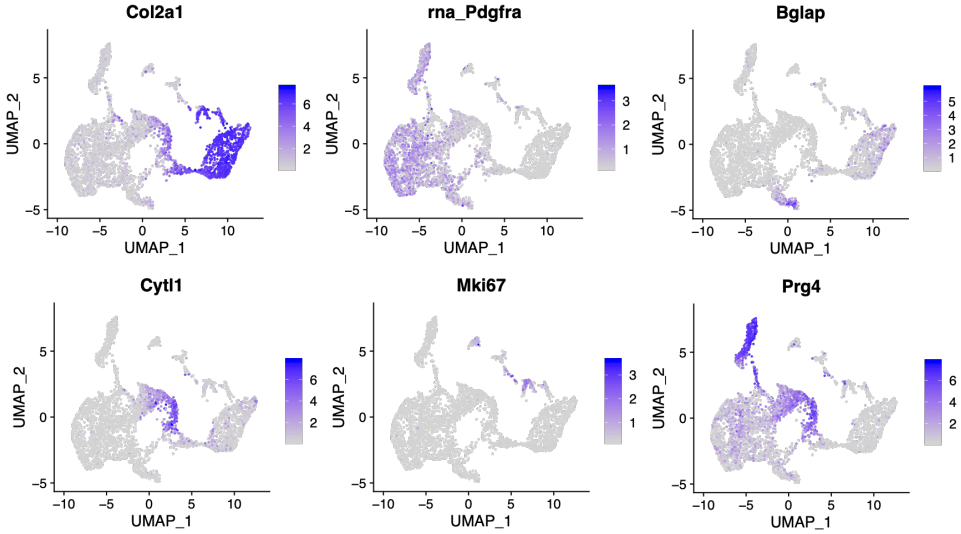

Figure 3. 21: Gene expression of re-clustered bone and cartilage cell populations. Marker genes specific for cartilage, bone, synoviocytes, fibroblasts and proliferating cells.

Cytl1high population of chondrocytes is layer restricted and expands post-injury

Immunohistochemical analysis of the cytokine-like 1 expression in the knee joints of MRL and B6 identified an expansion of cells expressing this protein after injury as show in the scRNAseq data (**Figure 3. *20***, **Figure 3. *21***). In both strains, there is limited expression prior to injury (**Figure 3. *22***a), while after injury MRL had an expansion of cells expressing

low amounts of *Cytl1*. In contrast, cells expressing *Cytl1* in B6 seemed to be similar in location and number but had stronger staining than their uninjured counterparts. Both strains showed robust expression in the intermediate layer of the articular cartilage, although MRL have a larger number of cells in this layer than B6.

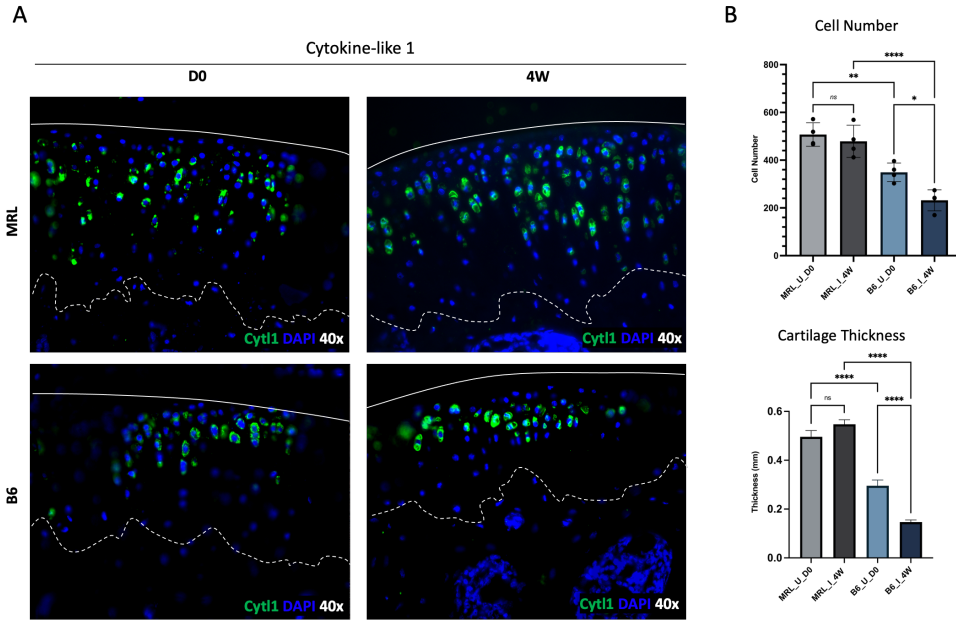

Figure 3. 22:Histomorphometry analysis of MRL and B6 cartilage tissue. Immunohistochemical analysis of Cytokine-like 1 protein expression in MRL and B6 knee joints after injury (A) Cell number (left) and cartilage thickness (right) analysis using histologically stained tissue sections of uninjured and injured joints. ns: not significant, *p<0.05, **p<0.01, ****p<0.0001 (B)

Histomorphometry analysis identifies stark differences in cartilage between MRL and B6

Examination of the cartilage as a whole tissue identified changes in cell number and tissue thickness as a result of injury (**Figure 3. *22***b). Prior to injury, B6 had less cells within the articular cartilage than MRL. At 4-weeks post injury, there appeared to be a significant loss of cells in B6 cartilage (nearly half), compared to MRL. Moreover, there was no significant change in cell number between injured and uninjured cartilage tissue in MRL. Furthermore, MRL cartilage was nearly twice as thick as B6 prior to injury (**Figure 3. *22***b). MRL also showed no significant difference in cartilage thickness between conditions.

Discussion

Within the last decade, studies that define the cellular makeup of the articular cartilage have been extremely limited in number [118, 147]. Most studies have focused on identifying the bone marrow microenvironment [148, 149] and in turn, its reaction to joint injury or fracture. Currently, there is a large gap in understanding of the function that chondrocytes have in joint recovery after trauma. This study identified multiple chondrocyte and supporting subpopulations in the articular joint that each have a distinct profile and potential function in homeostasis of the tissue. By comparing the articular cartilage of MRL and B6 using a TCI model, this study further identified changes at the cellular level in response to injury.

Of the stromal populations identified, endothelial cells had the largest expansion after injury as well as were much higher in population in MRL than B6. Endothelial cells functionally line vascular tissue and act to regulate nutrient exchange between the bloodstream and surrounding tissues. Within the bone marrow microenvironment, they are essential in producing growth factors and regulatory cytokines that aid in differentiation and movement of hematopoietic stem cells [150]. In addition, endothelial cells have been shown to aid in the development of new bone by promoting angiogenesis and stem cell recruitment [2]. While endothelial cells have been studied heavily in fracture repair, there is very little information pertaining to their role in cartilage homeostasis and regulation. Previously, research has shown that a reduction in vasculature or in angiogenesis in bone leads to impaired bone maintenance and repair, indicating that endothelial cells and pericytes are highly important in bone remodeling and healing [151]. Specifically, disruption of Notch signaling to endothelial cells led to a both bone and cartilage defects, indicating endothelial interact with chondrocytes to maintain the cartilage integrity [151] through delivery of nutrients via angiogenesis. Additionally, in ear cartilage, MRL have been shown to have an increase in CD31 positive cells indicating an influx of endothelial cells to the tissue after injury when compared to B6 [152, 153]. This alludes to the idea that an increase in vasculature in MRL aid in cartilage regeneration and tissue healing after traumatic injury.

MRL have been previously shown by several groups to have a regenerative capability in soft tissues, nerves, ear cartilage and full thickness articular cartilage lesions [73]. In addition, it has also been shown that MRL have more chondrocytes as well as a thicker cartilage layer than B6 [152] in uninjured joints. This study confirms that MRL have an increased number of chondrocytes compared to B6 both before TCI injury as well as out to 4-weeks post injury. MRL have also been shown to have an increase in cellular proliferation and very specific apoptotic cell profile in the articular cartilage. Prior to injury, MRL have very little apoptosis but after trauma there is clear apoptotic signal in the deep layer of the articular cartilage; a trend seen in **Error! Reference source not found.** where the deep layer of the AC has lost proteoglycan staining (Figure 3. 23). This indicates that MRLs have a more robust intermediate layer of chondrocytes that are not prone to cell death or ECM degradation. Additionally, more research is needed to understand what signaling is occurring at the cartilage-bone interface that is causing deep layer chondrocytes to undergo cell death. Furthermore, increases in proliferating chondrocytes seen in **Figure 3. *20***, identified that MRL joints are more proliferative than B6, specifically in their chondrocyte populations. Fitzgerald et al previously showed that B6 lack the capability to regenerate the articular cartilage after the induction of a full thickness lesion, while MRL could completely regenerate both chondrocytes and ECM [74].

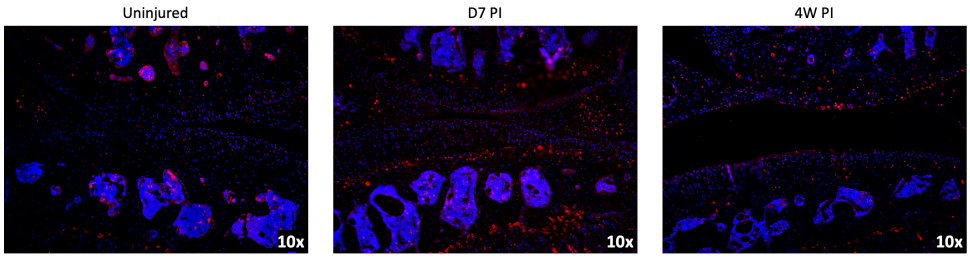

Figure 3. 23:TUNEL staining of formalin fixed paraffin embedded (FFPE) MRL joints at D0 (uninjured, left), Day 7 post injury(middle) and 4-weeks post injury (right). Apoptotic cells are marked by red staining indicating fragmented DNA. Dapi staining was used for identification of nuclei. Image magnification 10x.

In addition to the differences in cellular proliferation, MRL also have a more robust intermediate layer of chondrocytes that express *Cytl1*. *Cytl1* has been shown in many studies to have a positive effect on chondrogenesis and aids in cartilage homeostasis, increases pro-angiogenic signaling and regulates chemotactic capabilities [154]. *Cytl1*

expression has been shown to dramatically increase in mesenchymal stromal cells and induce chondrogenic differentiation in limb bud mesenchyme without altering hypertrophic chondrocytes [155]. When completely knocked down in mice, there are no changes to the development of bone and cartilage indicating Cytl1 is important in healing and homeostasis rather than maturation [156]. This function is mostly likely through binding to CCR2, which leads to downstream activation of ERK signaling and stimulation of transcription factor *Sox9*, as well as insulin growth factor 1 (*Igf1)* which promotes chondrogenesis. Additionally, Cytl1$^{-/-}$ mice show a more severe OA phenotype and advanced cartilage degradation when subjected to destabilization of the medial meniscus (DMM) surgery, indicating this gene is required for chondrocyte stability during injury and joint destabilization.

Furthermore, *Cytl1* has been identified as a novel cytokine produced by *CD34*+ bone marrow cells [157]. Structurally this cytokine has high affinity to adopt an IL-8-like chemokine fold that is particularly consistent with *CCL2* known as monocyte chemoattractant protein 1 (*MCP1*). *CCL2* has been shown to be involved in cartilage homeostasis and strongly binds to *CCR2*, a receptor on leukocytes that promotes chemotaxis of myeloid cells to regions of tissue destruction [158, 159]. Due to the high affinity of *CCL2* and *Cytl1* for binding *CCR2* [160], the increased population of *Cytl1*$^{+}$ chondrocytes in MRL, compared to B6, indicates that *Cytl1*$^{+}$chondrocytes may be functionally important in recruiting macrophages into the synovial joint to promote damage control through an anti-inflammatory pathway. Additionally, *Cytl1* has been shown to be expressed on endothelial cell progenitors and promote angiogenesis through a pathway similar to *VEGFa [161]*.

Furthermore, MRLs had a severe drop in *Col2*^{high} cells after injury compared to uninjured counterparts (**Figure 3. *20***), although they have an increase in collagen deposition in the matrix as shown by IHC (**Figure 3. *6***). Proteomic analysis previously showed that an increase in collagen 2 synthesis was associated with OA cartilage [162]. Additionally, studies of cartilage degradation identified aggrecan composition as important in preventing proteolytic degradation of collagen 2 and thus strengthening the articular cartilage [163].

While an increase in collagen 2 has been primarily associated with arthritic tissue, this protective effect of aggrecan may aid in recruitment of M2 polarized macrophages that help heal the joint tissues and potentially induce deposition of new GAGs in the ECM [164]. This phenomenon gives rise to the idea that MRL's *Acan+* intermediate layer of articular chondrocytes may aid in the protection of ECM breakdown compared to B6. Additionally, sustained collagen 2 and *Cytl1* expression in MRL chondrocytes may both recruit macrophage populations that positively respond to DAMPs in the joints space that further an anti-inflammatory phenotype. Molecules responsible for macrophage polarization have also been shown to promote chondrogenesis [165]. Additionally, Mannose Receptors on macrophages such as MRC1, have been shown to bind degraded collagens and internalize them; a function that decreases local DAMPs and promotes an anti-inflammatory environment [164-167]. In short, the initial shock of traumatic injury may be combatted by an interaction between chondrocytes and M2 macrophage populations by production of *IL-4, IL-10,* and *IGF [167]*. Increase production of these molecules has an anti-inflammatory joint effect, and in turn aids in chondrogenesis, ECM turnover, and cartilage repair as seen in MRL joints.

Chapter 4. Characterizing Immune Cell Infiltration in the Murine Joint Microenvironment after Traumatic Knee Injury

Abstract

Post Traumatic Osteoarthritis (PTOA) is a painful joint disease characterized by degradation of bone, cartilage, and connective tissues. PTOA is initiated by trauma to joint-stabilizing tissues, such as the anterior cruciate ligament, medial meniscus or by intra-articular fractures. In humans, nearly half of joint injuries progress to chronic PTOA, while the remainder spontaneously resolve without progressive degeneration. To understand molecular programs contributing to PTOA development, we examined injury induced fluctuations of immune cells and transcriptional shifts in the synovial joint microenvironment in PTOA-susceptible C57BL6/J (B6) and PTOA-resistant MRL/MpJ (MRL) mice strains. By inducing injury using a Tibial Compression Injury (TCI) model, this study could identify real-time changes occurring after injury that are essential in both joint protection and joint degradation. Single cell sequencing of synovial fluid and synovial tissue in both strains was conducted starting with uninjured mice and progressing over a time course of days 1, 3, 7 and weeks 2 and 4 post injury. Both tissue resident and infiltrating immune cell populations from the synovial capsule were identified. In addition, significant trends in monocyte and macrophage populations were identified in both MRL and B6 joints. these finding alluded to a potential myeloid driven anti-inflammatory response after injury in MRL that hinders pro-inflammatory signaling seen in B6 joints.

Overall, this data suggests that the PTOA resistant MRL/MpJ mice are more capable of clearing debris and apoptotic cells induced by the inflammatory response to injury because of their increase in activated macrophages within the synovial tissue and joint space. Additionally, this sustained population of macrophages may be responsible for tissue remodeling after ACL injury, allowing for decreased apoptosis of cartilage and bone cells and creating a joint more resistant to mechanical damage.

Introduction

In humans, nearly half of knee joint injuries progress to chronic Post-Traumatic Osteoarthritis (PTOA), while the remainder spontaneously resolve without progressive degeneration. The pathogenesis and onset of this disease is still not fully understood. It has been shown that multiple factors contribute to disease progression including genetics, epigenetics, and immune responses [168]. To better understand the molecular programs contributing to PTOA resistance, this chapter examines the role the immune system plays in inflammation and wound healing in response to ACL injury of both C57Bl6/J (B6) and the superhealer, MRL/MpJ (MRL) strain of mice [73].

PTOA progression can be classified into several early phases starting at trauma. These phases are categorized based on the response of the immune system, complex metabolic changes to joint resident cells and changes to cartilage composition and homeostasis that occur. After initial trauma, individuals enter the intermediate phase of disease progression where there is a high amount of cell necrosis, swelling of the cartilage, and loss of Proteoglycans (PGs) and Glycosaminoglycans (GAGs). Next, is the acute phase, which is characterized by an influx of immune cells that enter the synovial joint. This migration results in cell apoptosis, inflammation, cartilage degradation and sometimes internal joint bleeding [168]. Following this internal destruction of the joint is the asymptomatic phase in which many individuals undergo surgical interventions and pain management programs such as physical therapy. In those individuals that do not receive reconstructive surgery, this joint trauma can progress to chronic PTOA where individuals suffer from severe pain and potential immobility long term [169]. To better understand the advancement to chronic PTOA, it is important to reveal damages to the joint tissues that are triggered by the immune system and determine specifically when they occur in these early phases of trauma response. A more complete understanding of the immune systems role will aid in the development of future treatments and preventative measures that can be taken by individuals suffering from joint trauma.

Several studies have shown arthritis progression is dependent on the immune systems response to injury [170-174]. In early disease onset, initial damage to joint tissues

is caused by synovial inflammation and production of matrix degrading enzymes from myeloid derived immune cells. The immune system is divided into two sub-systems classified as innate and adaptive immunity. The innate immune systems has been previously shown to play specific roles in inflammation and wound healing in PTOA through inhibition of pro-inflammatory signaling by alternatively activated macrophage populations [175-177]. In response to injury, the first line of defense is mediated by the innate immune component that deploys a neutrophil and macrophage response. This initial response is non-specific and is designed to protect the body when triggered by specific certain molecular patterns [178] that are produced by stressed or apoptotic chondrocytes as well as by degraded fragments of the extracellular matrix (ECM). The dissemination of joint inflammation in PTOA is prolonged by the response of innate immune cells to these damage associated molecular patterns (DAMPs), complement factors, and secretion of other catabolic molecules by resident stromal cells, such as degrading enzymes known as matrix metalloproteins (MMPs) [179]. DAMPs play a large role in triggering damage early in the joint tissue since these signaling molecules are derived from products of degraded proteoglycans present in the articular ECM. After initial damage, cartilage, MMPs aid in the release of collagens and other ECM proteins from the cartilage caused by joint destabilization and mechanical tissue degradation [180]. These solubilized proteins can then interact with Pattern Recognition Receptors (PRRs), such as Toll-like receptors (TLRs) [181] on nearby synovial cells. This recognition leads to activation of the inflammasome, production of cytokines and chemokines, and promotion of inflammatory signaling resulting in recruitment of neutrophil and macrophage populations to the injury site [182].

Several studies have further reviewed the role of monocytes and macrophages in PTOA pathogenesis in human patient serum and synovial fluid samples [176]. Transcriptional identification of cellular markers and spatially identifying populations using *in vivo* labeling systems has shown that activated macrophage levels do correlate with the severity of PTOA [177]. Within the joint, there are several types of monocyte-derived and resident macrophage populations that are essential in maintaining bone and joint homeostasis in an anti-inflammatory environment [58]. Many immune cells,

including macrophages, reside in the infrapatellar fat pad; a small layer of white adipose tissue that is highly vascularized and sensitive to changes within the synovial joint, especially during injury. During injury, this tissue becomes a hub for infiltrating immune cells.

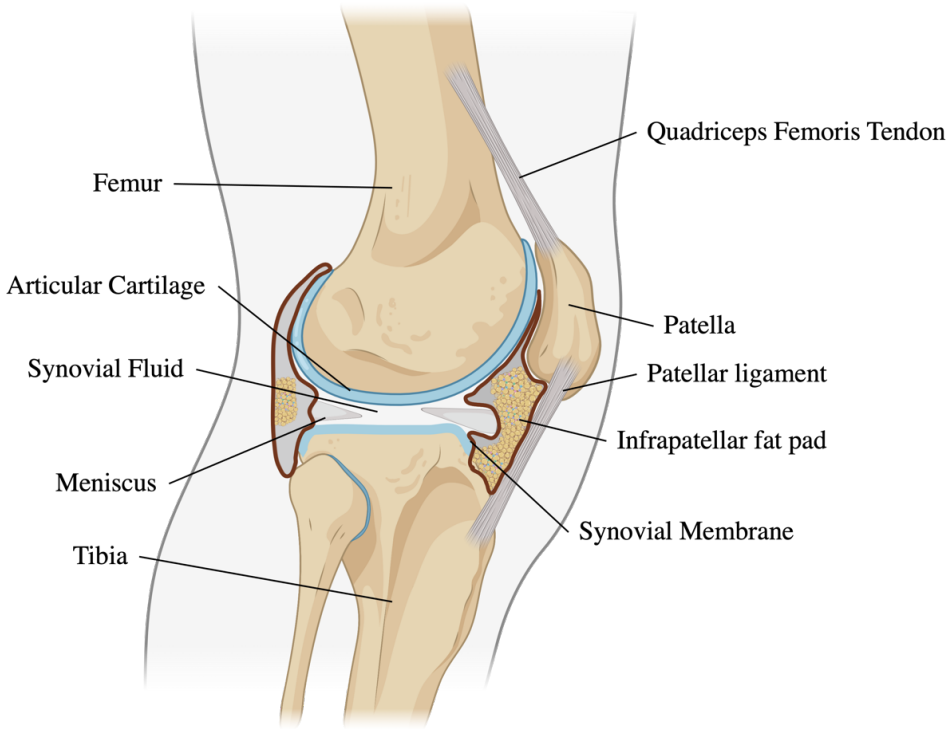

Figure 4. 1 Schematic of articular knee joint. The articular knee joint is encapsulated by a layer of fibroblasts and endothelial cells known as the synovial membrane [170]. Under this membrane is a layer of adipose tissue known as the infrapatellar fat pad (yellow). These structures surround the cartilage (blue) and meniscus (light grey). Image created with Biorender.

Error! Reference source not found. depicts a complex structure known as the synovial cavity that is supported by the fat pad. In a healthy joint, this capsule functions to support the joint and aid in movement through lubricating the joint surfaces to facilitate movement and reduce friction [183]. It is filled with a nutrient rich fluid, known as the synovial fluid and lined by a combination of Type A and Type B synovial fibroblasts, as well as and endothelial cells, lymphocytes, mast cells, adipocytes, and interstitial macrophages [184]. Synovial fluid is primarily composed of hyaluronan, lubricin, proteinase, collagenases, and prostaglandins [183, 185, 186]. Macrophages are the major immune cell present in healthy synovial tissue of the joint. A specific subset of

macrophages, known as *Lyve1* macrophages, line and maintain the integrity of the synovial cavity to keep the articular cartilage unperturbed by endogenous DAMPs that form from normal wear and tear of the joint [187]. During acute inflammation or chronic inflammatory diseases such as rheumatoid arthritis (RA), there is an increase in monocytes, activated macrophages, and synovial fibroblast populations that enter the joint space due to a disruption of this "lining" [188, 189]. This cellular influx leads to an expansion of the synovial pannus and increases degradation of the articular cartilage due to a spike in metalloproteinases secreted by infiltrating monocyte-derived macrophage populations [184]. These infiltrating macrophages are in large the main contributor to the sustained inflammation in the joint during OA progression [190]. They have been previously shown to have a more pro-inflammatory phenotype and release molecules associated with tissue degradation [191]. Although tissue resident macrophages are extremely important in resolving inflammation in RA the migration of non-resident macrophages can be detrimental to the tissue integrity. By identifying key cell types that push the tissue towards a more inflammatory phenotype, such as infiltrating macrophages, we can better understand their function in OA progression and potentially use them as drug targets for long term damage prevention.

To understand the progression of PTOA fully, the role of the immune system needs to be studied at a more detailed level than it has been previously attempted. The field has shown that a switch from a normal steady joint state to an inflammatory environment by infiltrating monocytes has a negative impact on joint integrity and disease outcome, although specific immune cell sub-types have still not been characterized. This chapter shows that by leveraging a non-surgical Tibial Compression Induced (TCI) injury model in mouse strains with varying susceptibilities to PTOA, we can study the immune response in the joint without inducing an immune response triggered by the surgery [192]. This study employed single-cell RNA sequencing (scRNAseq) to further identify tissue resident and infiltrating immune cell populations in the synovial capsule and infrapatellar fat pad with unprecedented resolution, from B6 and MRL mice at early and late stages of disease progression after trauma, to identify strain specific differences that may correlate with a disease protection phenotype.

Methods

Animal Care and Tibial Compression Joint Injury

All animal experimental procedures were completed using male mice in accordance with the Institutional Animal Care and Use Committee (IACUC) guidance at Lawrence Livermore National Laboratory and the University of California, Davis in AAALAC-accredited facilities. Male MRL (MRL/MpJ, Stock # 000486), B6 (C57Bl6/J, Stock # 000664) and *Trem2*$^{-/-}$ (C57BL/6J-Trem2^{em2Adiuj}/J, Stock # 027197) animals were purchased from Jackson Laboratory and bred in house using standard procedures. At 10-weeks MRL, B6 and *Trem2*$^{-/-}$ mice were placed under anesthesia using isoflurane inhalation and placed in a horizontal position to prepare for a non-invasive knee joint injury [129]. The right tibia was placed between two plates and subjected to single tibial compression overload at 1 mm/s displacement rate. Anterior Cruciate Ligament rupture occurred after a total compressive force, between 12N-18N was applied using an electromagnetic material testing system (ElectroForce 3200, TA Instruments, New Castle, DE, USA). Mice were given a single 50uL dose of 0.9% sterile saline (Becton, Dickinson and Company, Franklin Lakes, NJ, USA), and a single dose of Buprenorphine (0.01 mg/kg) administered immediately post-injury for pain relief. Post injury mice returned to normal cage activity and were housed in standard caging. Mice were allowed free range of the cage while on 12h light/dark cycles for up to 4 weeks, prior to euthanasia at specific time points, as indicated in Error! Reference source not found..

Histological assessment of the articular joint

Right hindlimbs were collected from uninjured (Day 0) and injured male mice at Day 7 (D7) and 4-weeks (4W) post-injury and processed for histological evaluation as previously described in chapters 1 and 2. Briefly, whole hindlimbs, without the foot, were fixed in 10% Neutral Buffered Formalin (NBF) overnight at 4ºC. Then decalcified using 0.5 M EDTA using the weight loss-weight gain method for measuring decalcification status and finally processed for paraffin embedding. Once embedded, joints were sectioned in the sagittal plane at 6µm and serial medial sections were prepared for histological assessment of joint tissue integrity at all timepoints. Sections were stained on charged glass slides using

0.1% Safranin-O (0.1%, Sigma, St. Louis, MO, USA; S8884) and 0.05% Fast Green (0.05%, Sigma, St. Louis, MO, USA; F7252) using standard procedures (IHC World, Woodstock, MD, USA). Slides were imaged using a Leica DM5000 microscope (Leica Microsystems, Wetzlar, Germany). ImagePro Plus V7.0 Software, a QIClick CCD camera (QImaging, Surrey, BC, Canada), and ImageJ V1.53 Software were used for imaging and photo editing.

OARSI Histological Scoring of Joint Degradation for Trem2$^{-/-}$ after injury

Selected serial medial sections from B6 and *Trem2*$^{-/-}$ were stained using Safranin-O and Fast Green as described above and subjected to a blind semi-quantitative scoring by five individual scientists using the OARSI Histopathology Scoring System [193]. All scores were collected, and the average score was plotted to determine the grade of joint damage that had occurred at 4W post injury compared to uninjured joints.

Immunohistochemistry

Sagittal sections from D0, D7, 4W knee joints of all mice strains were used for IHC. Primary antibodies were incubated overnight at 4°C in a dark, humid chamber following antigen retrieval with Unitrieve (NB325 Innovex Biosciences, Richmond, CA. USA) and blocking using Background Buster (NB306 Innovex Biosciences, Richmond, CA. USA) per manufacturer's instructions. Secondary antibodies were incubated for 2 hours at room temperature in a dark, humid chamber at 1:500. Negative control slides were incubated with secondary antibody-only. Stained slides were mounted with Prolong Gold with DAPI for nuclei staining (Molecular Probes, Eugene, OR. USA). Slides were imaged using a Leica DM5000 microscope. ImagePro Plus V7.0 Software, QIClick CCD camera (QImaging, Surrey, BC, Canada) and ImageJ V1.53 Software were used for imaging and photo editing. Primary antibodies include: Trem2 [1:100; ab95470 Abcam, Cambridge, UK], CD206 [1:100; ab64693, Abcam, Cambridge, UK]. Secondary Antibodies include: Goat anti-rabbit 594 (1:1000; A11037, Thermofisher, Waltham, MA. USA), Donkey anti-goat 488 (1:1000; A11055, ThermoFisher, Waltham, MA. USA).

Single-cell RNA sequencing

D0 and injured joints from D1, D3, D7, 2W, and 4W post-injury (n=5/group) were used for scRNA-seq analysis from both B6 and MRL joints. Briefly, right hindlimbs from injured and uninjured animals were dissected and of skin and muscle, while maintaining the integrity of the knee joint and retaining synovial fluid between tibia and femur. Cells residing in the synovial capsule were released by dissociating the joint and separating the femur and tibia into 7.5 mL of digestion cocktail containing 3% Collagenase 1 solution (Worthington Biochemical, Lakewood, NJ; CLS-1) and 100 µg/mL DNase I (Roche, Basel, Switzerland; 11284932001) in DMEM/F12. Joint tissue was digested while shaking at 37°C for two 1-hour digests, filtered through a 70µm nylon cell strainer into a 50mL conical, followed by a PBS wash step between each digest. After the final digest, cells were pelleted at 4°C under 600g centrifugation, and subjected to red blood cell (RBC) lysis using ammonium-chloride-potassium (ACK) lysis buffer (ThermoFisher Scientific, Waltham, MA, USA; A1049201). $CD45^+$ immune cells were enriched using CD45 conjugated magnetic microbeads followed by Miltenyi Biotech MACS separation with LC columns. Both the immune ($CD45^+$) and non-immune ($CD45^-$) cell populations were sequenced independently using a Chromium Single Cell 3' Reagent Kit and Chromium instrument (10X Genomics, Pleasanton, CA). Library preparation was performed according to manufacturer's protocol and sequenced on an Illumina NextSeq 500 (Illumina, San Diego, CA, USA).

scRNAseq data analysis

Raw scRNAseq data was processed using the 10x Genomics Cell Ranger software according to manufacturer's recommended protocols (10X Genomics, Pleasanton, CA, USA). Briefly, raw base call (BCL) files generated by Illumina NextSeq 500 sequencer were demultiplexed into FASTQ files using Cell Ranger 'mkfastq'. Aligning sequencing data to the mouse reference genome (mm10), barcode counting, and unique molecular identifier (UMI) counting were performed using Cell Ranger 'count'. Remaining analysis was performed using Seurat R package, which performs quality control and subsequent

analyses on the feature-barcode matrices produced by Cell Ranger. Output files from Cell Ranger were read into Seurat and cells with fewer than 500 detected genes/cell and genes that were expressed by fewer than 5 cells were filtered out. Next, the data was normalized by employing a global-scaling normalization method 'LogNormalize' and a set of highly variable genes was identified. Then the data from various timepoints were integrated for downstream analysis. After quality control procedures and integration were complete, data was scaled, and the dimensionality of the data was reduced by principal component analysis (PCA). Subsequently, cells were grouped into an optimal number of clusters for de novo cell type discovery using Seurat's 'FindNeighbors' and 'FindClusters' functions. A non-linear dimensional reduction was then performed via uniform manifold approximation and projection (UMAP) and various cell clusters were identified and visualized. Marker genes per cluster were calculated using Seurat's 'FindAllMarkers' function. To characterize monocytes and macrophages in detail, Mono/Mac cluster was extracted and analyzed as described above. Proliferating cells and a small subset of T cells identified among Mono/Macs were removed and Csf1r- and Cd14-positive monocyte and macrophage subclusters were further analyzed to identify various subtypes and cell type-specific changes. Gene expression plots were created using Seurat's 'VlnPlot', 'DotPlot', and 'FeaturePlot' functions. Differential gene expression analysis was performed using a pseudo-bulk RNAseq approach, treating each cell as a sample. The Deseq2 package[194] was utilized to perform differential expression analysis between experimental conditions. .. Genes with a p-value of <0.05 and a fold change ≥ 1.5 were considered differentially expressed. Ontology enrichment analysis on differentially expressed genes was performed using Enrichr[37].

Flow cytometry analysis

Single cell suspensions from all injured and uninjured knee joints were generated as previously described in the single-cell RNA sequencing section. Cells were blocked using Rat Anti-Mouse CD16/CD32 (Stock # 14-0161-82, Mouse Fc Block; BD ThermoFisher, Waltham, MA. USA) at 4^{o}C for 10 minutes. Samples were then incubated with an antibody cocktail (all purchased from Thermo Fisher) specific for macrophage characterization containing the following antibodies at a 1:100 dilution: PerCP CD45

Monoclonal Antibody (Clone: EM-05, Stock# MA110234), eFluor 506 CD11b Monoclonal Antibody (Clone: M1/70, Stock# 69-0112-82), PE F4/80 Monoclonal Antibody (Clone: QA17A29, Stock 157304), APC CD206/MMR Monoclonal Antibody (Clone: MR6F3, Stock# 17-2061-82), FITC TREM2 Monoclonal Antibody (Clone: 78.18, Stock# MA528223) and Sytox Blue Dead Cell stain for viability. Flow cytometric analysis was performed on a BD FACSMelody system.

Analysis software and statistical analysis

Statistical analyses were performed using GraphPad Prism. Flow cytometry data is presented from three to five biological replicates per strain (n= 3-5 males). A one-way ANOVA and post-hoc Bonferroni's Test were used to assess statistically significant differences of mean expression values. OARSI scoring is presented from four biological replicates (n=4 males) per strain and scored by five individual scientists. A one-way ANOVA and post-hoc Bonferroni's Test were used to assess statistically significant differences of mean expression values. Expression of immune cell marker in chondrocyte culture is presented from three (n=3 males) biological replicates. An unpaired students t-test and post-hoc Bonferroni's Test were used to assess statistically significant differences of mean expression values. All results were considered statistically significant for p values < 0.05.

Micro-computed tomography (uCT) Quantitative Analysis

Uninjured/Contralateral left and injured right hindlimbs from male B6 and Trem$^{-/-}$ were collected at 6-weeks post injury for quantification of bone structure and osteophyte formation. Samples fixed for overnight at 4^{o}C using 10% NBF and stored in 70% EtOH at 4^{o}C until scanned. Whole knees were scanned using a SCANO μCT 35 (Wangen-Brüttisellen, Switzerland) according to the rodent bone structure analysis guidelines (X-ray tube potential = 55kVp, intensity = 114 μA, 10 μm isotropic nominal voxel size, integration time = 900 ms) and as previously described [194, 195]. Trabecular bone in the distal femoral epiphysis was analyzed by manually drawing contours on 2D transverse slides; the volume of interest was designated as the region of trabecular bone enclosed by the growth plate and subchondral cortical bone plate. Trabecular bone volume per total

volume (BV/TV), trabecular thickness (Tb.Th), trabecular number (Tb.N), trabecular separation (Tb.Sp), and other microstructural outcomes were quantified using the manufacturer's analysis software. Osteophyte volume in injured joints were quantified by drawing contours around all heterotopic mineralized tissue attached to the distal femur, proximal tibia, patella, fabella, and menisci. Total mineralized osteophyte volume was calculated as the volumetric difference in mineralized tissue (excluding the femur and tibia) between injured and uninjured/contralateral joints.

Micro-Computed Tomography Statistics.

Statistical analysis was performed using two-way ANOVA and Student's T-test with a two-tailed distribution, with two-sample equal variance (homoscedastic test). For all tests, $p<0.05$ was considered statistically significant, after a Bonferroni correction.

Results

Profiling murine synovial immune populations using single cell RNA sequencing of MRL and B6 knee joints

As shown in Chapter 3, injured hindlimbs of MRLs show a significant difference in their resistance to cartilage breakdown in comparison to B6 4-weeks after ACL rupture using the tibial compression injury (TCI) model (**Error! Reference source not found.**); a phenotype that is sustained out to 12-weeks post-injury [99, 128].

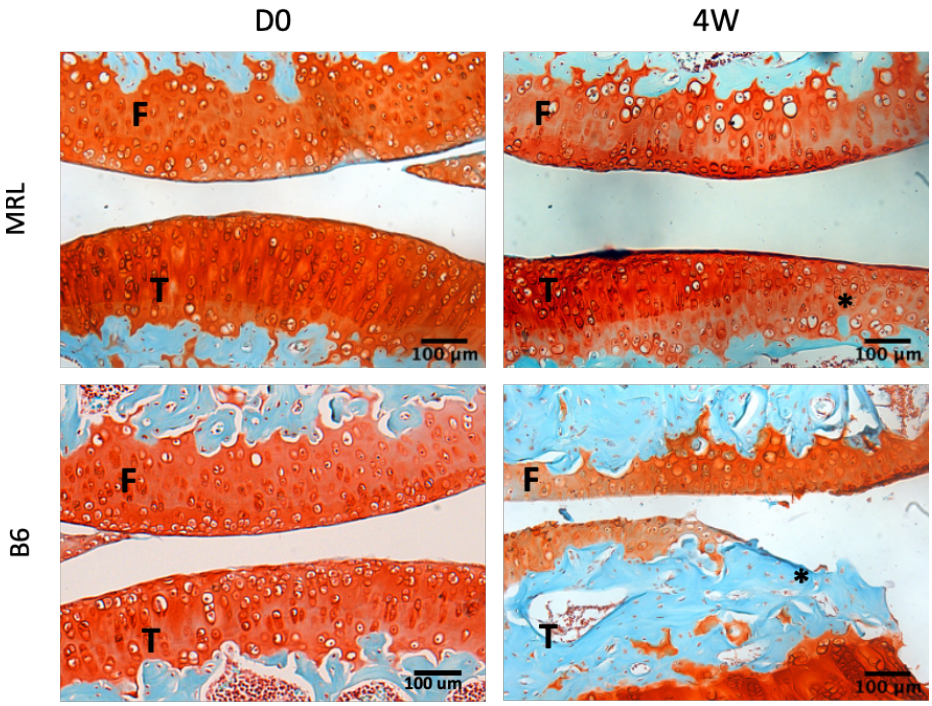

Figure 4. 2. Histological Assessment of PTOA onset in MRL and B6. Formalin-fixed, paraffin embedded murine hind knee joints were stained using safranin-o and fast green to identify differences in tissue morphology after injury. PTOA resistant MRL (top row) show little loss of staining after injury in the articular cartilage of the femur and tibia (red) indicating little to no loss of proteoglycan content in the cartilage matrix (top right, * asterisk). PTOA susceptible B6 (bottom row) show severe degradation of bone (blue,) and cartilage (red) in the tibia, and loss of some cartilage in the femur after injury (bottom right, * asterisk). Scale bar = 100um. Magnification 20X. F-Femur, T-Tibia.

To identify specific changes to the immune profile of these mice before and after TCI, synovial joints were enzymatically digested to a single cell suspension and Fluorescently Activated Cell Sorting (FACS) was used to enrich for viable, CD45+ immune cells from uninjured, day 1, day 3, day 7, 2-weeks and 4-weeks post injury (**Error! Reference source not found.**). Single-cell sequencing was conducted to comprehensively examine the immune profile of PTOA-susceptible and PTOA-resistant phenotypes of the synovial joint.

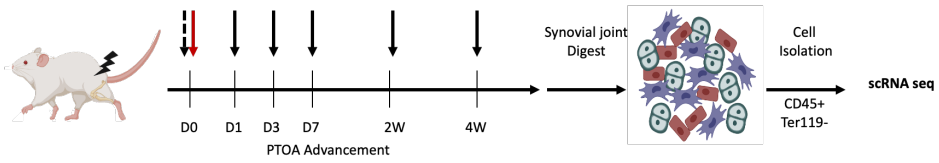

Figure 4. 3:Workflow for murine knee single-cell sequencing and flow cytometry. Uninjured murine joints were collected at Day 0 (dotted black arrow). Following tibial compression (red solid arrow), injured joints were collected at Days 1, 3, 7, 2-weeks and 4-weeks (solid black arrows) post injury and prepared for single-cell sequencing. Digested

immune cells (CD45+) were sorted using FACS to exclude stromal (CD45-) and erythroid lineage (Ter119+) cells before conducting single-cell RNA sequencing.

Single-cell sequencing identified seven (7) immune cell clusters including: Neutrophils, Macrophages, B cells, Proliferating Myeloid cells, Proliferating Neutrophils, T/NK cells, and Dendritic cells (**Error! Reference source not found.**a). All clusters highly expressed *Ptprc* (CD45) (**Error! Reference source not found.**b) and were identified based on specific cell markers of their respective cell types (**Error! Reference source not found.**c). Cells in Cluster 1 were high in expression of *s100a8* and *s100a9* were labeled as Neutrophils. Cluster 2 was labeled as Macrophages due to their high in expression of *CD14* and *Csfr1*. Cluster 3, B cells, robustly expressed *Ly6d* and *CD79a*/b. Proliferating populations in clusters 4 and 5 were high in makers of proliferation and cell cycle genes (*Top2a, Mki67, Ran*), cytoskeleton rearrangement (*Stmn1, Tubb, Pclaf*), and genes associated with the regulation of apoptosis (*Anp32b, Ptma, H1-5*). To differentiate the two clusters, expression of macrophage marker *Csfr1* and neutrophil markers s100a8/9 were used. T/NK cells were clustered together based on their expression of *Nkg7* and *Thy1* and are labeled as cluster 6. Finally, cluster 7 was identified as dendritic cells due to its high expression of *Ly6d* and *Ccr9* (**Error! Reference source not found.**a).

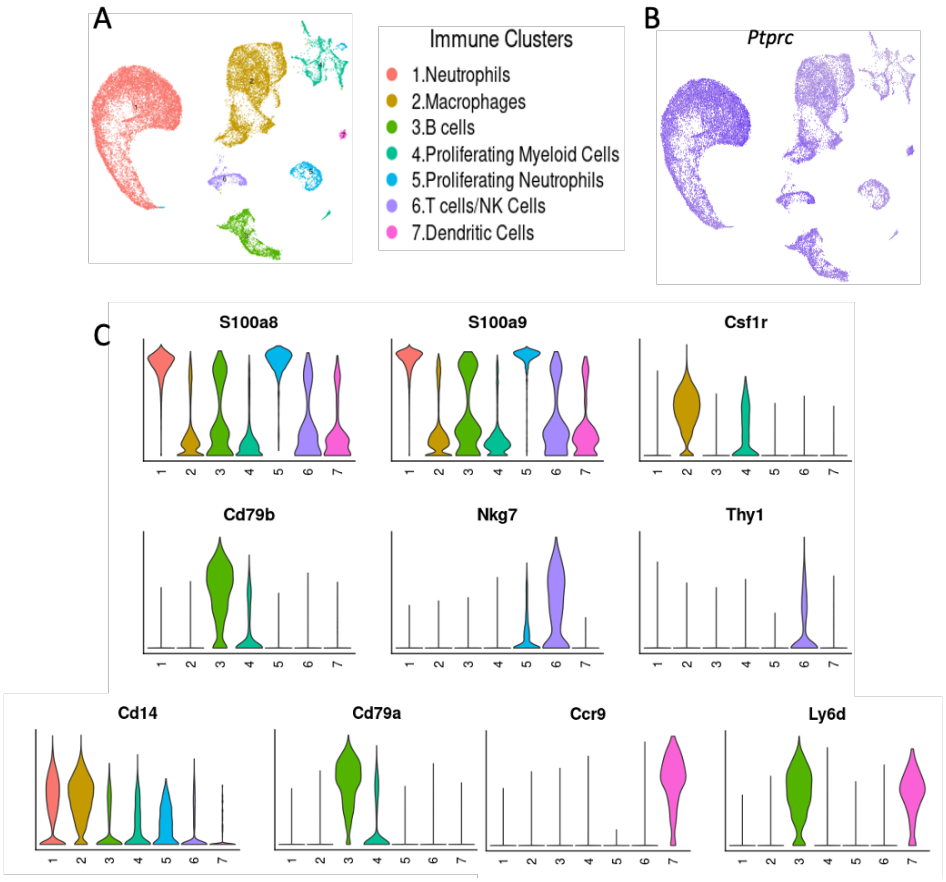

Figure 4. 4: Immune cell classification using scRNAseq and cluster-based gene expression. (A) Merged Uniform Manifold Approximation and Projection (UMAP) representing seven immune cell types within the synovial joint. (B) Feature plot of all populations showing well known transcriptional immune marker, Ptprc, which is expressed as CD45. (C) Violin plots identifying specific markers for each representative cell type. Height indicates cellular abundance and width indicates relative expression.

In uninjured joints of both strains, the neutrophil population was the largest, accounting for approximately 58% and 70% of the total cells sequenced in B6 and MRL, respectively. Macrophages comprised the 2nd largest population of sequenced cells with ~12% in B6 and ~10% in MRL. B6 had about 13% B cells, while MRL had roughly 6%. The remainder of the populations in B6 and MRL approximately included: 7% and 5% Proliferating Myeloid cells, 6% and 4% Proliferating Neutrophils, 4% T/NK cells for both strains, and 1.2% and 0.7% dendritic cells. After injury, several strain specific trends were observed in each cell type (**Error! Reference source not found.**b), the largest population shifts occurred at day 3 post-injury (**Error! Reference source not found.**, **Error! Reference source not found.**, Table 4. 1). The most dramatic shift was observed in the

neutrophil population of the MRLs, which decreased by 50% while neutrophil populations in B6 only decreased by ~15%. While macrophages in B6 and MRL were relatively comparable prior to injury, the population increased by ~52% in MRL, while the B6 population only increased by ~25%. Additionally, proliferating myeloid cell numbers increased by nearly 9% while B6 only increased by ~1.5%. At 4-weeks post injury, many populations in B6 stayed elevated from baseline D0 including an 11.5% increase in macrophages, 2.5% and 3% increase in proliferating myeloid and neutrophils respectively, as well as a 2% increase in T/NK cells. Additionally, the neutrophil population dropped by nearly 15%. In contrast, MRL had an 18% increase in macrophages, while other immune populations dropped below their baseline levels including a dramatic loss of neutrophils of nearly 15%: a similar trend for these cells seen in the B6 population. Changes in other populations are very minor and can be found in Table 4. 1 and Figure 4. 6: Percent of total Immune cells per timepoint. Graphical representation of the percent of each immune population sequenced across all injury timepoints. Colors are represented by cluster identities in figure 3.

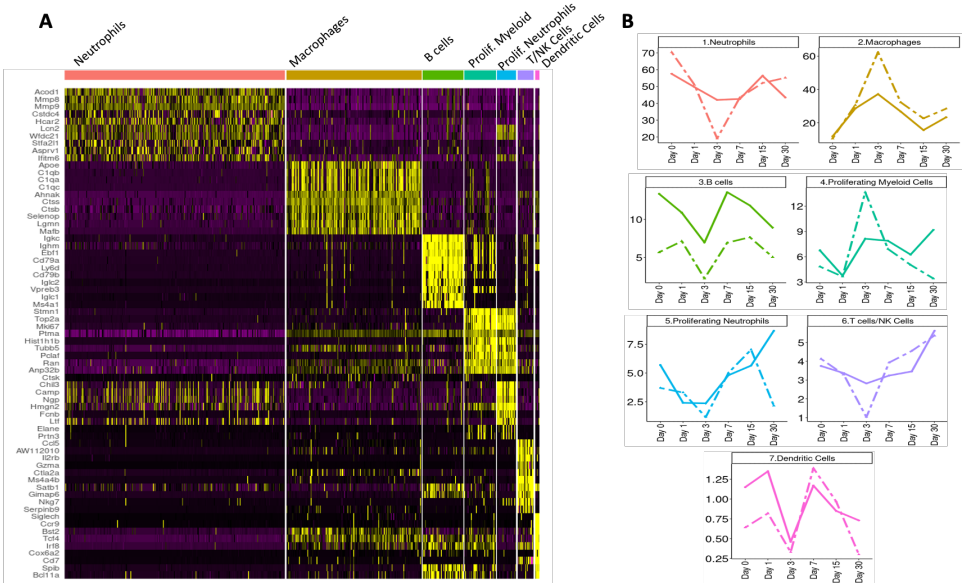

Figure 4. 5: Transcriptomic trends of differing joint immune populations after injury. Heat map of top genes contributing to each representative immune population's transcriptomic profile (A). Changes in proportion of each immune population after injury determined using single-cell RNA sequencing. Colors based on cluster identities in Figure 3 (B).

Table 4. 1: Percent of Immune cells per cluster. Raw percentages of total immune cells sequenced in each cluster at all timepoints in B6 (top) and MRL (bottom) joints.

	Percent of Total Cells Sequenced					
Population	B6 D0	B6 D1	B6 D3	B6 D7	B6 2W	B6 4W
Neutrophils	*57.5*	*49.68*	*42.05*	*42.61*	*56.38*	*43.54*
Macrophages	*11.82*	*28.58*	*37.21*	*26.74*	*15.61*	*23.34*
B cells	*13.31*	*10.85*	*6.96*	*13.53*	*11.79*	*8.9*
Proliferating Myeloid Cells	*6.77*	*3.76*	*8.14*	*7.9*	*6.26*	*9.19*
Proliferating Neutrophils	*5.7*	*2.41*	*2.36*	*4.81*	*5.65*	*8.68*
T cells/NK Cells	*3.75*	*3.37*	*2.82*	*3.24*	*3.46*	*5.62*
Dendritic Cells	*1.15*	*1.35*	*0.46*	*1.17*	*0.85*	*0.73*

	Percent of Total Cells Sequenced					
Population	MRL D0	MRL D1	MRL D3	MRL D7	MRL 2W	MRL 4W
Neutrophils	*70.39*	*51.1*	*19.16*	*43.48*	*52.09*	*55.18*
Macrophages	*10.6*	*30.69*	*62.39*	*32.31*	*22.65*	*28.49*
B cells	*5.69*	*7.13*	*2.27*	*6.93*	*7.65*	*5.07*
Proliferating Myeloid Cells	*4.84*	*3.65*	*13.67*	*6.93*	*5.04*	*3.43*
Proliferating Neutrophils	*3.7*	*3.3*	*1.16*	*5.02*	*7.04*	*2.16*
T cells/NK Cells	*4.13*	*3.3*	*1.03*	*3.93*	*4.55*	*5.37*
Dendritic Cells	*0.64*	*0.82*	*0.33*	*1.39*	*0.97*	*0.3*

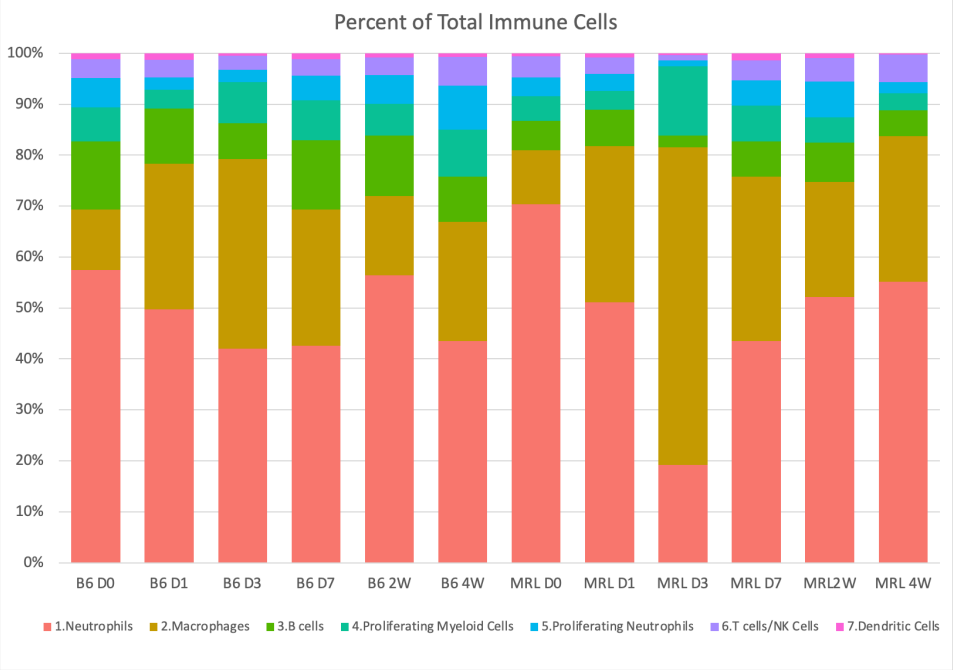

Figure 4. 6: Percent of total Immune cells per timepoint. Graphical representation of the percent of each immune population sequenced across all injury timepoints. Colors are represented by cluster identities in figure 3.

Single-cell sequencing uncovers multiple subpopulations of macrophages induced by TCI injury

Populations of monocytes and macrophages have been previously identified in the synovial joint [187, 196] that have distinct functions associated with homeostasis, joint protection and the inflammatory response in RA [197]. These cells are extremely diverse in function, tissue region and transcriptionally; alluding to specific responses they may have early in PTOA progression. To determine the role this population plays in disease onset, the parent macrophage cluster (Mono-Mac) was further analyzed to identify sub-populations of monocytes and macrophages at baseline as well as in response to joint injury at D1, D3, D7, D14 and D30. Analysis of this cluster identified nine (9) different sub-populations (**Error! Reference source not found.**) with distinct gene expression profiles. All clusters expressed *CD14,* and clusters 1, 2, 4, and 6 were consistent in expression of *Adgre* (*F4/80*) (**Error! Reference source not found.**b) compared to previously published data identifying these cells as macrophages [198]. Further analysis showed clusters 3, 5, and 7 shared expression of *Plac8*, an established monocyte marker [199].

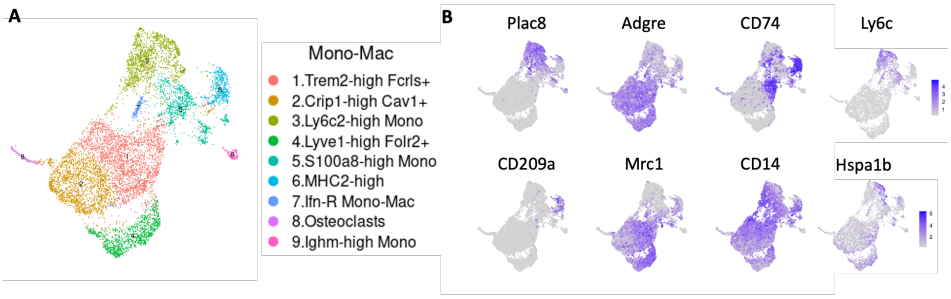

Figure 4. 7 :Myeloid and macrophage sub-clusters have distinct gene expression profiles. Identification of monocyte and macrophage populations from the parent Macrophage single-cell cluster (A). Feature plots of restricted gene expression to certain sub-populations used to identify clusters (B).

In addition to these classically defined macrophage and monocyte clusters, clusters 8 and 9 had distinct gene expression profiles corresponding to osteoclasts (cluster 8) and Ighm^{high} monocytes (cluster 9). The osteoclast cluster had strong expression of *Cstk*, *Acp5, Nfatc1, and Mmp9*, all transcripts known to be highly expressed in osteoclasts [200]. Ighm^{high} cells represented a smaller cluster of monocytes that displayed high expression of

genes associated with B cell differentiation and proliferation (*CD79a/b, Myb, IghM, Vpreb3, Igkc, Mmp9*) [201, 202], but did not cluster with B cells in the parent immune cluster (**Error! Reference source not found.**, **Error! Reference source not found.**). In addition, this subpopulation expressed *Plac8* at lower levels than the other monocyte clusters (**Error! Reference source not found.**b).

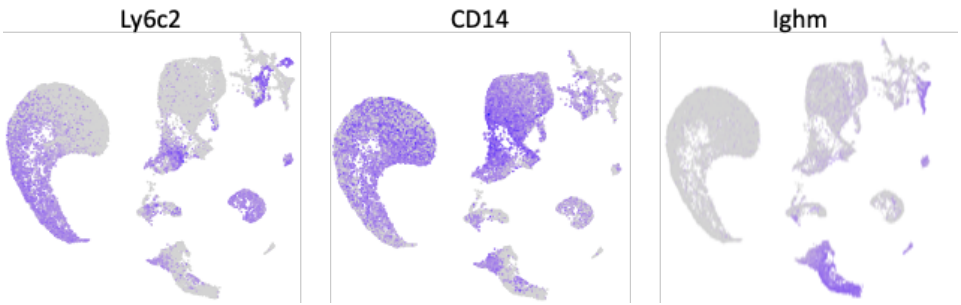

Figure 4. 8: Expression of monocyte, macrophage and B cell markers present in parent clusters of immune cells. Feature plots showing Ly6c2 expression in neutrophil populations, some myeloid, and B cells (Left). Robust CD14 expression in neutrophils and all myeloid derived cells (Middle). Limited expression of Ighm to B cells and some proliferating myeloid cell populations (Right).

Clusters 1, 2, and 4 had relatively high expression of *Mrc1 (CD206)* ***(Error! Reference source not found.****b).* This suggests that these clusters are each separate sub-populations of alternatively activated or M2 macrophages commonly known for tissue repair and wound healing [60]. Clusters 1 and 2 are moderately comparable transcriptionally (**Error! Reference source not found.**, **Error! Reference source not found.**) and cluster together closely in UMAP projections. While both exhibit little to no expression of *Ly6c* ***(Error! Reference source not found.)****,* they robustly express *CD14, Adgre, Crip1* and *Trem2* ***(Error! Reference source not found.****b,* ***Error! Reference source not found.)***. The Crip1^{high}Cav1^{+} (cluster 2) has lower *Mrc1* expression when compared to Trem2^{high}Fcrls^{+} (cluster 1), but robustly expressed *Cav1* (Caveolin-1) ***(Error! Reference source not found.****,* ***Error! Reference source not found.)***; a gene that has been shown to promote monocyte to macrophage differentiation [203]. In addition to its classical macrophage expression, cluster 1 is high in expression of *Apoe, IL-10*, and *Cxcl1/2* (**Error! Reference source not found.**). Apoprotein E, *Apoe*, is an HDL protein secreted by macrophages to aid in lipid efflux, cholesterol homeostasis, and can limit pro-inflammatory cytokine and chemokine signaling to promote an M2 macrophage phenotype [204, 205].

Interlukin-10 (*IL-10*) is an anti-inflammatory cytokine produced by macrophages and is vastly associated with macrophage activation and switching from a pro-inflammatory M1 state to a reparative M2 state by a downregulation of Tumor Necrosis Factor (TNF) [206].

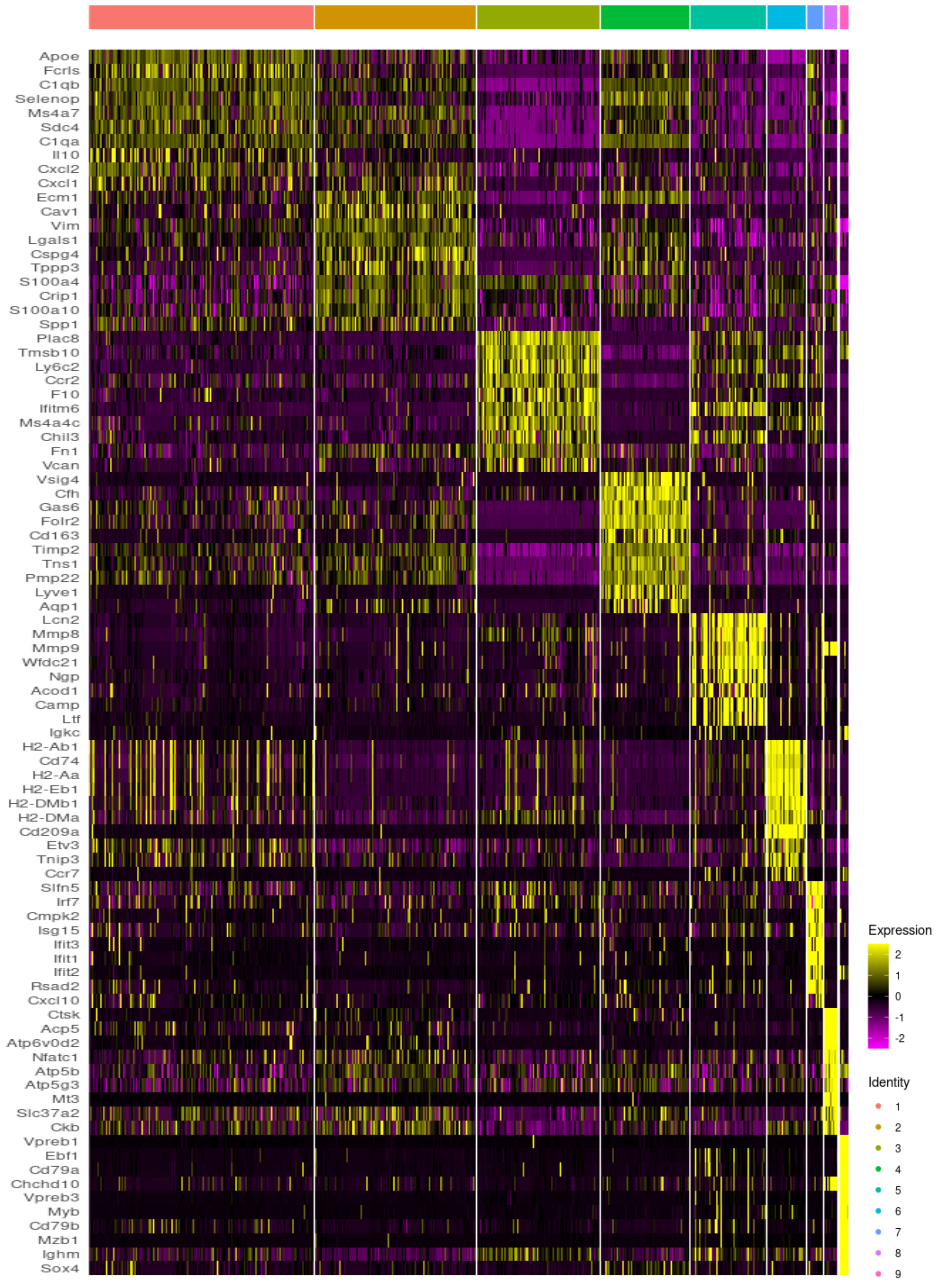

Figure 4. 9:Heatmap expression of top expressed genes from each Mono-Mac sub-population. Scaled expression of most highly enriched genes of each monocyte-macrophage subpopulation. Colors are indicative of clusters identity in figure 5, expression

is based on average logarithmic fold change where yellow expression is two-fold higher and purple is two-fold lower.

Cluster 4 was classified as the *Lyve1*^{high}*Folr2*$^{+}$ sub-population of macrophages and broadly expresses *Mrc1* and *Adgre* ***(Error! Reference source not found.)***. It is characterized by its high expression of lymphatic vessel endothelial hyaluronan receptor-*1 (Lyve1)* ***(Error! Reference source not found.)*** and clusters closely with the Crip1^{high}Cav1 and Trem2^{high}Fcrls^{+} populations. While the *Lyve1*^{high}*Folr2* subpopulation shares some expression (**Error! Reference source not found.**) it differs transcriptionally by expressing another set of genes associated with fibroblast proliferation, tissue remodeling, stress response, and monocyte migration including *Vsig4, Tim2, Lyve1, and Aqp1 [132, 207, 208]* (**Error! Reference source not found.**). In addition, its high expression of *Folr2,* a gene previously shown to act as a marker for tissue resident macrophages [209], coincides with the previously published studies on resident *Lyve1* expressing macrophages in the synovial lining of joints and other soft tissues [187, 198].

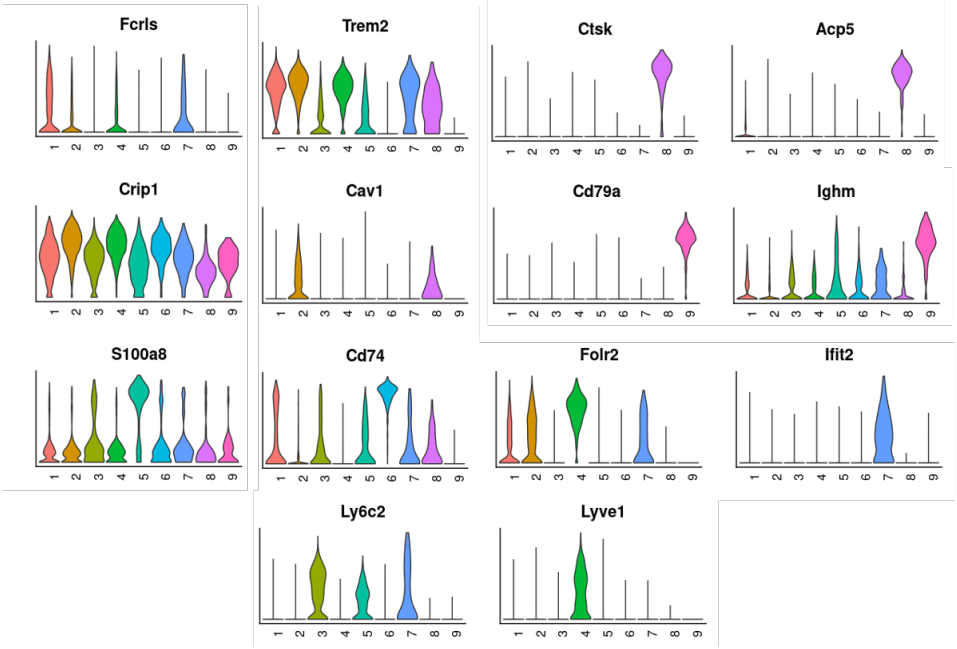

Figure 4. 10:Established markers differentiating Mono-Mac subpopulations from scRNAseq. Violin plots representing genes used to distinguish monocyte and macrophage subpopulations. Height indicates cellular abundance and width indicated relative expression. Colors are indicative of cluster identities in Figure 5.

Cluster 5 has variable expression of monocyte and macrophage makers including Plac8, CD14, Ly6c, and Adgre, while having robust expression of s100a8 and s100a9

(**Error! Reference source not found.**, **Error! Reference source not found.**), two widely accepted markers of neutrophils and monocytes. Previous research has shown that these proteins make up nearly 45% of cytoplasmic protein in neutrophils and DCs while monocytes have been shown to have lower expression levels, suggesting that these are tissue resident monocytes [210, 211], and was thus named s100a8high monocytes. This cluster is dominant in markers associated with endothelial proliferation and angiogenesis, Lcn2 [212, 213], and robust in markers associated with monocyte differentiation into macrophages [214] [215] such as *Wfdc21*, and *Mmp8*, as well as genes related to monocyte activation and recruitment such as *Ngp* [216].

Cluster 6 denoted as MHC2^{high} is a population of monocytes that is high in *CD74, CD209a,* and *CD14* expression (**Error! Reference source not found.**, **Error! Reference source not found.**) and has robust expression of genes associated with myeloid cell pathways involving antigen processing and presentation [217], TLR signaling [218], and interactions with cytokines affecting monocyte migration [219] (*H2-Ab1, H2-Aa, H2-Eb1, H2-Dmb1, H2-Dma1, Ccr7, Tnip3*). Cluster 7 is high in interferon signaling genes (*Ifit1, Ifit2, Ifit3, Irf7*), and macrophage activation and recruitment (*Cxcl10*) [220], suggesting that this subpopulation plays a role in regulating macrophage activation. In short, these two subpopulations may play a highly important role in monocyte and macrophage recruitment through cytokine and interferon signaling cascades.

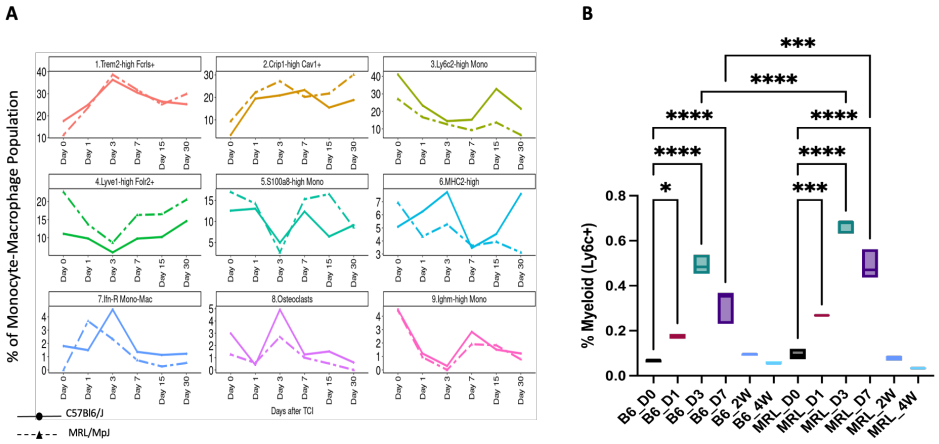

Figure 4. 11:Injury induced spikes in myeloid populations are consistent across platforms. Analysis of monocyte and macrophage subpopulations from single-cell sequencing analysis shows a large change in each myeloid population after injury that progressed until

day 3 post injury and returned to baseline starting at 2W post injury (A). Flow cytometric analysis of digested myeloid cells confirmed the largest significant changes in myeloid cell populations occurred at day three post injury and returned to baseline around 4-weeks post injury(B).

Myeloid cell populations change dramatically at early timepoints after injury

Nearly all Mono-Mac sub-populations suffered from severe shifts at day 3 or day 7 post injury. In addition, these changes were strain dependent and in MRL some sustained to nearly 4 weeks post injury (**Error! Reference source not found.**). B6 joints showed a slight increase from baseline of nearly 3% at day 3 post injury in both the MHC2^{high} monocytes and Ifn-R monocytes, while in MRL only the Ifn-R monocytes increased from baseline by roughly 2%. Comparatively, s100a8^{high} monocytes and Ighm^{high} monocytes decreased slightly from baseline in both MRL and B6. S100a8^{high} monocytes decreased about 8% in B6 and 14% in MRL, while the Ighm^{high} monocyte population declined about 4% in both strains. This trend in monocytes was also confirmed by FACS analysis, where the myeloid population peaked at day 3 post injury and began to decline in both MRL and B6 synovial joints (Table 4. 2).

Table 4. 2. Percent of Mono-Mac Subpopulations. Raw percentages of each subpopulation in total cells of Mono-Mac parent cluster at all timepoints in B6 (top) and MRL (bottom) joints.

	Percent of Total Cells Sequenced					
Population	B6 D0	B6 D1	B6 D3	B6 D7	B6 2W	B6 4W
1.Trem2-high Fcrls+	*17.66*	*25*	*36.3*	*30.5*	*26.42*	*25.23*
2.Crip1-high Cav1+	*3.29*	*19.43*	*20.91*	*23.27*	*15.47*	*18.84*
3.Ly6c2-high Mono	*41.02*	*23.37*	*14.42*	*15.2*	*32.83*	*21.58*
4.Lyve1-high Folr2+	*11.08*	*9.78*	*5.91*	*9.75*	*10.19*	*14.59*
5.S100a8-high Mono	*12.57*	*13.04*	*4.94*	*12.37*	*6.42*	*9.12*
6.MHC2-high	*5.09*	*6.25*	*7.74*	*3.46*	*4.53*	*7.6*
7.Ifn-R Mono-Mac	*1.8*	*1.49*	*4.55*	*1.36*	*1.13*	*1.22*
8.Osteoclasts	*2.99*	*0.41*	*4.94*	*1.26*	*1.51*	*0.61*
9.Ighm-high Mono	*4.49*	*1.22*	*0.29*	*2.83*	*1.51*	*1.22*

	Percent of Total Cells Sequenced					
Population	MRL D0	MRL D1	MRL D3	MRL D7	MRL 2W	MRL 4W
1.Trem2-high Fcrls+	*11.32*	*23.7*	*38.65*	*31.76*	*25.13*	*29.87*
2.Crip1-high Cav1+	*9.43*	*22.19*	*27.2*	*20.2*	*21.73*	*30.13*
3.Ly6c2-high Mono	*27.04*	*16.62*	*12.6*	*9.19*	*13.61*	*6.49*
4.Lyve1-high Folr2+	*22.64*	*13.69*	*8.62*	*16.29*	*16.49*	*20.52*
5.S100a8-high Mono	*16.98*	*14.26*	*2.64*	*15.29*	*16.49*	*8.57*
6.MHC2-high	*6.92*	*4.34*	*5.27*	*3.64*	*3.93*	*3.12*
7.Ifn-R Mono-Mac	*0*	*3.68*	*2.32*	*0.73*	*0.26*	*0.52*
8.Osteoclasts	*1.26*	*0.57*	*2.7*	*1*	*0.52*	*0*
9.Ighm-high Mono	*4.4*	*0.94*	*0*	*1.91*	*1.83*	*0.78*

The largest shift in macrophages was observed in the Trem2^{high}Fcrls^{+} subpopulation at day 3 post-injury. This subpopulation increased nearly 19% and 27% from baseline Day

0, in B6 and MRL, respectively (**Error! Reference source not found.**a). A similar increase was observed at 3 days post-injury in the Crip1^{high}Cav1^{+} subpopulation where both strains had an increase of about 17% from baseline (**Error! Reference source not found.**a). In addition, this subpopulation had a second spike at 4-weeks post injury in both strains.

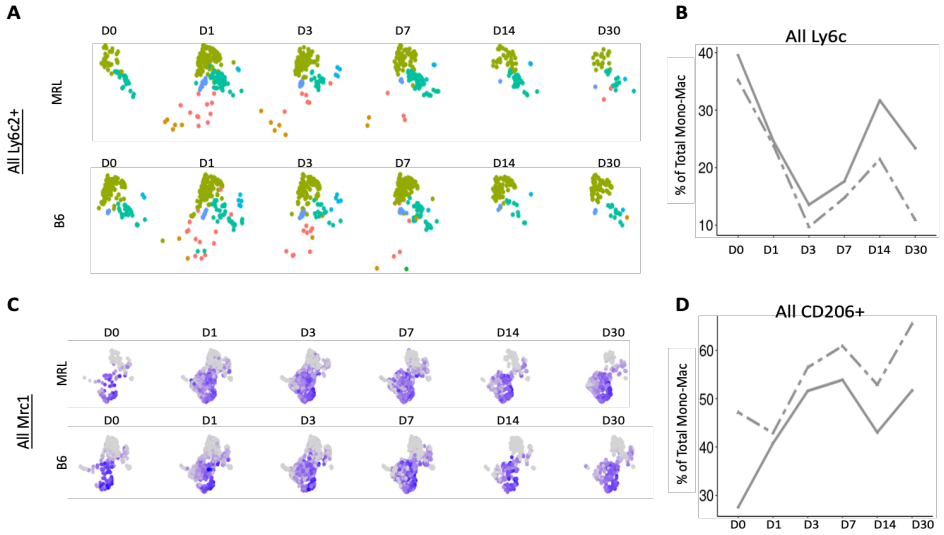

Figure 4. 12: Changes to monocyte influx and macrophage activation over injury progression. Split UMAP of all cells expressing Ly6c2 in Mono-Mac parent cluster (A). Percent of total Ly6c2 expressing cells across injury timepoints showing B6 (solid line) and MRL (dotted line) specific subpopulations (B) Feature plots of all Mrc1 (CD206) expressing cells in Mono-Mac cluster at all timepoints post-injury (C). Percent of total cells sequenced expressing Mrc1 (CD206) in both B6 (solid line) and MRL (dotted line) across all injury timepoints (D).

In the Ly6c^{+} monocyte subpopulation (cluster 3), the largest spike from baseline occurs at day 3 in B6, and day 7 in MRL. This trend can also be seen in all Ly6c^{+} cells using flow cytometry to analyze the percent of myeloid cells present in the synovial joint at all timepoints: D0 (uninjured), D1, D3, D7, 2W-, and 4W-post injury (**Error! Reference source not found.**b). When all clusters were analyzed together, *Ly6c* expression was most prevalent in clusters 3, 5, and 7 (**Error! Reference source not found.**a). Interestingly, B6 have an increased number of Ly6c^{+} monocytes at all timepoints when compared to MRL (**Error! Reference source not found.**b), suggesting there is less macrophage differentiation and more monocyte recruitment occurring in B6 joints after injury. Additionally, there were an increasing number of *CD206+* cells in both MRL and B6 (**Error! Reference source not found.**c, d). MRL joints had a larger baseline level of alternatively activated (M2) macrophages that sustains high levels after injury when

compared to B6 (**Error! Reference source not found.**c, d). These activated macrophages robustly expressed *Mrc1,* and primarily clustered with the Crip1^{high}Cav1^{+} and Trem2^{high}Fcrls^{+} populations (**Error! Reference source not found.**c). These trend suggests that MRL have an increased shift in their differentiation from monocytes to macrophages as well as increased macrophage infiltration into the joint after injury that may play a role in their resistant phenotype.

Moreover, all *CD206*+ cells were further separated into all CD206^{+}Lyve1^{+} and all CD206^{+}Trem2^{+} cells (**Error! Reference source not found.**). Initially, MRL had more Lyve1^{+} and Trem2^{+} cells which coincides with the increased number of M2 activated macrophages seen in **Error! Reference source not found.**. Over the course of injury, these macrophage populations spiked at two different timepoints early on post-injury. Initially the Lyve1^{+} population suffered from a large decrease in population at day 3 in both strains, although levels of Lyve1+ cells were still higher in MRL. This population began to recover at day 7, and continued to increase above pre-injury levels in both strains (**Error! Reference source not found.**a,b). In addition, *Lyve1* expression was restricted to the Lyve1^{high}Folr2^{+} cluster (**Error! Reference source not found.**a).

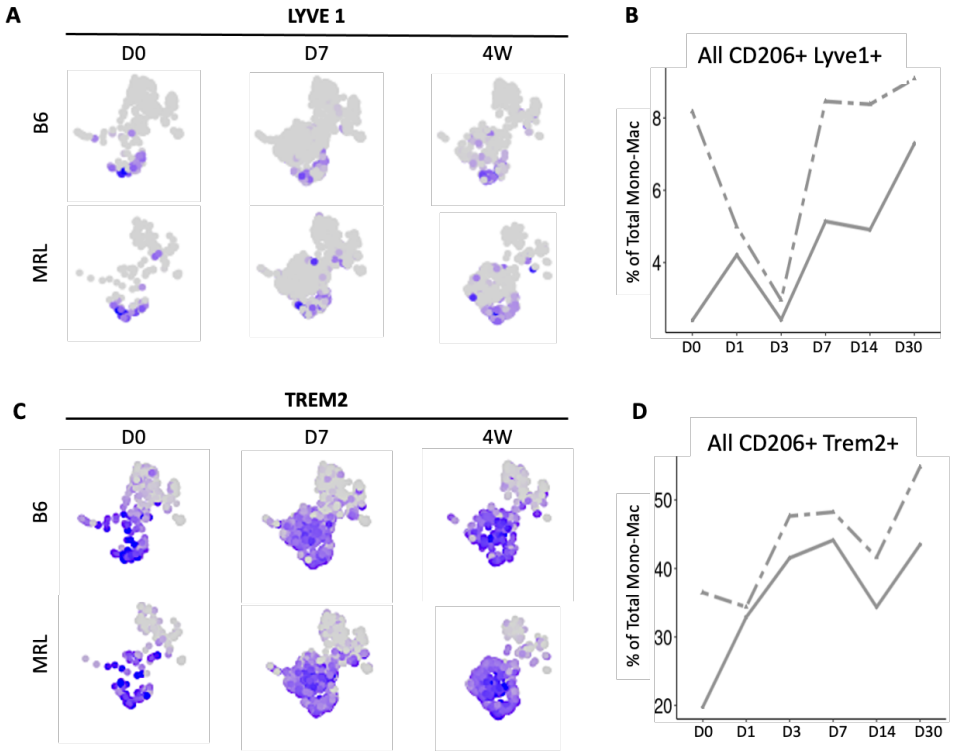

Figure 4. 13: Subpopulations of all Mono-Mac populations expressing alternative activated macrophage markers. Split feature plots representing injury induced expression in all Mono-Mac subpopulations (A). Line graph showing percent of cells in the Mono-Mac subpopulations coexpressing CD206 and Lyve1 at all timepoints in B6 (solid line) and MRL (dotted line) (B). Split feature plots of Trem2 expressing cells at day 0, day 7, and 4-weeks post injury in all subpopulations (C). Line graph representative of the percent of CD206 and Trem2 expressing cells in Mono-Mac subpopulations of both MRL (dotted line) and B6 (solid line) strains across all timepoints (D).

In contrast, *Trem2* expression expanded across the Crip1^{high}Cav1^{+}, Trem2^{high}Fcrls^{+} and Lyve1^{high}Folr2^{+} subpopulations (**Error! Reference source not found.**c). *Trem2*+ cells instantly began to increase after injury, peaking at day 7 for both B6 and MRL. The same trend was also seen in the *Trem2*+ cells as in the *Lyve1*+ population, in which MRL had a consistently higher population at all timepoints (**Error! Reference source not found.**c, d). The trends seen in macrophage subpopulations suggest that *Trem2* expression may be vital in the immune systems injury response and that these cells may provide an essential role in promoting healing of the injured joint after trauma has occurred.

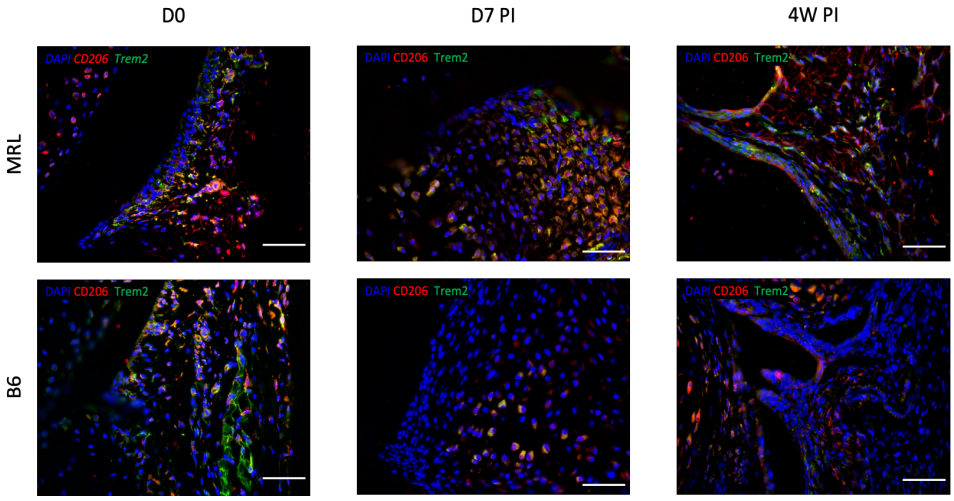

Figure 4. 14:Trem2 expression in synovium of MRL and B6. Immunohistochemical stain of Trem2 protein providing spatial expression of cells in the synovium. MRL (top) and B6 (bottom) were stained concurrently with CD206 (red) and Trem2 (green) antibodies to indicate activated M2 macrophages that co-express Trem2 over the course of injury (D0, D7, and 4W post injury. Scale bar 100um, magnification 40X.

Sustained Trem2^{high}Fclrs^{+} macrophage populations in MRL may aid in tissue resistance to PTOA

Transcriptional trends in the Trem2 populations shown were also seen at the protein level through immunohistochemical analysis of synovial joints at different injury timepoints (**Error! Reference source not found.**). In uninjured joints of MRL, *Trem2* signal was stronger than in B6 (**Error! Reference source not found.**, D0). Robust expression of CD206 (*Mrc1*) was seen throughout the synovium of the knee joint. In addition, CD206 expression was stronger at nearly all timepoints in MRL. At day 7, *Trem2*$^{+}$*CD206*$^{+}$ cells spiked in MRL joints as indicated by the yellow co-expression of *Trem2* and CD206 (**Error! Reference source not found.**). This fluorescent signal was still present in the joints of B6 but at lower levels than the synovium of MRL.

To further distinguish changes to these populations in response to injury, flow cytometry was conducted on uninjured (D0) and injured (D7) joints of MRL and B6. In this study, *CD45*$^{+}$ *CD11b*$^{+}$ *F4/80*$^{+}$ cells were gated as the Mon-Mac population (**Error! Reference source not found.**a). This population was then analyzed for different combinations of *CD206* and *Trem2* expression (**Error! Reference source not found.**b-d). After injury, B6 had a higher percent of *CD45*$^{+}$ *CD11b*$^{+}$ *F4/80*$^{+}$ myeloid cells than MRL. These cells were CD206-Trem2- and most likely represented of monocytes that had not yet

differentiated into macrophages (**Error! Reference source not found.**b). This corresponded with the single-cell data in **Error! Reference source not found.**, in which B6 had more Ly6c^{+} cells in the synovial joint than MRL. In addition, the CD206+Trem2- population showed no significant difference between B6 and MRL at day 7(**Error! Reference source not found.**c), while the single-cell data indicated that there was a small difference in CD206+ cells on the order of a few percent. The CD206+Trem2+ population exhibited a blatant difference between injured joints of MRL and B6, indicating that MRL had a higher number of alternatively activated macrophages expressing Trem2 after injury than B6. (**Error! Reference source not found.**d) This data was consistent with the single-cell analysis as well as the immunohistochemical analysis in **Error! Reference source not found.**in which MRL and B6 have comparable numbers prior to injury, but by 7 days after injury MRL showed significantly more activated (*CD206*$^{+}$), *Trem2*$^{+}$ expressing macrophages than B6 (**Error! Reference source not found.**d). While there was a significant reduction in population of CD206-Trem2+ macrophages at day 7, B6 synovial joints still had a significantly higher percentage of these cells post injury than MRL. This indicates that B6 mice have an additional Trem2+ population that are not an alternatively activated macrophage phenotype (**Error! Reference source not found.**d)

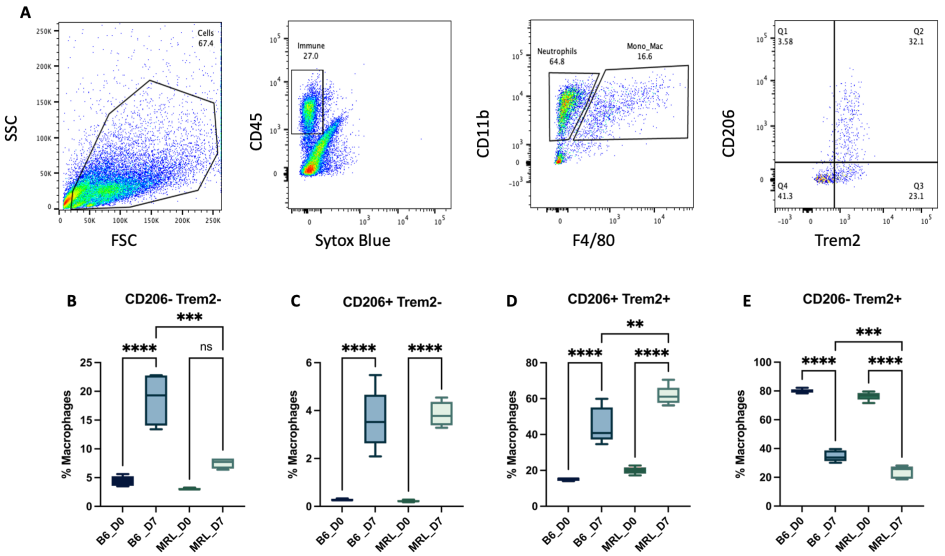

Figure 4. 15:FACS analysis of Trem2+ macrophages in joints of MRL/MpJ and C57Bl6/J. Representative gating scheme for analysis of CD206+ Trem2+ macrophages using flow cytometry (A). Proportion of cells in B6 and MRL with macrophage expression profiles

of: CD206-Trem2- (B) CD206+Trem2- (C) CD206+Trem2+ (D) CD206-Trem2+ (E). n=5; ** p<0.01, ***p<0.001, ****p<0.0001

Gene ontology indicates Trem2+ macrophages have strain specific functions after injury

Enriched gene ontology terms were determined by analyzing significant genes expressed by the Trem2highFclrs+ subpopulation. These genes were determined using a pseudobulk analysis comparing D0 to each injury timepoint. Genes at day 7 post injury were selected from each strain with average expression values greater than 1.5-fold and a p-value < 0.05 (Table 4. 2, Table 4. 3). Both strains shared the top 10 enriched GO terms, but MRL had slightly higher enrichment scores than B6 (**Error! Reference source not found.**).

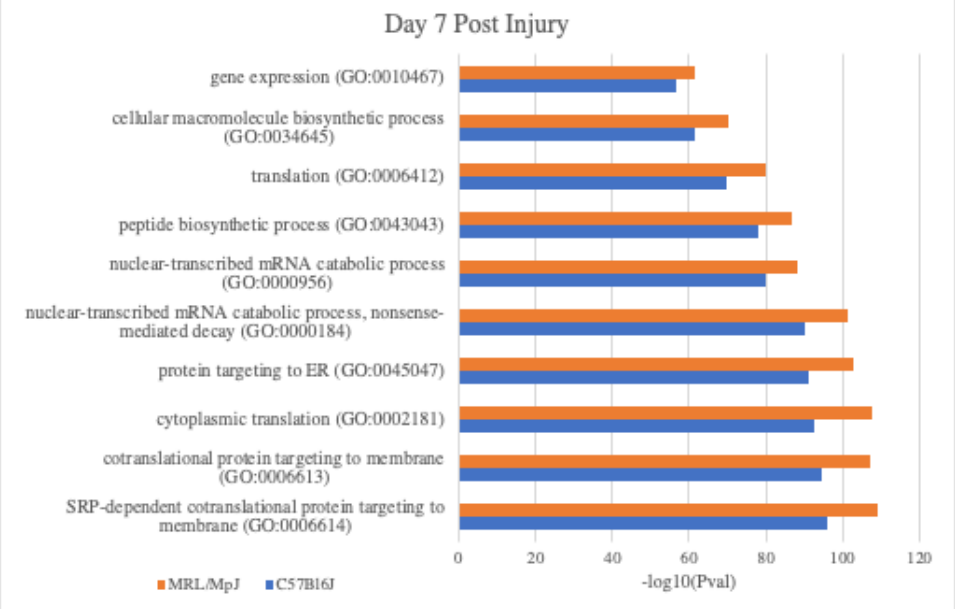

Figure 4. 16: Enriched Gene Ontology Terms Associated with Trem2+ Subpopulation. Top 10 GO terms from the Trem2^{high}Fclrs^{+} macrophage subpopulation. Significant genes upregulated at 7 days post injury (Table 4. 2 and Table 4. 3) in both MRL (orange) and B6 (blue) were identified based on average expression >1.5 fold and p<0.05.

To identify strain specific ontologies related to injury response, the top 100 GO terms were analyzed using Venny2.1 (***Error! Reference source not found.***). At day 7 post injury, the top ontology terms identified in B6 related to apoptotic signaling, leukocyte differentiation, production of TNFa and IFNy, as well as changes to cellular metabolism (***Error! Reference source not found.***). In contrast, highly enriched ontology terms in MRL were related to cellular senescence, immune cell activation, endocytosis and TLR-2 signaling (***Error! Reference source not found.***).

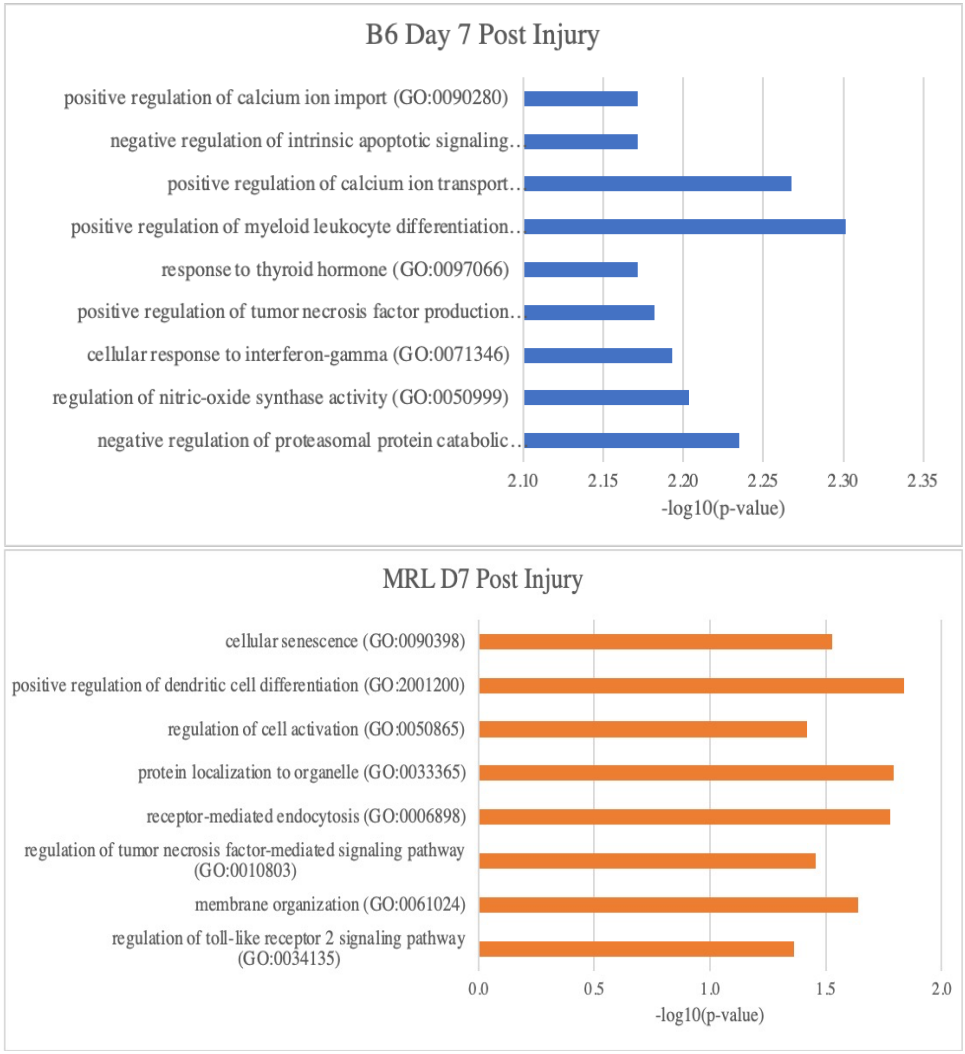

Figure 4. 17:Strain Specific Enriched Gene Ontologies from Trem2+ cells. Top ontologies isolated to B6 (top, blue) or MRL (bottom, orange) $Trem2^{high}Fclrs^{+}$ macrophage subpopulation post injury. GO terms are only present in each representative strain at day 7 post injury identifying GO terms associated with strain specific injury response.

Table 4. 3:Significant genes expressed in Trem2^{high}Fclrs^{+}+ subpopulation of MRL and B6 samples.

Trem2 Subpopulation DEGs - MRL D7			
Tmem176b	mt-Nd5	Ctsc	Rplp2
Ly6e	Clic1	Npc2	Lamp1
Tagln2	Gabarap	Prdx1	Btg1
Alox5ap	Ifrd1	Iqgap1	Rps21
Cd68	Sdcbp	Rps26	Rpl26
Cdkn1a	Sat1	Atp2b1	Rps6
Trem2	Ctsz	Marcksl1	Rpl10a
Npm1	Gm10260	H2afz	Rpl37
Rpl27	Rpl38	Arpc1b	Rpl5
Gadd45b	Rpl22	Cstb	Cd63
Rpl4	Egr1	Mrc1	Plek
Serf2	Cd44	Laptm5	Lgals3
Slfn2	Cox4i1	Hspa5	Rpl14
Naca	Cdc42	Hspa1b	Rps25
Myl6	Tgfbi	Cfl1	Hsp90aa1
Zfand5	Eef2	Rpl36	Pfn1
Calr	Fxyd5	Cxcl1	Rpl6
F13a1	Fosb	Klf2	Rpl18
Clta	Ifi207	Serinc3	H2-K1
Plin2	Rpl23a	Csf1r	Rack1
Pabpc1	Rap1b	Emp3	Cyba
Anxa5	Grn	Gpx1	Emp1
Ier5	Zeb2	Rps15	Ms4a7
Rpl7a	Ccl7	Oaz1	Ccl2
Rpl35	Eif4a1	Pltp	Ctsd
Eef1b2	Pim1	Rpl15	Id2
Ifitm2	Ybx1	Rpl24	S100a10
Rps17	Arpc2	Dusp1	Ier3
Dab2	Klf4	Gnai2	Rpl34
Cxcl2	mt-Co3	mt-Co3	mt-Atp6
Srgn	Rpl11	Rps10	Lyz2
Rpl12	Rps5	Rps19	Tmsb4x
Calm1	Mt1	Rps3a1	Malat1
Zfp36	Lgmn	H2-Ab1	C1qb
Rps28	Rpl17	S100a8	mt-Nd2
Rpl3	Rps13	Jund	Actg1
Lyz1	Rpl13a	Rpl19	Rps24
Lgals1	Rpl28	Rpl27a	H2-Aa
Rpl7	Rps15a	Rps16	S100a9
Rpl39	H2-D1	Cd74	H3f3b
Atp6v0c	Ctss	Cebpb	Fau
Rpl30	Hspa1a	Ptma	mt-Nd4
Ppia	Ddx5	Rps11	Ubb
Mafb	Lmna	Rps23	Selenop
Nfkbia	S100a6	H2-Eb1	Ctsb
Rpl41	S100a4	Rpl32	Neat1
B2m	Fcer1g	Rps9	Hspa8
Hsp90ab1	Rpl37a	Psap	Rplp1
Hmox1	Rpsa	Eif1	Apoe
Rpl35a	Rps29	Rps4x	mt-Cytb
Rpl8	Rps8	Rps27a	C1qa
Rps3	Fos	Rps14	Cst3
Rps7	Mcl1	Rplp0	Itm2b
H3f3a	C1qc	Junb	Eef1a1
Atf3	Rpl18a	Rps12	Actb
Tyrobp	Cd14	Rpl13	Vim
Pf4	Ahnak	mt-Nd1	Tpt1
Klf6	Ubc	Crip1	mt-Co2
Jun	Rps20	Rpl23	mt-Co1
Ftl1	Fth1		

Trem2 Subpopulation DEGs – B6 D7			
Lilrb4a	Atp2b1	Plek	Mafb
Cdkn1a	Marcksl1	Lgals3	Nfkbia
Sqstm1	H2afz	Rpl14	Rpl41
Rpl27	Arpc1b	Rps25	B2m
Gadd45b	Cstb	Hsp90aa1	Hsp90ab1
Serf2	Mrc1	Pfn1	Hmox1
Slfn2	Laptm5	Rpl6	Rpl35a
Pabpc1	Hspa5	Rpl18	Rpl8
Anxa5	Cfl1	H2-K1	Rps3
Ifitm2	Cxcl1	Rack1	Rps7
Gabarap	Serinc3	Cyba	H3f3a
Ifrd1	Csf1r	Emp1	Tyrobp
Sdcbp	Gpx1	Ms4a7	Pf4
Sat1	Rps15	Ccl2	Klf6
Ctsz	Oaz1	Ctsd	Rpl11
Cd44	Rpl15	Id2	Rps5
Fxyd5	Rpl24	S100a10	Mt1
Fosb	Dusp1	Ier3	Lgmn
Rpl23a	Gnai2	Rpl34	Rpl17
Rap1b	Rplp2	Srgn	Rps13
Zeb2	Lamp1	Rpl12	Rpl13a
Ccl7	Btg1	Calm1	Rpl28
Pim1	Rps21	Zfp36	Rps15a
Arpc2	Rpl26	Rpl3	H2-D1
Ctsc	Rps6	Rpl7	Ctss
Npc2	Rpl10a	Rpl39	Ddx5
Prdx1	Rpl37	Atp6v0c	Lmna
Iqgap1	Rpl5	Rpl30	S100a6
Rpl27a	Rps23	Cebpb	Lyz2
Fcer1g	Rps9	mt-Cytb	Rps26
Rpl37a	Psap	C1qa	Cd63
Rpsa	Eif1	Cst3	Ppia
Rps29	Rps4x	Itm2b	S100a4
Rps8	Rps27a	Eef1a1	Rpl32
Fos	Rps14	Actb	Gm42418
Mcl1	Rplp0	Vim	Rplp1
C1qc	Junb	Tpt1	H2-Eb1
Rpl18a	Rps12	mt-Co2	Fau
Cd14	Rpl13	mt-Co1	mt-Nd4
Ahnak	mt-Nd1	Cxcl2	Ubb
Ubc	Crip1	mt-Co3	Selenop
Rps20	Rpl23	mt-Atp6	Ctsb
Rps10	C1qb	Ftl1	Neat1
Rps19	mt-Nd2	Fth1	Hspa8
Rps3a1	Actg1	Tmsb4x	S100a9
H2-Ab1	Rps24	Malat1	H3f3b
S100a8	H2-Aa	Apoe	Cd74
Jund	Ptma	Rps16	Rps11
Rpl19			

Trem2+ macrophages further cluster ino transcriptionally unique subpopulations

When Trem2^{high}Fclrs^{+} macrophages were analyzed, five transcriptionally different clusters were identified as individual subpopulations(***Error! Reference source not found.***a, b). In addition, each cluster had a different response to injury throughout the timecourse (***Error! Reference source not found.***c). There was no strain specific trend when these populations were examined, although the s100a4^{high}, Hmox1^{high}, and Ms4a6b^{high} subpopulations all had significant changes to their population at day 3 post injury. Both s100a4^{high} and Ms4a6b^{high} subpopulations peaked at day 3, while the Hmox1^{high} subpopulation dropped to nearly 10% of its original population in both strains (***Error! Reference source not found.***c). Each Trem+ subpopulation had a separate response to injury based on population totals (***Error! Reference source not found.***) and molecular fucntion denoted by its transcriptomic profile (***Error! Reference source not found.***). When all Trem2+ cells including those not restricted to the Mono-Mac parent cluster were observed, there were specific expression patterns between subpopulations (***Error! Reference source not found.***). Genes strongly associated with each cluster were used to perform an ontology enrichment analysis through Enrichr. This analysis identified ontologies associated with specific functions of Trem2+ subpopulations. Cluster 0 expressed genes associated with antigen presentation, cytokine signaling, and lymphocyte development. Cluster 1 genes were linked to integrin signaling and peptide response. Cluster 2 genes were specific to activation of the complement sysytem and fibroblast proliferation. Cluster 3 genes corresponded to neutrophil signaling pathways. Cluster 4 genes were associated with osteoclast pathways and lipid metabolism (***Error! Reference source not found.***).

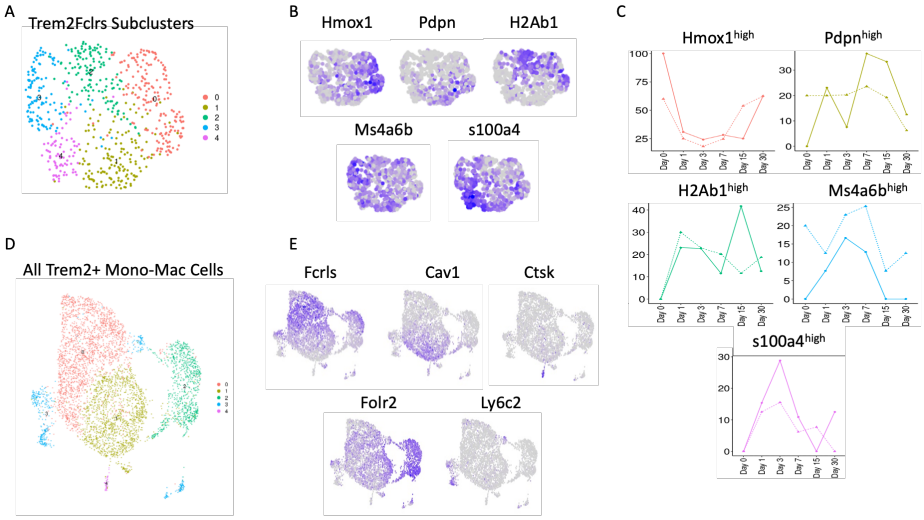

Figure 4. 18:Single-Cell Resolution of Trem2+ Subclusters Induced Over Injury. Merged UMAP showing Trem2highFclrs+ macrophage cluster further grouped into 5 individual sub-populations (A) Feature plot representing top genes associated with individual Trem2highFclrs+ macrophage subpopulations (B) Trem2highFclrs+ subpopulation expression over injury time course showing changes to cellular proportion at each timepoint (C) Merged UMAP of all Trem2 expressing cells in parent Mono-Mac cluster

(D) Feature plots of highly expressing cluster markers enriched in defined subpopulations (E).

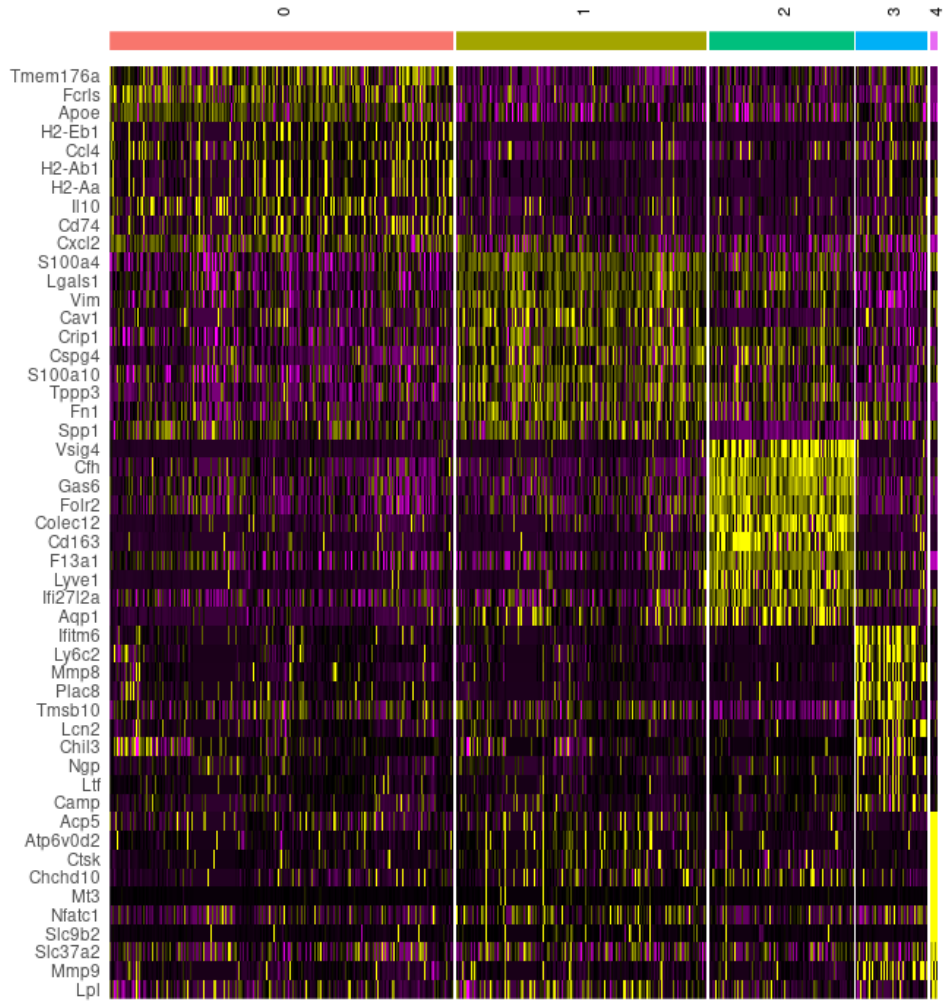

Figure 4. 19: Gene expression profile of Trem2 subpopulation. Heatmap of genes specific to each subpopulation identified in the Trem2^{high}Fcrls^{+} subpopulation.

MRL and B6 chondrocytes express macrophage markers prior to and following injury

While analyzing Trem2 expressson in the synovium of B6 and MRL, expression of Mrc1 and Trem2 was noted in the articular cartilage of the knee. To further elicidate this phenomenon, joint tissues were stained with Trem2 and Aggrecan (Acan) to identify potential colocalization of these transcipits in chondrocytes of the articular joint (***Error! Reference source not found.***). In uninjured samples, there was an unambiguous colocalization of these two markers in the intermediate layers of the articular cartilage in

in both strains In addition, Trem2 expression was also seen in the deep layers of the artcular cartilage and the growth plate of both MRL and B6, albeit MRL had a more robust expression profile in both locations***Error! Reference source not found.***e. Further research through Gene Expression Omnibus *[132]* identified a study in which chondrocytes were isolated from mice and treated with IL-1B to induce an in vitro inflammatory response to replicate an OA phenotype [221]. Re-analyzing the gene expression data from RNA sequencing conducted during this study confirmed cellular phenotype by expression of two chondorcyte markers, Acan and Col2a1, before and after IL-1B dosing (***Error! Reference source not found.***a, b). In addition, CD206 and Trem2 were also both identified in the gene expression data (***Error! Reference source not found.***c, d). After treatment, CD206 levels in chondrocytes decreased significantly from untreated counterparts (***Error! Reference source not found.***c). Comparatively, Trem2 levels increased nearly 3-fold when compared to untreated chondrocytes (***Error! Reference source not found.***d). This data confirms that both CD206 and Trem2 are expressed in chondrocytes and macrophages before and after an induced injury or arthritic environment.

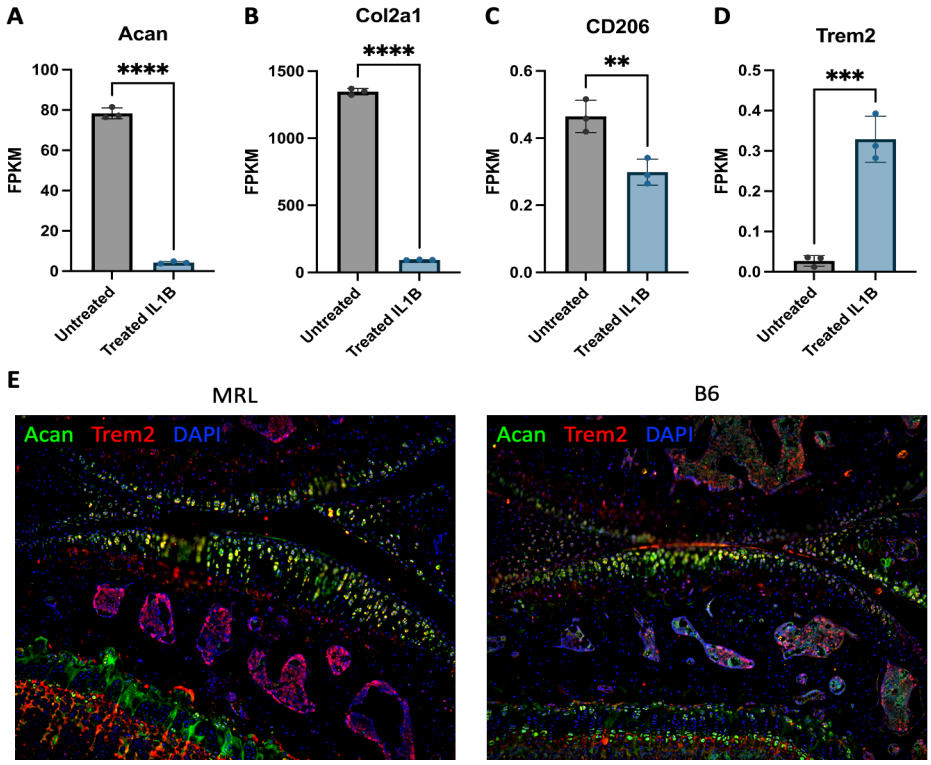

Figure 4. 20: Highly prevalent macrophage markers expressed in articular chondrocytes. Expression of chondrocyte markers Aggrecan (A) and Collagen 2 (B) after induction of an OA phenotype in vitro using IL-1B. Chondrocytes also expressed CD206 at high levels before and after OA induction (C) Chondrocytes had a significant increase in Trem2 expression after OA induction with IL-1B (D) IHC confirmation of Trem2 and Acan expression in MRL and B6 joints using immunohistochemistry to show regional and strain specific expression profiles in uninjured joints (E).

Injured joints of Trem2 knockout mice have similar PTOA phenotype to B6

Single-cell analysis of immune response to early PTOA onset highlights that *Trem2*+ macrophages are important in promotion of an anti-inflammatory joint phenotype and joint protection after injury. To determine if *Trem2*+ macrophages were responsible in deterring the severe PTOA phenotype, Trem2 knockout mice ($Trem2^{-/-}$) were injured, and histological analysis was conducted to grade the severity of their joint phenotypes (**Error! Reference source not found.**, **Error! Reference source not found.**). Right hindlimbs of $Trem2^{-/-}$and B6 animals were collected for analysis at 4-weeks post-injury. Sections from each strain were stained using safranin-o and fast green (**Error! Reference source not found.**). Histological evaluation showed that $Trem2^{-/-}$ (**Error! Reference source not found.**-bottom left panel) have loss of proteoglycan staining (black crosses, red tissue) prior to injury. Furthermore, by 4-weeks post injury, both strains had a severe PTOA phenotype. Semi-quantitative OARSI scoring [193] to blindly grade the severity of PTOA phenotype indicated $Trem2^{-/-}$ had a significantly higher OA score, on average, prior to injury when compared to B6 (**Error! Reference source not found.**a). Assessment of PTOA severity at 4-weeks post injury showed no significant difference between OARSI scores of $Trem2^{-/-}$and B6 joints (**Error! Reference source not found.**a). To identify additional changes in the bone between B6 and $Trem2^{-/-}$, both strains were injured and hindlimbs were collected at 6-weeks post injury to perform μCT analysis as previously described [194, 195].

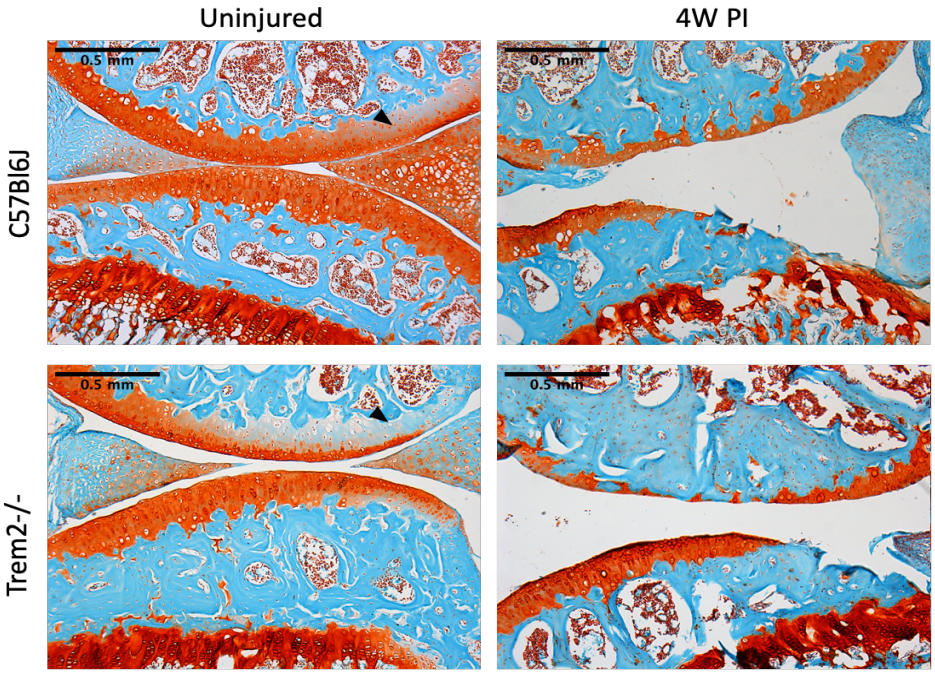

Figure 4. 21:Histological evaluation of Trem2 Knockout joints. Joints from Trem2-/- animals were compared to B6 at day 0 and 4-weeks post injury for PTOA phenotype by staining with Safranin-O and Fast Green. Scale bars = 0.5m, (500um), 10X magnification. Arrows indicate loss of proteoglycan staining.

Examination of bone remodeling in Trem2$^{-/-}$ and B6 animals found that Trem2$^{-/-}$ joints had significantly less (~60%) ectopic bone formation than B6 joints at 6-weeks post injury (**Error! Reference source not found.**b). There was no significant difference between uninjured hindlimbs of Trem2$^{-/-}$ and B6, although injured B6 hindlimbs had significantly more subchondral bone than injured Trem2$^{-/-}$ hindlimbs (**Error! Reference source not found.**c). Furthermore, both strains showed significant loss in subchondral bone after injury compared to their uninjured counterparts. Overall, these parameters indicate that injury induces significantly more subchondral bone loss in Trem2$^{-/-}$ hindlimbs than B6, less ectopic bone formation at 6-weeks post injury, but no significant change in PTOA severity.

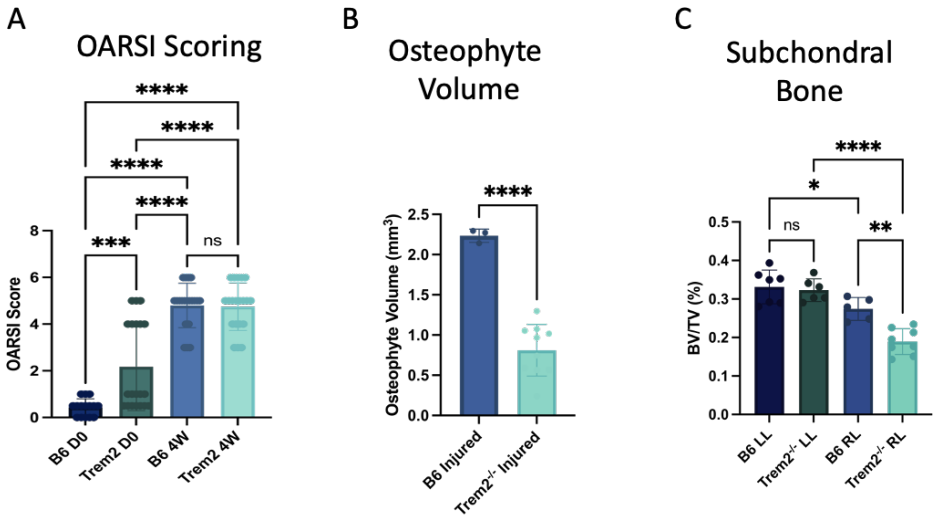

Figure 4. 22: Bone histomorphology parameters of B6 and Trem2$^{-/-}$ post injury. OARSI scoring of PTOA phenotype of B6 and Trem2$^{-/-}$ joints at D0 (Uninjured) and 4-weeks post injury on a scale of least severe (0) to most severe (6) (A) uCT analysis indicating volume of osteophyte formation at 6-weeks post injury in B6 and Trem2$^{-/-}$ animals (B) Bone volume to total volume expressed as a ratio indicating changes to subchondral bone before and after injury in B6 and Trem2$^{-/-}$ animals (C). ns, not significant; *p<0.05, **p<0.01 ***p<0.001, **** p<0.0001.

Discussion

This study demonstrates the important modulatory role immune cells have in the prevention and onset of chronic joint degeneration. The use of single-cell RNA sequencing has expedited research of immune heterogeneity [91, 222] in many tissues including the synovial knee joint [118, 198, 223, 224]. Figures 3 and 4 demonstrate murine immune responses to a tibial compression induced injury model that mimics human injury and PTOA onset [168]. This non-surgical injury method allows unbiased examination of the immune response in joint tissues of PTOA-susceptible (C57Bl6/J) and PTOA-resistant (MRL/MpJ) strains. Specifically, immune cell interference from surgery or enzymatic OA induction is avoided.

Previous studies have identified resident and infiltrating Myeloid-derived populations as culprits of a pro-inflammatory joint state after injury [168]. These cells are responsible for the production of proinflammatory cytokines and chemokines, such as IL-1B, TNFa, IL-6, IL-10, IL-17, as well as many others from the CCL/CXCL family [179].

Many of these molecular signals induce infiltration of innate (macrophages, neutrophils, NK) and adaptive (T, B) immune cells into the synovial joint, as shown in figure 3 and 4. These populations of immune cells, although present in both mouse strains, have distinctly different responses across early and late injury timepoints (Fig4). Previous research of B6 joints has shown that neutrophils, macrophages, and B cells play vital roles in the production of inflammatory cytokines, tissue repair, and protease expression, respectively [198], indicating their response to injury may be responsible for the pro-inflammatory state of the knee joint. As shown **Error! Reference source not found.**, B6 have a decrease in Neutrophil populations and a corresponding increase in Macrophage and proliferating myeloid populations after injury. Changes to neutrophil and macrophage homeostatic levels is likely indicate a pro-inflammatory response and classical activation of resident monocytes that produces an influx of M1 macrophages. Upon activation infiltrating macrophages are responsible for production of pro-inflammatory cytokines (TNFa, IL-1B, IL-6) and growth factors (FGFs, BMPs) as previously shown [198], and aid in degradation of joint tissue as well as PTOA progression [58].

MRLs showed a more extreme response to injury in neutrophil, macrophage, and proliferating myeloid cell populations (**Error! Reference source not found.**) indicating a higher recruitment of monocytic cells into the joints of MRL than B6. Subsequent analysis of these cells revealed MRL and B6 mice have differing responses to injury, indicated by a 6-fold increase of total Mono-Macs from baseline at day 3 post-injury and alterations to individual subpopulations of Mono-Macs identified in figure 5. This signifies a higher infiltration of monocytes into MRL joints after injury than B6.

During tissue injury, circulating cytokines (e.g. IL-6, IL-10) drive monocytes and steady state macrophages towards a pro-inflammatory (M1) phenotype. When local stromal cells produce molecules known to reverse this polarization (e.g. IL-4), macrophages and monocytes are deactivated and begin “priming” towards a wound healing or anti-inflammatory (M2) macrophage state [225]. During this time, M2 macrophages are responsible for cleaning up tissue debris and apoptotic cells, while promoting healing by producing anti-inflammatory signaling molecules and growth factors [58]. Within the

parent Mono-Mac cluster, 9 transcriptionally distinct monocyte and macrophage subpopulations with pro- or anti-inflammatory profiles were represented in both strains after injury. Both MRL and B6 showed a distinct response to injury in these subpopulations, indicating the influx of monocytes and subsequent activation of these cells was potentially responsible for successive joint damage that occurs at later timepoints post-injury. The largest changes in subpopulations occurred in the Ly6c+ Monocytes and Crip1^{high}Cav1^{+}, Trem2^{high}Fcrls^{+}, and Lyve1^{high}Folr^{+} macrophage populations.

Previous literature has determined that Ly6c^{high} monocytes are recruited to the joints in response to traumatic knee injury and act as pro-inflammatory effector cells in tissues with perturbed homeostasis [58]. This population is slightly attenuated in MRL joints after injury, as compared to B6, indicating there is a lack of pro-inflammatory signals, such as Reactive Oxygen Species (ROS), TNF-a, and IL-6, to further exacerbate inflammation in the joint and the progression of a severe PTOA phenotype.

Environmental cues within the joint are responsible for activation of monocytes into terminally differentiated macrophages. These signals, like those affecting Ly6c+ monocytes, will polarize macrophages towards a classically activated, inflammatory M1 phenotype or alternatively activated, healing M2 phenotype [59, 60]. Decades of research have alluded to a dichotomy of macrophage states; however, new research has revealed a spectrum of activation states that macrophages can develop into [226]. **Error! Reference source not found.**, **Error! Reference source not found.**, **Error! Reference source not found.**show multiple subpopulations of macrophages in MRL and B6 that transcriptionally align towards the M2 phenotype of the activation spectrum.

Lyve1^{high}Folr^{+} macrophages have been previously identified as an M2 macrophage population with a role in tissue repair in lung, heart, vasculature, and adipose tissues [227]. *Lyve1*+ macrophages, which have been shown to line the synovial membrane of the joint [196], are transcriptionally similar to tissue resident populations. Additionally, Lyve1^{+} macrophages are responsible for maintaining synovial lining integrity to prevent pro-inflammatory immune cells from infiltrating the joint cavity and synovial fluid. The population of tissue resident macrophages is depleted in B6 during PTOA progression, as

demonstrated by a decrease in the Lyve1^{high}Folr^{+} subpopulation at day 3 post-injury (**Error! Reference source not found.**). As shown in **Error! Reference source not found.**, uninjured MRL joints have nearly double the population of Lyve1^{high}Folr^{+} macrophages compared to B6. This indicates MRLs have a more prevalent population of tissue resident macrophages and potentially more robust synovial lining prior to injury. Previous groups have hypothesized that the presence of Lyve1 macrophages helps control fibrosis and limits the influx of inflammatory neutrophils, classically activated (M1) macrophages, and other antigen presenting cells into the synovial capsule [228]. Lyve1 macrophages are essential in forming a tight junction mediated protective barrier [58], helping to resolve inflammation, and inducing a reparative fibroblast phenotype in synovial, cardiac, and vascular tissue [196]. Single-cell RNA sequencing in **Error! Reference source not found.** substantiates that an increased baseline population of tissue resident macrophages in MRL may aid in keeping the synovial lining intact post-injury.

In addition to Lyve1^{high}Folr^{+} macrophages, uninjured joint tissue has additional populations of resident macrophages that line the synovial capsule and protect the integrity of synovial joints [190]. These joint resident macrophages are highly specialized cells responsible for antigen presentation, phagocytosis, and debris clearance from the joint, as well as modulation of ECM and synovial fluid production [187]. Crip1^{high}Cav1^{+} and Trem2^{high}Fcrls^{+} macrophages (**Error! Reference source not found.**) robustly express markers of alternatively activated macrophage populations, such as *Cxcl2, Cxcl, IL-10, Ccr2, Mrc1,* and *Apoe (***Error! Reference source not found.***).* In addition, both of these populations robustly express Trem2 (Triggering Receptor Expressed on Myeloid Cells 2) and have previously been identified as additional cells responsible for forming a protective barrier in B6 synovial joints [187, 198]. Trem2 macrophages are responsible for driving an anti-inflammatory tissue environment and promoting damage repair through alternative activation via stromal cell interaction [229, 230]. Both MRL and B6 show an increase in these Trem2 macrophage populations soon after injury. After injury, the synovial joint has an influx of immune cells, specifically Ly6c+ monocytes in the case of B6 joints. Cellular infiltration of monocyte populations results in an increase of classically activated

macrophages. These M1 macrophages contribute to pannus formation and inflamed synovial tissue [231] both of which are hallmarks of PTOA.

Previous examination of *Trem2* and its ligand, *Apoe*, indicates that both are expressed in the Lyve1^{high}Folr^{+} and Trem2^{high}Fclrs^{+} macrophage populations [198] and contribute to the M2 phenotype. *Trem2* is part of a large membrane complex that includes *Dap12*; a signaling adapter protein expressed in stromal and myeloid cells, that participate in the innate immune response. When activated, this complex inhibits pro-inflammatory signaling cascades [232] and interacts with several ligands (**Error! Reference source not found.**) to promote macrophage polarization towards alternative activation following, a shift from proinflammatory signaling to wound healing is seen in the tissue of interest. Analysis of close protein contacts to *Trem2* were used to identify potential interactions of *Trem2* expressing macrophages and other immune (**Error! Reference source not found.**b) or stromal (**Error! Reference source not found.**c) joint populations. *Apoe* is shown to be expressed in monocyte-derived macrophage populations, while *CD33, Tyrobp, and Syk* have relatively high expression in neutrophils and dendritic cells (**Error! Reference source not found.**b) as well as some stromal cell populations as previously described [229, 230] (**Error! Reference source not found.**b). These transcripts are primarily involved in immune cell activation [233] and myeloid cell maturation [234]. In addition, expression of *Clu* in proliferating myeloid cells and stromal chondrocyte populations is crucial for promoting cellular survival and proliferation, as well as reducing inflammatory signaling [235].

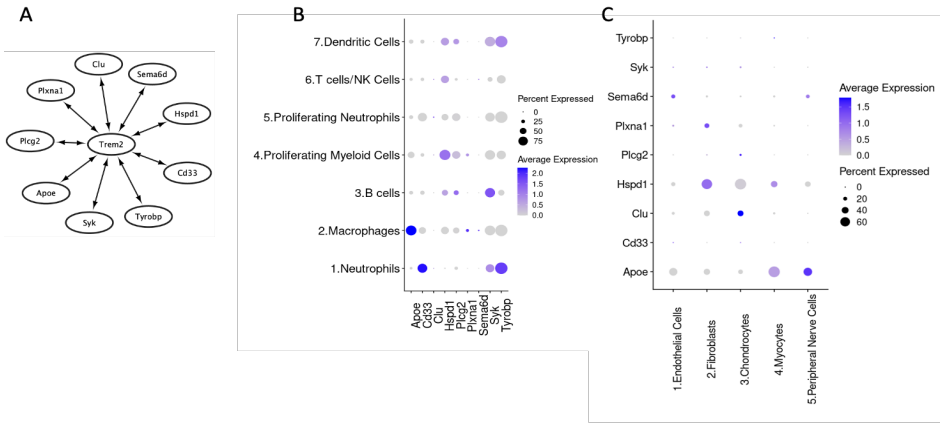

Figure 4. 23: STRING Interactome's network of genes that interact directly with Trem2 and are an integral part of the Trem2 membrane complex (A). Dot plot mapping expression of genes in network in other immune cell types including macrophages (B). Dot plot mapping expression of genes in network expressed in stromal cell populations including chondrocytes, (C). Dot size represents percent of cells expressing marker while color indicated average expression values.

Starting at day 3 post-injury, MRL synovium sustains high levels of $Trem2^{+}$ M2 macrophages (**Error! Reference source not found.**-14). However, this $Trem2^{+}$ populations in B6 begin to decrease towards baseline levels after day 7 post-injury, indicating a prolonged M1 macrophage response. Sustained levels indicate that this population of M2 macrophages in MRL are more capable of phagocytosis, debris clearance, and removal of apoptotic cells induced by the initial inflammatory response to injury. Moreover, B6 mice have an additional population of Trem2 expressing myeloid cells, CD206-Trem2+, not transcriptionally representative of an alternatively activated macrophage phenotype (**Error! Reference source not found.**a). While expressing myeloid lineage markers, these CD206-Trem2+ cells may be Trem2+ expressing macrophages that are classically activated, and contribute to joint inflammation [236, 237]. Previous studies have shown that Trem2+ M1 macrophages contribute to changes in stromal cell differentiation through WNT/b-catenin signaling, [238] and to lipid metabolism, as previously shown in several obesity studies and nervous system diseases [239].

Gene ontology analysis (**Error! Reference source not found.**) of both strains showed that Trem2 expressing cells in B6 are enriched in ontologies related to calcium ion transport, TNFa regulation, and Interferon response. Published data suggests that inflammatory cytokines like TNFa and DAMPs, e.g. calcium containing crystals, initiate a Pattern Recognition Receptor (PRR) response in monocytes and macrophages. These PRRs are present in immune and synovial cells as well as chondrocytes and osteoblasts. As ECM fragments from proteolytic cleavage continue to be produced by apoptotic cells in the joint, dysregulation of intracellular (calcium binding proteins) and extracellular (collagens, PGs, GAGs) DAMP production occurs. Production of cytokines like TNF and IL-1B leads to a decrease in matrix protein production by chondrocytes like collagens ad aggrecan. Additionally increased TNF and IL-1B leads to an increase catabolic factors

[58], including MMPs, chemokines, and cytokines, that further exacerbate the inflammatory response in B6 and eventually lead to severe PTOA [240]. Furthermore, collagen and aggrecan biproducts from the catabolism of cartilage post-injury have been shown to stimulate inflammatory TLR signaling pathways [241] and promote joint degradation.

MRL ontologies are enriched in TNF-a signaling pathways, antigen presenting cell differentiation, endocytosis, and TLR2 signaling. TLR signaling recognizes ECM-derived DAMPs like collagen and aggrecan [167]. These ontologies indicate that Trem2+ macrophages in MRL initiate additional innate immune signaling to manage TNFa production by other pro-inflammatory immune cells and promote macrophage polarization to the alternative pathway (**Error! Reference source not found.**). Additionally, this sustained population of $Trem2^{+}$ macrophages may be responsible for tissue remodeling based on their projected interactions with other stromal cell population in **Error! Reference source not found.** and expression of *MRC1* [166]. Trem2 macrophages regulate ECM turnover through collagen recognition, internalization, and degradation via MRC1 [166, 242]. In addition, collagen 2 products have been shown to promote M2 polarization and several *in vitro* and *in vivo* studies have shown that treatment with soluble collagen 2 promotes a pro-chondrogenic joint microenvironment by modulation of inflammation, TGF-b production, and decreased apoptosis [164, 243].

While genetic depletion of *Trem2* showed no significant changes to PTOA severity when compared to B6 joints (**Error! Reference source not found.**, **Error! Reference source not found.**), scRNAseq data suggests that an increase of Trem2 expressing M2 macrophages is essential in maintaining cartilage integrity and prohibiting prolonged inflammation after injury. In short, this sustained population of Trem2 expressing macrophages in MRL joints is essential for successful cartilage tissue remodeling, macrophage turnover, and joint protection during early injury response, preventing severe chronic PTOA.

Chapter 5. Conclusion

For decades, PTOA has been at the forefront of inflammatory joint disease research. Although preventative measures are still unavailable, new developments in the field have advanced our understanding of the joint microenvironment and helped begin development of potential new treatments. While PTOA is not an aggressive disease, its delayed progression and lack of sound detection makes its resolution an extremely important topic in the bone and cartilage field. Additionally, newly developed scientific technologies have given researchers insight to the joint as a whole tissue rather than individual parts. The joint microenvironment is constantly changing due to environmental cues and internal signaling. The work presented in this thesis exemplifies the use of new technological advances for identifying transcriptional changes at the single cell level. Moreover, it also deconstructs the synovial joint and reveals the cellular heterogeneity that exists within the tissue.

A thorough analysis of the synovial knee joint was performed by using single-cell RNA sequencing to identify transcriptionally unique subpopulations of bone, cartilage, synovial, stromal, and immune cells within the joint. Initial hypotheses predicted that chondrocyte populations were inherently different between mouse strains with differing susceptibilities to PTOA. Chondrocyte populations from MRL and B6 mouse strains were relatively similar in transcriptional identity of their chondrocyte populations, although there were severe differences in the number of chondrocytes between different condition. Specifically, a stark decrease in chondrocytes was seen in MRL and may potentially imply that these mice have a difference in their cartilage matrix composition. While this hypothesis would also support that their lack of cartilage degradation after traumatic injury is due to a hardier matrix less prone to enzymatic digestion than B6, additional experimentation is necessary to determine protein composition of their ECM. In addition, a full protein analysis using mass spectrometry would provide novel insights into differences in collagens, proteoglycans, glycosaminoglycans and other potential cartilage proteins responsible for the resilient articular cartilage of MRL joints.

While there were minor differences within the subpopulations of chondrocytes and some trends in response to injury, key mediators in PTOA progression are predicted to

stem from stromal cell populations as well as the immune system. Supporting joint cells, like endothelial cells and fibroblasts, have previously been studied in the context of inflammation through their interactions with myeloid populations [244, 245]. Additionally, the work demonstrated in this dissertation has shown that endothelial and fibroblast populations robustly change after injury, indicating they also play a role in joint maintenance in response to trauma. Specifically, MRL have an higher number of endothelial cells after injury compared to B6 and sustained level of lymphatic cells, indicating an increase of angiogenesis in the joints. The mostly likely mechanism is through interactions with the immune system to promote recruitment of macrophages into the synovial joint. Additionally, these cells may directly interact with chondrocytes by producing anti-apoptotic signaling molecules and growth factors to halt the severe tissue destruction that occurs in late stage PTOA. While endothelial cells seemed to form a distinct population in the single-cell data, further analysis may result in several subpopulations that could potentially be restricted to the joint tissues. An interesting approach to determining the true function of these cells would be to further explore the result of injury on genetically modified knockout animals. A lack of PECAM/*CD31*+ cells may be lethal as endothelial cells are essential in the formation of vasculature, but used in a targeted approach, may result in a tangible study to identify the role of endothelial cells in PTOA progression.

Of the results collected, the most likely mechanism associated with joint regeneration and resistance to severe tissue degradation stems from the immune system. From first glance, the most severe change in cellular populations were from neutrophils. Shortly after injury induction, neutrophil populations in MRL joints dropped to fractions of their baseline levels. While neutrophils have been primarily identified as first responders to tissue trauma, they have also been shown to promote inflammation and cause additional tissue damage when left unregulated [246]. While further analysis is necessary to determine the direct role neutrophils have in PTOA progression, the stark difference between B6 and MRL is enough to hypothesize that the lack of this population in MRL may contribute to an anti-inflammatory joint environment essential for tissue healing. Furthermore, the

neutrophil population in both strains can be further analyzed into subpopulations that may each have a distinct metabolic functional.

In addition to the severe drop in neutrophil populations seen in MRL, there is also a large increase in macrophage populations and stark decrease in monocytes populations early after injury. When further identifying subpopulations of macrophages, MRLs have a higher number of all subpopulations that resembled an alternatively activated macrophage (M2). M2 macrophages are activated by the production of anti-inflammatory signaling molecules, specifically IL-4 and IL-10. In this study, three populations of macrophages were identified that transcriptionally represented an M2 phenotype. Two of the three populations were extremely high in expression of *Trem2*, a receptor complex located on the plasma membrane of macrophages, myeloid cells, and dendritic cells [247]. *Trem2* is part of a large complex that includes *Dap12*; a signaling adapter protein expressed in stromal and myeloid cells. When activated, this complex inhibits pro-inflammatory signaling cascades [232] and thus promotes additional macrophage polarization. In contrast, *Trem2* has been studied highly in neurological disorders and has previously been shown to have a proinflammatory effect on nervous system tissues. Moreover, *Trem2* has been identified in microglial studies to elicit cell survival as well as a proinflammatory signaling response [248]. More recently, *Trem2*+ macrophages have been shown to help control metabolism through interactions with resident adipocytes [249].

While past research of this receptor has had conflicting results, this study identified a population of *Trem2*+ macrophages in the joints of MRLs that also highly express *CD206*, a known marker of activated M2 macrophages. The increase in M2 population is mirrored by a concurrent drop in *Ly6c*+ monocyte populations. This indicates that MRL have a decrease in monocytes due to a phenotypic switch to activated macrophage populations driven by surrounding cells. In addition, *Trem2* and *CD206* are both highly expressed in chondrocytes, indicating there is potential crosstalk between joint resident and infiltrating immune cells after injury. Additionally, using immunohistochemistry to spatially validate transcriptional trends showed that MRL joints have a sustained level of

CD206+Trem2+ macrophages. These sustained levels indicate that an influx of these cells after injury is crucial for joint recovery.

In further analyzing the role of *Trem*2 this study utilized a knockout mouse model to completely remove *Trem2* cells from the injury response. Prior to injury, $Trem2^{-/-}$ joints had a decrease in proteoglycan staining when compared to B6 controls. This indicates that Trem2 has a role in supporting the cartilage matrix and may be essential in ECM homeostasis. Additionally, after injury, $Trem2^{-/-}$ joints had no change from B6 in the severity of their PTOA phenotype, when blindly scored by OARSI standards. This phenotypic similarity indicates that simple removal of Trem2 may not actually exasperate the PTOA phenotype as originally thought. While additional experimentation is needed to determine the true function of Trem2 in the MRL joint, the current findings indicate that Trem2 may need to be overexpressed to alter the PTOA phenotype; a trend also seen in other bone research [250]. Additionally, while Trem2 may be a future target for cartilage and bone regeneration research, identifying the mechanism in MRL that prompts macrophage polarization after injury may be more of interest. This study shows that continued levels of M2 macrophages in MRL joints aid in promoting an anti-inflammatory joint microenvironment and promoting wound healing.

The work presented in this dissertation has identified several key regulators of knee joints healing after traumatic injury induction. While identifying cellular populations with distinct role in PTOA progression is important in understanding the underlying mechanism of onset, additional translational research is necessary to move the field forward. Future research focusing on promoting an angiogenic, anti-inflammatory joint environment would aid in targeted pharmacologic interventions. Currently, this research adds value by fully illuminating specific interactions between chondrocytes within the articular cartilage, stromal cells supporting the joint and resident or infiltrating myeloid derived immune cells. While there is conflicting evidence suggesting Trem2 is an anti-inflammatory marker, the influx of M2 macrophages expressing this marker makes it an interesting new target for potential research. Future research should aim to better understand what molecular signals

that M2 macrophages receive within the joints space to keep this population sustained after injury.

Additionally, this study only identified cellular populations in male mice. With the average age of the population in the United States aging rapidly, female counterparts are also at risk PTOA and OA. Past research has identified several histological differences in PTOA onset and progression between male and female mice [125, 126]. Additional research into the immune system and stromal populations of female mice should be analyzed to determine if there are sex related changes to the joint space after injury. While age is not a determining factor in PTOA, new information gained by analyzing the female response to injury in joint cell population may provide insight to potential targets to aid in the onset of Osteoporosis and osteopenia seen in aging women [251].

The findings of this research will continue to improve our understanding of the cellular response to injury and PTOA progression. While PTOA is still a complex disease that has been shown to encompass crosstalk from many cells, this research lays a foundation for identifying key regulators in disease progression and prevention. In summation, this work identified specific changes to chondrocytes over an injury time course. Additionally, specific subpopulations of chondrocytes were classified and found to reside in restricted locations within the cartilage tissue; a phenomenon previously identified histologically but not at the single cell level. Furthermore, this study identified a specific immune profile in a regenerative strain of mouse. Particularly, macrophage polarization was identified as a regulator of tissue damage and healing in the early stages of PTOA progression. While bone and cartilage research continues to provide challenges to researchers, the work performed here reduces the complexity of the joint by providing a cellular landscape of interacting populations responsible for maintenance and homeostasis in uninjured and PTOA joints, alike.

References

1. Barbour, K.E., et al., *Vital Signs: Prevalence of Doctor-Diagnosed Arthritis and Arthritis-Attributable Activity Limitation - United States, 2013-2015.* MMWR Morb Mortal Wkly Rep, 2017. **66**(9): p. 246-253.

2. Petrillo, S., et al., *Endothelial Cells Promote Osteogenesis by Establishing a Functional and Metabolic Coupling With Human Mesenchymal Stem Cells.* Front Physiol, 2021. **12**: p. 813547.

3. Pereira, D., et al., *The effect of osteoarthritis definition on prevalence and incidence estimates: a systematic review.* Osteoarthritis Cartilage, 2011. **19**(11): p. 1270-85.

4. Thomas, A.C., et al., *Epidemiology of Posttraumatic Osteoarthritis.* J Athl Train, 2017. **52**(6): p. 491-496.

5. Hawker, G.A., *Osteoarthritis is a serious disease.* Clin Exp Rheumatol, 2019. **37 Suppl 120**(5): p. 3-6.

6. Stewart, M.C., et al., *Phenotypic stability of articular chondrocytes in vitro: the effects of culture models, bone morphogenetic protein 2, and serum supplementation.* J Bone Miner Res, 2000. **15**(1): p. 166-74.

7. Wang, L.J., et al., *Post-traumatic osteoarthritis following ACL injury.* Arthritis Res Ther, 2020. **22**(1): p. 57.

8. Jiménez, G., et al., *Osteoarthritis: Trauma vs Disease.* Adv Exp Med Biol, 2018. **1059**: p. 63-83.

9. Watt, F.E., *Posttraumatic osteoarthritis: what have we learned to advance osteoarthritis?* Curr Opin Rheumatol, 2021. **33**(1): p. 74-83.

10. Cui, A., et al., *Global, regional prevalence, incidence and risk factors of knee osteoarthritis in population-based studies.* EClinicalMedicine, 2020. **29-30**: p. 100587.

11. Dieleman, J.L., et al., *US Health Care Spending by Payer and Health Condition, 1996-2016.* Jama, 2020. **323**(9): p. 863-884.

12. Novakofski, K.D., et al., *High-Resolution Methods for Diagnosing Cartilage Damage In Vivo.* Cartilage, 2016. **7**(1): p. 39-51.

13. Rickey, E.J., et al., *Evaluation of experimental impact injury for inducing post-traumatic osteoarthritis in the metacarpophalangeal joints of horses.* Am J Vet Res, 2012. **73**(10): p. 1540-52.

14. Bansal, P.N., et al., *Cationic contrast agents improve quantification of glycosaminoglycan (GAG) content by contrast enhanced CT imaging of cartilage.* J Orthop Res, 2011. **29**(5): p. 704-9.

15. Bansal, P.N., et al., *Contrast enhanced computed tomography can predict the glycosaminoglycan content and biomechanical properties of articular cartilage.* Osteoarthritis Cartilage, 2010. **18**(2): p. 184-91.

16. Blaker, C.L., E.C. Clarke, and C.B. Little, *Using mouse models to investigate the pathophysiology, treatment, and prevention of post-traumatic osteoarthritis.* J Orthop Res, 2017. **35**(3): p. 424-439.

17. Feucht, C.L. and D.R. Patel, *Analgesics and anti-inflammatory medications in sports: use and abuse.* Pediatr Clin North Am, 2010. **57**(3): p. 751-74.

18. Camu, F. and C. Vanlersberghe, *Pharmacology of systemic analgesics.* Best Pract Res Clin Anaesthesiol, 2002. **16**(4): p. 475-88.

19. Matthew, M.T. and P.W. Nance, *Analgesics. Opioids, adjuvants, and others.* Phys Med Rehabil Clin N Am, 1999. **10**(2): p. 255-73, vii.

20. Ricciotti, E. and G.A. FitzGerald, *Prostaglandins and inflammation.* Arterioscler Thromb Vasc Biol, 2011. **31**(5): p. 986-1000.

21. Thau, L., J. Gandhi, and S. Sharma, *Physiology, Cortisol*, in *StatPearls*. 2022, StatPearls Publishing
Copyright © 2022, StatPearls Publishing LLC.: Treasure Island (FL).

22. Lim, J., et al., *Pharmacopuncture and joint movement manual therapy for post-traumatic phalangeal osteoarthritis: A case report.* Medicine (Baltimore), 2021. **100**(38): p. e27081.

23. Brittberg, M., et al., *Cartilage repair in the degenerative ageing knee.* Acta Orthop, 2016. **87**(sup363): p. 26-38.

24. Ralphs, J.R. and M. Benjamin, *The joint capsule: structure, composition, ageing and disease.* J Anat, 1994. **184 (Pt 3)**(Pt 3): p. 503-9.

25. Chang, L.R., G. Marston, and A. Martin, *Anatomy, Cartilage*, in *StatPearls*. 2022: Treasure Island (FL).

26. Hoemann, C.D., et al., *The cartilage-bone interface.* J Knee Surg, 2012. **25**(2): p. 85-97.

27. Chen, S., et al., *Meniscus, articular cartilage and nucleus pulposus: a comparative review of cartilage-like tissues in anatomy, development and function.* Cell Tissue Res, 2017. **370**(1): p. 53-70.

28. Safshekan, F., et al., *Viscoelastic Properties of Human Tracheal Tissues.* J Biomech Eng, 2017. **139**(1).

29. Loy, B.N., et al., *A Biomechanical and Structural Comparison of Articular Cartilage and Subchondral Bone of the Glenoid and Humeral Head.* Orthop J Sports Med, 2018. **6**(7): p. 2325967118785854.

30. Sofat, N., V. Ejindu, and P. Kiely, *What makes osteoarthritis painful? The evidence for local and central pain processing.* Rheumatology (Oxford), 2011. **50**(12): p. 2157-65.

31. Lenoch, F., *Disturbance of nourishment of the articular cartilage and its relation to the development of osteoarthrosis.* Rev Czech Med, 1970. **16**(3): p. 113-7.

32. Isojima, T. and N.A. Sims, *Cortical bone development, maintenance and porosity: genetic alterations in humans and mice influencing chondrocytes, osteoclasts, osteoblasts and osteocytes.* Cell Mol Life Sci, 2021. **78**(15): p. 5755-5773.

33. Oftadeh, R., et al., *Biomechanics and mechanobiology of trabecular bone: a review.* J Biomech Eng, 2015. **137**(1).

34. Kivell, T.L., *A review of trabecular bone functional adaptation: what have we learned from trabecular analyses in extant hominoids and what can we apply to fossils?* J Anat, 2016. **228**(4): p. 569-94.

35. Hu, Y., et al., *Subchondral bone microenvironment in osteoarthritis and pain.* Bone Res, 2021. **9**(1): p. 20.

36. Freemont, A.J., *Microscopic analysis of synovial fluid--the perfect diagnostic test?* Ann Rheum Dis, 1996. **55**(10): p. 695-7.

37. Seidman, A.J. and F. Limaiem, *Synovial Fluid Analysis*, in *StatPearls*. 2022, StatPearls Publishing
Copyright © 2022, StatPearls Publishing LLC.: Treasure Island (FL).

38. Scanzello, C.R. and S.R. Goldring, *The role of synovitis in osteoarthritis pathogenesis.* Bone, 2012. **51**(2): p. 249-57.

39. Primorac, D., et al., *Knee Osteoarthritis: A Review of Pathogenesis and State-Of-The-Art Non-Operative Therapeutic Considerations.* Genes (Basel), 2020. **11**(8).

40. Belluzzi, E., et al., *Contribution of Infrapatellar Fat Pad and Synovial Membrane to Knee Osteoarthritis Pain.* Biomed Res Int, 2019. **2019**: p. 6390182.

41. Paduszyński, W., et al., *Hoffa's Fat Pad Abnormality in the Development of Knee Osteoarthritis.* Adv Exp Med Biol, 2018. **1039**: p. 95-102.

42. Eymard, F. and X. Chevalier, *Inflammation of the infrapatellar fat pad.* Joint Bone Spine, 2016. **83**(4): p. 389-93.

43. Ushiyama, T., et al., *Cytokine production in the infrapatellar fat pad: another source of cytokines in knee synovial fluids.* Ann Rheum Dis, 2003. **62**(2): p. 108-12.

44. Barboza, E., et al., *Profibrotic Infrapatellar Fat Pad Remodeling Without M1 Macrophage Polarization Precedes Knee Osteoarthritis in Mice With Diet-Induced Obesity.* Arthritis Rheumatol, 2017. **69**(6): p. 1221-1232.

45. Parkin, J. and B. Cohen, *An overview of the immune system.* Lancet, 2001. **357**(9270): p. 1777-89.

46. Katz, J.N., K.R. Arant, and R.F. Loeser, *Diagnosis and Treatment of Hip and Knee Osteoarthritis: A Review.* Jama, 2021. **325**(6): p. 568-578.

47. Janeway, C.A., Jr. and R. Medzhitov, *Innate immune recognition.* Annu Rev Immunol, 2002. **20**: p. 197-216.

48. Yatim, K.M. and F.G. Lakkis, *A brief journey through the immune system.* Clin J Am Soc Nephrol, 2015. **10**(7): p. 1274-81.

49. Dranoff, G., *Cytokines in cancer pathogenesis and cancer therapy.* Nat Rev Cancer, 2004. **4**(1): p. 11-22.

50. Sattler, S., *The Role of the Immune System Beyond the Fight Against Infection.* Adv Exp Med Biol, 2017. **1003**: p. 3-14.

51. Hsueh, M.F., et al., *Synergistic Roles of Macrophages and Neutrophils in Osteoarthritis Progression.* Arthritis Rheumatol, 2021. **73**(1): p. 89-99.

52. Li, Z., Z. Huang, and L. Bai, *Cell Interplay in Osteoarthritis.* Front Cell Dev Biol, 2021. **9**: p. 720477.

53. Saxne, T., et al., *Inflammation is a feature of the disease process in early knee joint osteoarthritis.* Rheumatology (Oxford), 2003. **42**(7): p. 903-4.

54. Chen, L., et al., *Inflammatory responses and inflammation-associated diseases in organs.* Oncotarget, 2018. **9**(6): p. 7204-7218.

55. Turner, M.D., et al., *Cytokines and chemokines: At the crossroads of cell signalling and inflammatory disease.* Biochim Biophys Acta, 2014. **1843**(11): p. 2563-2582.

56. Benigni, G., et al., *CXCR3/CXCL10 Axis Regulates Neutrophil-NK Cell Cross-Talk Determining the Severity of Experimental Osteoarthritis.* J Immunol, 2017. **198**(5): p. 2115-2124.

57. Jabbour, H.N., et al., *Inflammatory pathways in female reproductive health and disease.* Reproduction, 2009. **138**(6): p. 903-19.

58. Haubruck, P., et al., *Monocytes, Macrophages, and Their Potential Niches in Synovial Joints - Therapeutic Targets in Post-Traumatic Osteoarthritis?* Front Immunol, 2021. **12**: p. 763702.

59. Sica, A. and A. Mantovani, *Macrophage plasticity and polarization: in vivo veritas.* J Clin Invest, 2012. **122**(3): p. 787-95.

60. Gordon, S. and F.O. Martinez, *Alternative activation of macrophages: mechanism and functions.* Immunity, 2010. **32**(5): p. 593-604.

61. Fujiwara, N. and K. Kobayashi, *Macrophages in inflammation.* Curr Drug Targets Inflamm Allergy, 2005. **4**(3): p. 281-6.

62. Kramer, W.C., K.J. Hendricks, and J. Wang, *Pathogenetic mechanisms of posttraumatic osteoarthritis: opportunities for early intervention.* Int J Clin Exp Med, 2011. **4**(4): p. 285-98.

63. Szczodry, M., et al., *Progressive chondrocyte death after impact injury indicates a need for chondroprotective therapy.* Am J Sports Med, 2009. **37**(12): p. 2318-22.

64. DiMicco, M.A., et al., *Mechanisms and kinetics of glycosaminoglycan release following in vitro cartilage injury.* Arthritis Rheum, 2004. **50**(3): p. 840-8.

65. Lee, J.H., et al., *Mechanical injury of cartilage explants causes specific time-dependent changes in chondrocyte gene expression.* Arthritis Rheum, 2005. **52**(8): p. 2386-95.

66. Grigull, N.P., et al., *Chondrogenic Potential of Pellet Culture Compared to High-Density Culture on a Bacterial Cellulose Hydrogel.* Int J Mol Sci, 2020. **21**(8).

67. Giannoni, P. and R. Cancedda, *Articular chondrocyte culturing for cell-based cartilage repair: needs and perspectives.* Cells Tissues Organs, 2006. **184**(1): p. 1-15.

68. Fu, Y., et al., *Engineering Cartilage Tissue by Co-culturing of Chondrocytes and Mesenchymal Stromal Cells.* Methods Mol Biol, 2021. **2221**: p. 53-70.

69. Gosset, M., et al., *Primary culture and phenotyping of murine chondrocytes.* Nat Protoc, 2008. **3**(8): p. 1253-60.

70. Stiffel, V., et al., *A Mouse Noninvasive Intraarticular Tibial Plateau Compression Loading-Induced Injury Model of Posttraumatic Osteoarthritis.* Calcif Tissue Int, 2020. **106**(2): p. 158-171.

71. Narez, G.E., K.M. Fischenich, and T.L.H. Donahue, *Experimental animal models of post-traumatic osteoarthritis of the knee.* Orthop Rev (Pavia), 2020. **12**(2): p. 8448.

72. Khella, C.M., et al., *An Evidence-Based Systematic Review of Human Knee Post-Traumatic Osteoarthritis (PTOA): Timeline of Clinical Presentation and Disease Markers, Comparison of Knee Joint PTOA Models and Early Disease Implications.* Int J Mol Sci, 2021. **22**(4).

73. Heydemann, A., *The super super-healing MRL mouse strain.* Front Biol (Beijing), 2012. **7**(6): p. 522-538.

74. Fitzgerald, J., et al., *Evidence for articular cartilage regeneration in MRL/MpJ mice.* Osteoarthritis Cartilage, 2008. **16**(11): p. 1319-26.

75. Jablonski, C.L., et al., *p21(-/-) Mice Exhibit Spontaneous Articular Cartilage Regeneration Post-Injury.* Cartilage, 2021. **13**(2_suppl): p. 1608s-1617s.

76. Kwiatkowski, A., et al., *Superior angiogenesis facilitates digit regrowth in MRL/MpJ mice compared to C57BL/6 mice.* Biochem Biophys Res Commun, 2016. **473**(4): p. 907-912.

77. Rai, M.F. and L.J. Sandell, *Regeneration of articular cartilage in healer and non-healer mice.* Matrix Biol, 2014. **39**: p. 50-5.

78. Ward, B.D., et al., *Absence of posttraumatic arthritis following intraarticular fracture in the MRL/MpJ mouse.* Arthritis Rheum, 2008. **58**(3): p. 744-53.

79. Clark, L.D., R.K. Clark, and E. Heber-Katz, *A new murine model for mammalian wound repair and regeneration.* Clin Immunol Immunopathol, 1998. **88**(1): p. 35-45.

80. Michalopoulos, G.K. and M.C. DeFrances, *Liver regeneration.* Science, 1997. **276**(5309): p. 60-6.

81. Sacco, A., et al., *Self-renewal and expansion of single transplanted muscle stem cells.* Nature, 2008. **456**(7221): p. 502-6.

82. Rajnoch, C., et al., *Regeneration of the ear after wounding in different mouse strains is dependent on the severity of wound trauma.* Dev Dyn, 2003. **226**(2): p. 388-97.

83. Kanno, H., et al., *Immune complex-degradation ability of macrophages in MRL/Mp-lpr/lpr lupus mice and its regulation by cytokines.* Clin Exp Immunol, 1994. **95**(1): p. 115-21.

84. Al Barashdi, M.A., et al., *Protein tyrosine phosphatase receptor type C (PTPRC or CD45).* J Clin Pathol, 2021. **74**(9): p. 548-552.

85. Cieza, A., et al., *Global estimates of the need for rehabilitation based on the Global Burden of Disease study 2019: a systematic analysis for the Global Burden of Disease Study 2019.* Lancet, 2021. **396**(10267): p. 2006-2017.

86. McMahon, S.B., et al., *The burden of musculoskeletal pain and the role of topical non-steroidal anti-inflammatory drugs (NSAIDs) in its treatment. Ten underpinning statements from a global pain faculty.* Curr Med Res Opin, 2021. **37**(2): p. 287-292.

87. Dai, X. and L. Shen, *Advances and Trends in Omics Technology Development.* Front Med (Lausanne), 2022. **9**: p. 911861.

88. Mereu, E., et al., *Benchmarking single-cell RNA-sequencing protocols for cell atlas projects.* Nat Biotechnol, 2020. **38**(6): p. 747-755.

89. Hon, C.C., et al., *The Human Cell Atlas: Technical approaches and challenges.* Brief Funct Genomics, 2018. **17**(4): p. 283-294.

90. Ofengeim, D., et al., *Single-Cell RNA Sequencing: Unraveling the Brain One Cell at a Time.* Trends Mol Med, 2017. **23**(6): p. 563-576.

91. Lei, Y., et al., *Applications of single-cell sequencing in cancer research: progress and perspectives.* J Hematol Oncol, 2021. **14**(1): p. 91.

92. He, S., et al., *Single-cell transcriptome profiling of an adult human cell atlas of 15 major organs.* Genome Biol, 2020. **21**(1): p. 294.

93. Chen, M., et al., *Generation of a transgenic mouse model with chondrocyte-specific and tamoxifen-inducible expression of Cre recombinase.* Genesis, 2007. **45**(1): p. 44-50.

94. Madisen, L., et al., *A robust and high-throughput Cre reporting and characterization system for the whole mouse brain.* Nat Neurosci, 2010. **13**(1): p. 133-40.

95. Jenzer, H.R. and F. Burkart, *[Exercise in the hemodynamic assessment of the mitral valve diseases].* Schweiz Med Wochenschr, 1973. **103**(8): p. 277-9.

96. Schneider, C.A., W.S. Rasband, and K.W. Eliceiri, *NIH Image to ImageJ: 25 years of image analysis.* Nat Methods, 2012. **9**(7): p. 671-5.

97. Nagao, M., C.W. Cheong, and B.R. Olsen, *Col2-Cre and tamoxifen-inducible Col2-CreER target different cell populations in the knee joint.* Osteoarthritis Cartilage, 2016. **24**(1): p. 188-91.

98. Salvat, C., et al., *Immature murine articular chondrocytes in primary culture: a new tool for investigating cartilage.* Osteoarthritis Cartilage, 2005. **13**(3): p. 243-9.

99. Sebastian, A., et al., *Comparative Transcriptomics Identifies Novel Genes and Pathways Involved in Post-Traumatic Osteoarthritis Development and Progression.* Int J Mol Sci, 2018. **19**(9).

100. Goldring, M.B., *Human chondrocyte cultures as models of cartilage-specific gene regulation.* Methods Mol Med, 2005. **107**: p. 69-95.

101. Lian, C., et al., *Collagen type II suppresses articular chondrocyte hypertrophy and osteoarthritis progression by promoting integrin β1-SMAD1 interaction.* Bone Res, 2019. **7**: p. 8.

102. Honvo, G., et al., *Role of Collagen Derivatives in Osteoarthritis and Cartilage Repair: A Systematic Scoping Review With Evidence Mapping.* Rheumatol Ther, 2020. **7**(4): p. 703-740.

103. Poole, A.R., et al., *Type II collagen degradation and its regulation in articular cartilage in osteoarthritis.* Ann Rheum Dis, 2002. **61 Suppl 2**(Suppl 2): p. ii78-81.

104. Yoon, H.J., et al., *Type II collagen and glycosaminoglycan expression induction in primary human chondrocyte by TGF-β1.* BMC Musculoskelet Disord, 2015. **16**: p. 141.

105. Carballo, C.B., et al., *Basic Science of Articular Cartilage.* Clin Sports Med, 2017. **36**(3): p. 413-425.

106. Rahmati, M., et al., *Aging and osteoarthritis: Central role of the extracellular matrix.* Ageing Res Rev, 2017. **40**: p. 20-30.

107. Hamada, T., et al., *Surface markers and gene expression to characterize the differentiation of monolayer expanded human articular chondrocytes.* Nagoya J Med Sci, 2013. **75**(1-2): p. 101-11.

108. Li, X., et al., *Influence of microporous gelatin hydrogels on chondrocyte functions.* J Mater Chem B, 2017. **5**(29): p. 5753-5762.

109. Liebman, J. and R.L. Goldberg, *Chondrocyte culture and assay.* Curr Protoc Pharmacol, 2001. **Chapter 12**: p. Unit12.2.

110. Gage, B.E., et al., *Epidemiology of 6.6 million knee injuries presenting to United States emergency departments from 1999 through 2008.* Acad Emerg Med, 2012. **19**(4): p. 378-85.

111. Ondresik, M., et al., *Management of knee osteoarthritis. Current status and future trends.* Biotechnol Bioeng, 2017. **114**(4): p. 717-739.

112. Swann, D.A., et al., *The isolation and partial characterization of the major glycoprotein (LGP-I) from the articular lubricating fraction from bovine synovial fluid.* Biochem J, 1977. **161**(3): p. 473-85.

113. Swann, D.A., et al., *The lubricating activity of synovial fluid glycoproteins.* Arthritis Rheum, 1981. **24**(1): p. 22-30.

114. Ayral, X., et al., *Synovitis: a potential predictive factor of structural progression of medial tibiofemoral knee osteoarthritis -- results of a 1 year longitudinal arthroscopic study in 422 patients.* Osteoarthritis Cartilage, 2005. **13**(5): p. 361-7.

115. Buckwalter, J.A., *Articular cartilage.* Instr Course Lect, 1983. **32**: p. 349-70.

116. Redler, I., et al., *The ultrastructure and biomechanical significance of the tidemark of articular cartilage.* Clin Orthop Relat Res, 1975(112): p. 357-62.

117. Temenoff, J.S. and A.G. Mikos, *Review: tissue engineering for regeneration of articular cartilage.* Biomaterials, 2000. **21**(5): p. 431-40.

118. Sebastian, A., et al., *Single-Cell RNA-Seq Reveals Transcriptomic Heterogeneity and Post-Traumatic Osteoarthritis-Associated Early Molecular Changes in Mouse Articular Chondrocytes.* Cells, 2021. **10**(6).

119. Archer, C.W. and P. Francis-West, *The chondrocyte.* Int J Biochem Cell Biol, 2003. **35**(4): p. 401-4.

120. Yoshitomi, H., *Regulation of Immune Responses and Chronic Inflammation by Fibroblast-Like Synoviocytes.* Front Immunol, 2019. **10**: p. 1395.

121. Bartok, B. and G.S. Firestein, *Fibroblast-like synoviocytes: key effector cells in rheumatoid arthritis.* Immunol Rev, 2010. **233**(1): p. 233-55.

122. Li, N., et al., *Synovial membrane mesenchymal stem cells: past life, current situation, and application in bone and joint diseases.* Stem Cell Res Ther, 2020. **11**(1): p. 381.

123. Thomson, A. and C.M.U. Hilkens, *Synovial Macrophages in Osteoarthritis: The Key to Understanding Pathogenesis?* Front Immunol, 2021. **12**: p. 678757.

124. Sophia Fox, A.J., A. Bedi, and S.A. Rodeo, *The basic science of articular cartilage: structure, composition, and function.* Sports Health, 2009. **1**(6): p. 461-8.

125. Mendez, M.E., et al., *Antibiotic Treatment Prior to Injury Improves Post-Traumatic Osteoarthritis Outcomes in Mice.* Int J Mol Sci, 2020. **21**(17).

126. Mendez, M.E., et al., *LPS-Induced Inflammation Prior to Injury Exacerbates the Development of Post-Traumatic Osteoarthritis in Mice.* J Bone Miner Res, 2020. **35**(11): p. 2229-2241.

127. Sebastian, A., et al., *Global Gene Expression Analysis Identifies Age-Related Differences in Knee Joint Transcriptome during the Development of Post-Traumatic Osteoarthritis in Mice.* Int J Mol Sci, 2020. **21**(1).

128. Chang, J.C., et al., *Global molecular changes in a tibial compression induced ACL rupture model of post-traumatic osteoarthritis.* J Orthop Res, 2017. **35**(3): p. 474-485.

129. Christiansen, B.A., et al., *Musculoskeletal changes following non-invasive knee injury using a novel mouse model of post-traumatic osteoarthritis.* Osteoarthritis Cartilage, 2012. **20**(7): p. 773-82.

130. Ji, Q., et al., *Single-cell RNA-seq analysis reveals the progression of human osteoarthritis.* Ann Rheum Dis, 2019. **78**(1): p. 100-110.

131. Pastoureau, P.C., E.B. Hunziker, and J.P. Pelletier, *Cartilage, bone and synovial histomorphometry in animal models of osteoarthritis.* Osteoarthritis Cartilage, 2010. **18 Suppl 3**: p. S106-12.

132. Di Gregoli, K., et al., *Differential effects of tissue inhibitor of metalloproteinase (TIMP)-1 and TIMP-2 on atherosclerosis and monocyte/macrophage invasion.* Cardiovasc Res, 2016. **109**(2): p. 318-30.

133. Trapnell, C., et al., *The dynamics and regulators of cell fate decisions are revealed by pseudotemporal ordering of single cells.* Nat Biotechnol, 2014. **32**(4): p. 381-386.

134. Qiu, X., et al., *Single-cell mRNA quantification and differential analysis with Census.* Nat Methods, 2017. **14**(3): p. 309-315.

135. Qiu, X., et al., *Reversed graph embedding resolves complex single-cell trajectories.* Nat Methods, 2017. **14**(10): p. 979-982.

136. Chen, J., et al., *Improved human disease candidate gene prioritization using mouse phenotype.* BMC Bioinformatics, 2007. **8**: p. 392.

137. Chen, J., B.J. Aronow, and A.G. Jegga, *Disease candidate gene identification and prioritization using protein interaction networks.* BMC Bioinformatics, 2009. **10**: p. 73.

138. Chen, J., et al., *ToppGene Suite for gene list enrichment analysis and candidate gene prioritization.* Nucleic Acids Res, 2009. **37**(Web Server issue): p. W305-11.

139. Zhou, Y., et al., *Metascape provides a biologist-oriented resource for the analysis of systems-level datasets.* Nat Commun, 2019. **10**(1): p. 1523.

140. Qadri, M., et al., *Proteoglycan-4 regulates fibroblast to myofibroblast transition and expression of fibrotic genes in the synovium.* Arthritis Res Ther, 2020. **22**(1): p. 113.

141. James, A.W., et al., *Pericytes for the treatment of orthopedic conditions.* Pharmacol Ther, 2017. **171**: p. 93-103.

142. Kohashi, K., I. Kinoshita, and Y. Oda, *Soft Tissue Special Issue: Skeletal Muscle Tumors: A Clinicopathological Review.* Head Neck Pathol, 2020. **14**(1): p. 12-20.

143. de Bellard, M.E., *Myelin in cartilaginous fish.* Brain Res, 2016. **1641**(Pt A): p. 34-42.

144. Ducoli, L. and M. Detmar, *Beyond PROX1: transcriptional, epigenetic, and noncoding RNA regulation of lymphatic identity and function.* Dev Cell, 2021. **56**(4): p. 406-426.

145. de Crombrugghe, B., et al., *Transcriptional mechanisms of chondrocyte differentiation.* Matrix Biol, 2000. **19**(5): p. 389-94.

146. Graefe, C., et al., *Optimized Ki-67 staining in murine cells: a tool to determine cell proliferation.* Mol Biol Rep, 2019. **46**(4): p. 4631-4643.

147. Rios-Arce, N.D., et al., *Preexisting Type 1 Diabetes Mellitus Blunts the Development of Posttraumatic Osteoarthritis.* JBMR Plus, 2022. **6**(5): p. e10625.

148. Oetjen, K.A., et al., *Human bone marrow assessment by single-cell RNA sequencing, mass cytometry, and flow cytometry.* JCI Insight, 2018. **3**(23).

149. Tikhonova, A.N., et al., *The bone marrow microenvironment at single-cell resolution.* Nature, 2019. **569**(7755): p. 222-228.

150. Yin, Y., et al., *Insights into the mechanism of vascular endothelial cells on bone biology.* Biosci Rep, 2021. **41**(1).

151. Zhu, S., et al., *Endothelial cells produce angiocrine factors to regulate bone and cartilage via versatile mechanisms.* Theranostics, 2020. **10**(13): p. 5957-5965.

152. Deng, Z., et al., *Characterization of articular cartilage homeostasis and the mechanism of superior cartilage regeneration of MRL/MpJ mice.* Faseb j, 2019. **33**(8): p. 8809-8821.

153. Bara, J.J., et al., *Articular cartilage glycosaminoglycans inhibit the adhesion of endothelial cells.* Connect Tissue Res, 2012. **53**(3): p. 220-8.

154. Zhu, S., et al., *Protein Cytl1: its role in chondrogenesis, cartilage homeostasis, and disease.* Cell Mol Life Sci, 2019. **76**(18): p. 3515-3523.

155. Kim, J.S., Z.Y. Ryoo, and J.S. Chun, *Cytokine-like 1 (Cytl1) regulates the chondrogenesis of mesenchymal cells.* J Biol Chem, 2007. **282**(40): p. 29359-67.

156. Jeon, J., et al., *Cytokine-like 1 knock-out mice (Cytl1-/-) show normal cartilage and bone development but exhibit augmented osteoarthritic cartilage destruction.* J Biol Chem, 2011. **286**(31): p. 27206-13.

157. Liu, X., et al., *Molecular cloning and chromosomal mapping of a candidate cytokine gene selectively expressed in human CD34+ cells.* Genomics, 2000. **65**(3): p. 283-92.

158. Tomczak, A. and M.T. Pisabarro, *Identification of CCR2-binding features in Cytl1 by a CCL2-like chemokine model.* Proteins, 2011. **79**(4): p. 1277-92.

159. Bakos, E., et al., *CCR2 Regulates the Immune Response by Modulating the Interconversion and Function of Effector and Regulatory T Cells.* J Immunol, 2017. **198**(12): p. 4659-4671.

160. Wang, X., et al., *Cytokine-like 1 Chemoattracts Monocytes/Macrophages via CCR2.* J Immunol, 2016. **196**(10): p. 4090-9.

161. Schneller, D., et al., *Cytokine-Like 1 Is a Novel Proangiogenic Factor Secreted by and Mediating Functions of Endothelial Progenitor Cells.* Circ Res, 2019. **124**(2): p. 243-255.

162. Hermansson, M., et al., *Proteomic analysis of articular cartilage shows increased type II collagen synthesis in osteoarthritis and expression of inhibin betaA (activin A), a regulatory molecule for chondrocytes.* J Biol Chem, 2004. **279**(42): p. 43514-21.

163. Pratta, M.A., et al., *Aggrecan protects cartilage collagen from proteolytic cleavage.* J Biol Chem, 2003. **278**(46): p. 45539-45.

164. Dai, M., et al., *Cartilage repair in degenerative osteoarthritis mediated by squid type II collagen via immunomodulating activation of M2 macrophages, inhibiting apoptosis and hypertrophy of chondrocytes.* Biomaterials, 2018. **180**: p. 91-103.

165. Fernandes, T.L., et al., *Macrophage: A Potential Target on Cartilage Regeneration.* Front Immunol, 2020. **11**: p. 111.

166. Martinez-Pomares, L., et al., *Carbohydrate-independent recognition of collagens by the macrophage mannose receptor.* Eur J Immunol, 2006. **36**(5): p. 1074-82.

167. Frevert, C.W., et al., *Danger-Associated Molecular Patterns Derived From the Extracellular Matrix Provide Temporal Control of Innate Immunity.* J Histochem Cytochem, 2018. **66**(4): p. 213-227.

168. Punzi, L., et al., *Post-traumatic arthritis: overview on pathogenic mechanisms and role of inflammation.* RMD Open, 2016. **2**(2): p. e000279.

169. Anderson, D.D., et al., *Post-traumatic osteoarthritis: improved understanding and opportunities for early intervention.* J Orthop Res, 2011. **29**(6): p. 802-9.

170. Dymock, D.C., et al., *Concentrations of stromal cell-derived factor-1 in serum, plasma, and synovial fluid of horses with osteochondral injury.* Am J Vet Res, 2014. **75**(8): p. 722-30.

171. El-Hadi, M., et al., *Expression of interleukin-8 and intercellular cell adhesion molecule-1 in the synovial membrane and cranial cruciate ligament of dogs after rupture of the ligament.* Can J Vet Res, 2012. **76**(1): p. 8-15.

172. Ferrándiz, M.L., et al., *Influence of age on osteoarthritis progression after anterior cruciate ligament transection in rats.* Exp Gerontol, 2014. **55**: p. 44-8.

173. Shen, P.C., et al., *Lentiviral small hairpin RNA knockdown of macrophage inflammatory protein-1γ ameliorates experimentally induced osteoarthritis in mice.* Hum Gene Ther, 2013. **24**(10): p. 871-82.

174. Loeser, R.F., et al., *Disease progression and phasic changes in gene expression in a mouse model of osteoarthritis.* PLoS One, 2013. **8**(1): p. e54633.

175. Delaunay, A. and J. Pages, *Complement and phagocytosis.* C R Seances Soc Biol Fil, 1945. **139**(11-12): p. 557.

176. Liu, B., et al., *Imbalance of M1/M2 macrophages is linked to severity level of knee osteoarthritis.* Exp Ther Med, 2018. **16**(6): p. 5009-5014.

177. Kraus, V.B., et al., *Direct in vivo evidence of activated macrophages in human osteoarthritis.* Osteoarthritis Cartilage, 2016. **24**(9): p. 1613-21.

178. Schaefer, L., *Complexity of danger: the diverse nature of damage-associated molecular patterns.* J Biol Chem, 2014. **289**(51): p. 35237-45.

179. Lieberthal, J., N. Sambamurthy, and C.R. Scanzello, *Inflammation in joint injury and post-traumatic osteoarthritis.* Osteoarthritis Cartilage, 2015. **23**(11): p. 1825-34.

180. Ravindra, K.C., et al., *Chemoproteomics of matrix metalloproteases in a model of cartilage degeneration suggests functional biomarkers associated with posttraumatic osteoarthritis.* J Biol Chem, 2018. **293**(29): p. 11459-11469.

181. Suresh, R. and D.M. Mosser, *Pattern recognition receptors in innate immunity, host defense, and immunopathology.* Adv Physiol Educ, 2013. **37**(4): p. 284-91.

182. Guo, H., J.B. Callaway, and J.P. Ting, *Inflammasomes: mechanism of action, role in disease, and therapeutics.* Nat Med, 2015. **21**(7): p. 677-87.

183. Kosinska, M.K., et al., *A comparative study on the lipidome of normal knee synovial fluid from humans and horses.* PLoS One, 2021. **16**(4): p. e0250146.

184. Knab, K., D. Chambers, and G. Krönke, *Synovial Macrophage and Fibroblast Heterogeneity in Joint Homeostasis and Inflammation.* Front Med (Lausanne), 2022. **9**: p. 862161.

185. Hui, A.Y., et al., *A systems biology approach to synovial joint lubrication in health, injury, and disease.* Wiley Interdiscip Rev Syst Biol Med, 2012. **4**(1): p. 15-37.

186. Gibson, D.S. and M.E. Rooney, *The human synovial fluid proteome: A key factor in the pathology of joint disease.* Proteomics Clin Appl, 2007. **1**(8): p. 889-99.

187. Culemann, S., et al., *Locally renewing resident synovial macrophages provide a protective barrier for the joint.* Nature, 2019. **572**(7771): p. 670-675.

188. Croft, A.P., et al., *Distinct fibroblast subsets drive inflammation and damage in arthritis.* Nature, 2019. **570**(7760): p. 246-251.

189. Orr, C., et al., *Synovial tissue research: a state-of-the-art review.* Nat Rev Rheumatol, 2017. **13**(8): p. 463-475.

190. Kurowska-Stolarska, M. and S. Alivernini, *Synovial tissue macrophages: friend or foe?* RMD Open, 2017. **3**(2): p. e000527.

191. Shi, C. and E.G. Pamer, *Monocyte recruitment during infection and inflammation.* Nat Rev Immunol, 2011. **11**(11): p. 762-74.

192. Christiansen, B.A., et al., *Non-invasive mouse models of post-traumatic osteoarthritis.* Osteoarthritis Cartilage, 2015. **23**(10): p. 1627-38.

193. Glasson, S.S., et al., *The OARSI histopathology initiative - recommendations for histological assessments of osteoarthritis in the mouse.* Osteoarthritis Cartilage, 2010. **18 Suppl 3**: p. S17-23.

194. Bouxsein, M.L., et al., *Guidelines for assessment of bone microstructure in rodents using micro-computed tomography.* J Bone Miner Res, 2010. **25**(7): p. 1468-86.

195. Lockwood, K.A., et al., *Comparison of loading rate-dependent injury modes in a murine model of post-traumatic osteoarthritis.* J Orthop Res, 2014. **32**(1): p. 79-88.

196. Alivernini, S., et al., *Distinct synovial tissue macrophage subsets regulate inflammation and remission in rheumatoid arthritis.* Nat Med, 2020. **26**(8): p. 1295-1306.

197. Kurowska-Stolarska, M. and S. Alivernini, *Synovial tissue macrophages in joint homeostasis, rheumatoid arthritis and disease remission.* Nat Rev Rheumatol, 2022. **18**(7): p. 384-397.

198. Sebastian, A., et al., *Single-cell RNA-Seq reveals changes in immune landscape in post-traumatic osteoarthritis.* Front Immunol, 2022. **13**: p. 938075.

199. Monaghan, K.L., et al., *Monocytes and Monocyte-Derived Antigen-Presenting Cells Have Distinct Gene Signatures in Experimental Model of Multiple Sclerosis.* Front Immunol, 2019. **10**: p. 2779.

200. Zhao, Q., et al., *Osteoclast differentiation and gene regulation.* Front Biosci, 2007. **12**: p. 2519-29.

201. Audzevich, T., et al., *Pre/pro-B cells generate macrophage populations during homeostasis and inflammation.* Proc Natl Acad Sci U S A, 2017. **114**(20): p. E3954-e3963.

202. Xie, H., et al., *Stepwise reprogramming of B cells into macrophages.* Cell, 2004. **117**(5): p. 663-76.

203. Fu, Y., et al., *Caveolin-1 plays a critical role in the differentiation of monocytes into macrophages.* Arterioscler Thromb Vasc Biol, 2012. **32**(9): p. e117-25.

204. O'Connor, M., D. Brighouse, and C.J. Glynn, *Unusual complications of the treatment of chronic spinal arachnoiditis.* Clin J Pain, 1990. **6**(3): p. 240-2.

205. Getz, G.S. and C.A. Reardon, *Apoproteins E, A-I, and SAA in Macrophage Pathobiology Related to Atherogenesis.* Front Pharmacol, 2019. **10**: p. 536.

206. Iyer, S.S. and G. Cheng, *Role of interleukin 10 transcriptional regulation in inflammation and autoimmune disease.* Crit Rev Immunol, 2012. **32**(1): p. 23-63.

207. Tyteca, D., et al., *Regulation of macrophage motility by the water channel aquaporin-1: crucial role of M0/M2 phenotype switch.* PLoS One, 2015. **10**(2): p. e0117398.

208. Li, J., et al., *VSIG4 inhibits proinflammatory macrophage activation by reprogramming mitochondrial pyruvate metabolism.* Nat Commun, 2017. **8**(1): p. 1322.

209. Samaniego, R., et al., *Folate Receptor β (FRβ) Expression in Tissue-Resident and Tumor-Associated Macrophages Associates with and Depends on the Expression of PU.1.* Cells, 2020. **9**(6).

210. Wang, S., et al., *S100A8/A9 in Inflammation.* Front Immunol, 2018. **9**: p. 1298.

211. Hey, Y.Y., T.J. O'Neill, and H.C. O'Neill, *A novel myeloid cell in murine spleen defined through gene profiling.* J Cell Mol Med, 2019. **23**(8): p. 5128-5143.

212. Puranik, A.S., et al., *Kidney-resident macrophages promote a proangiogenic environment in the normal and chronically ischemic mouse kidney.* Sci Rep, 2018. **8**(1): p. 13948.

213. Santiago-Sánchez, G.S., et al., *Biological Functions and Therapeutic Potential of Lipocalin 2 in Cancer.* Int J Mol Sci, 2020. **21**(12).

214. Xie, Z., Z. Guo, and J. Liu, *Whey Acidic Protein/Four-Disulfide Core Domain 21 Regulate Sepsis Pathogenesis in a Mouse Model and a Macrophage Cell Line via the Stat3/Toll-Like Receptor 4 (TLR4) Signaling Pathway.* Med Sci Monit, 2018. **24**: p. 4054-4063.

215. Wen, G., et al., *A Novel Role of Matrix Metalloproteinase-8 in Macrophage Differentiation and Polarization.* J Biol Chem, 2015. **290**(31): p. 19158-72.

216. Soehnlein, O., C. Weber, and L. Lindbom, *Neutrophil granule proteins tune monocytic cell function.* Trends Immunol, 2009. **30**(11): p. 538-46.

217. Fukuda, Y., et al., *Correction: Interplay between soluble CD74 and macrophage-migration inhibitory factor drives tumor growth and influences patient survival in melanoma.* Cell Death Dis, 2022. **13**(5): p. 422.

218. Park, K.T., et al., *Phenotype and Function of CD209+ Bovine Blood Dendritic Cells, Monocyte-Derived-Dendritic Cells and Monocyte-Derived Macrophages.* PLoS One, 2016. **11**(10): p. e0165247.

219. Sánchez-Sánchez, N., L. Riol-Blanco, and J.L. Rodríguez-Fernández, *The multiple personalities of the chemokine receptor CCR7 in dendritic cells.* J Immunol, 2006. **176**(9): p. 5153-9.

220. Tomita, K., et al., *CXCL10-Mediates Macrophage, but not Other Innate Immune Cells-Associated Inflammation in Murine Nonalcoholic Steatohepatitis.* Sci Rep, 2016. **6**: p. 28786.

221. Ding, D.F., et al., *Similarities and differences between rat and mouse chondrocyte gene expression induced by IL-1β.* J Orthop Surg Res, 2022. **17**(1): p. 70.

222. Papalexi, E. and R. Satija, *Single-cell RNA sequencing to explore immune cell heterogeneity.* Nat Rev Immunol, 2018. **18**(1): p. 35-45.

223. Li, X., et al., *Combining bulk and single-cell RNA-sequencing data to reveal gene expression pattern of chondrocytes in the osteoarthritic knee.* Bioengineered, 2021. **12**(1): p. 997-1007.

224. Kouroupis, D., et al., *Single-Cell RNA-Sequencing Identifies Infrapatellar Fat Pad Macrophage Polarization in Acute Synovitis/Fat Pad Fibrosis and Cell Therapy.* Bioengineering (Basel), 2021. **8**(11).

225. Lech, M. and H.J. Anders, *Macrophages and fibrosis: How resident and infiltrating mononuclear phagocytes orchestrate all phases of tissue injury and repair.* Biochim Biophys Acta, 2013. **1832**(7): p. 989-97.

226. Martinez, F.O. and S. Gordon, *The M1 and M2 paradigm of macrophage activation: time for reassessment.* F1000Prime Rep, 2014. **6**: p. 13.

227. Dick, S.A., et al., *Self-renewing resident cardiac macrophages limit adverse remodeling following myocardial infarction.* Nat Immunol, 2019. **20**(1): p. 29-39.

228. Chakarov, S., et al., *Two distinct interstitial macrophage populations coexist across tissues in specific subtissular niches.* Science, 2019. **363**(6432).

229. MacDonald, L., et al., *COVID-19 and RA share an SPP1 myeloid pathway that drives PD-L1+ neutrophils and CD14+ monocytes.* JCI Insight, 2021. **6**(13).

230. Coelho, I., et al., *Trem-2 Promotes Emergence of Restorative Macrophages and Endothelial Cells During Recovery From Hepatic Tissue Damage.* Front Immunol, 2020. **11**: p. 616044.

231. de Seny, D., et al., *New Proteins Contributing to Immune Cell Infiltration and Pannus Formation of Synovial Membrane from Arthritis Diseases.* Int J Mol Sci, 2021. **23**(1).

232. Zhong, L., et al., *TREM2/DAP12 Complex Regulates Inflammatory Responses in Microglia via the JNK Signaling Pathway.* Front Aging Neurosci, 2017. **9**: p. 204.

233. Lu, J., et al., *Elevated TYROBP expression predicts poor prognosis and high tumor immune infiltration in patients with low-grade glioma.* BMC Cancer, 2021. **21**(1): p. 723.

234. Ferlazzo, G., et al., *Engagement of CD33 surface molecules prevents the generation of dendritic cells from both monocytes and CD34+ myeloid precursors.* Eur J Immunol, 2000. **30**(3): p. 827-33.

235. Tarquini, C., et al., *Clusterin exerts a cytoprotective and antioxidant effect in human osteoarthritic cartilage.* Aging (Albany NY), 2020. **12**(11): p. 10129-10146.

236. Harasymowicz, N.S., et al., *Single-cell RNA sequencing reveals the induction of novel myeloid and myeloid-associated cell populations in visceral fat with long-term obesity.* Faseb j, 2021. **35**(3): p. e21417.

237. Li, R.Y., et al., *TREM2 in the pathogenesis of AD: a lipid metabolism regulator and potential metabolic therapeutic target.* Mol Neurodegener, 2022. **17**(1): p. 40.

238. Park, M., et al., *Triggering receptor expressed on myeloid cells 2 (TREM2) promotes adipogenesis and diet-induced obesity.* Diabetes, 2015. **64**(1): p. 117-27.

239. Kobayashi, M., et al., *TREM2/DAP12 Signal Elicits Proinflammatory Response in Microglia and Exacerbates Neuropathic Pain.* J Neurosci, 2016. **36**(43): p. 11138-11150.

240. Rahmati, M., A. Mobasheri, and M. Mozafari, *Inflammatory mediators in osteoarthritis: A critical review of the state-of-the-art, current prospects, and future challenges.* Bone, 2016. **85**: p. 81-90.

241. Lees, S., et al., *Bioactivity in an Aggrecan 32-mer Fragment Is Mediated via Toll-like Receptor 2.* Arthritis Rheumatol, 2015. **67**(5): p. 1240-9.

242. Engelholm, L.H., et al., *uPARAP/Endo180 is essential for cellular uptake of collagen and promotes fibroblast collagen adhesion.* J Cell Biol, 2003. **160**(7): p. 1009-15.

243. Mantovani, A., et al., *Macrophage plasticity and polarization in tissue repair and remodelling.* J Pathol, 2013. **229**(2): p. 176-85.

244. Mescher, A.L., *Macrophages and fibroblasts during inflammation and tissue repair in models of organ regeneration.* Regeneration (Oxf), 2017. **4**(2): p. 39-53.

245. Kalucka, J., et al., *Interaction of endothelial cells with macrophages-linking molecular and metabolic signaling.* Pflugers Arch, 2017. **469**(3-4): p. 473-483.

246. Rosales, C., *Neutrophil: A Cell with Many Roles in Inflammation or Several Cell Types?* Front Physiol, 2018. **9**: p. 113.

247. Do, T.H., et al., *TREM2 macrophages induced by human lipids drive inflammation in acne lesions.* Sci Immunol, 2022. **7**(73): p. eabo2787.

248. Zhong, L., et al., *Soluble TREM2 induces inflammatory responses and enhances microglial survival.* J Exp Med, 2017. **214**(3): p. 597-607.

249. Jaitin, D.A., et al., *Lipid-Associated Macrophages Control Metabolic Homeostasis in a Trem2-Dependent Manner.* Cell, 2019. **178**(3): p. 686-698.e14.

250. Chang, J.C., et al., *SOST/Sclerostin Improves Posttraumatic Osteoarthritis and Inhibits MMP2/3 Expression After Injury.* J Bone Miner Res, 2018. **33**(6): p. 1105-1113.

251. Varacallo, M., et al., *Osteopenia*, in *StatPearls*. 2022, StatPearls Publishing Copyright © 2022, StatPearls Publishing LLC.: Treasure Island (FL).